MODELING OF ECM CONTROLLED SERIES FAN-POWERED VAV TERMINAL UNITS

A Thesis

by

PENG YIN

Submitted to the Office of Graduate Studies of
Texas A&M University
in partial fulfillment of the requirements for the degree of

MASTER OF SCIENCE

August 2010

Major Subject: Mechanical Engineering

Modeling of ECM Controlled Series Fan-powered VAV Terminal Units

MODELING OF ECM CONTROLLED SERIES FAN-POWERED VAV TERMINAL UNITS

A Thesis

by

PENG YIN

Submitted to the Office of Graduate Studies of
Texas A&M University
in partial fulfillment of the requirements for the degree of

MASTER OF SCIENCE

Approved by:

Co-Chairs of Committee,	Dennis O'Neal
	Michael B. Pate
Committee Members,	Warren Heffington
	Jorge L. Alvarado
Head of Department,	Dennis O'Neal

August 2010

Major Subject: Mechanical Engineering

ABSTRACT

Modeling of ECM Controlled Series Fan-powered VAV Terminal Units. (August 2010)

Peng Yin, B.S., Shanghai Ocean University

Co-Chairs of Advisory Committee: Dr. Dennis O'Neal
Dr. Michael B. Pate

Semi-empirical models for series fan-powered variable air volume terminal units (FPTUs) were developed based on models of the primary, plenum, fan airflow and the fan power consumption. The experimental setups and test procedures were developed respectively for primary, plenum and fan airflow to test each component of the FPTUs at typical design pressures and airflows. Two sizes of the terminal units from three manufacturers were used in this study. All of the FPTUs were equipped with electronically commutated motors (ECM). Data provided by the models were compared against the data from previous experiments to prove the models' validity. Regression modeling was performed by using SigmaStat.

The model of primary airflow had an R^2 above 0.948 for all the terminal units evaluated while the plenum airflow model had an R^2 above 0.99. For all the terminal units, the R^2 of the fan airflow model was ranged from 0.973 to 0.998. Except for one

fan, the fan power consumption model was able to characterize the power performance and had an R^2 above 0.986.

By combining the airflow and power models, the model for series FPTU was developed. Verification was made to prove the FPTU model's validity by comparing the measured and predicted data of airflow and power consumption. Correction factors were used in the primary airflow model to compensate for the difference caused by large measurement errors and the system effects. The predicted values were consistent with measurements and no offset was needed in the primary airflow model. Generally, the newly established model was able to describe the airflow performance as well as power consumption of series FPTUs without adding complexity.

DEDICATION

To my parents.

ACKNOWLEDGEMENTS

This study was organized and funded by several VAV fan-powered terminal unit manufacturers. I would like to thank General Electric, A.O Smith Corp, Krueger, Metalaire, and Nailor Industries for their financial support.

I would like to thank Dr. Dennis O'Neal, Dr. Michael B. Pate, Dr. Warren Heffington, and Dr. Jorge L. Alvarado who served as my committee advisers. Since I joined this research group Dr. Dennis O'Neal has given me guidance of great value for this project. Dr. Michael B. Pate helped me to coordinate the use of the experimental devices.

I would like to thank Mr. Kelly Milligan at the Riverside Energy System Laboratory. His advice and help was very valuable while working through technical difficulties in setting up the test rigs. Also, I would like to thank Mr. Jake Edmondson, the previous graduate student who worked on this project. He taught me how to operate the experimental devices and showed me the future research directions.

At last, I would like to give my heartfelt appreciation to my Mum and Dad for their continuous influence and encouragement. Without their support and help it would have been impossible for me to study abroad and became what I am now. Thank you.

NOMENCLATURE

AC	Alternating Current
AHU	Air Handling Unit
ASHRAE	American Society of Heating, Refrigeration and Air-Conditioning Engineers
A_d	Flow-through Area of a Damper at Certain Control Voltage
A_{d0}	Flow-through Area of a Damper at Fully Open Position
A_p	Inlet Area of Plenum Airflow
A_{p0}	Inlet Area of Terminal Unit S12B
BF	Butterfly Damper
CAV	Constant Air Volume
CFM	Cubic Feet per Minute
DAQ	Data Acquisition
DC	Direct Current
ECM	Electronically Commutated Motor
FPTU	Fan Powered Terminal Unit
HVAC	Heating, Ventilation, Air-Conditioning

k	Pressure Loss Coefficient
OB	Opposed-blade Damper
PCI	Peripheral Component Interconnect
$P_{upstream}$	Upstream Static Pressure
$P_{downstream}$	Downstream Static Pressure
$P_{internal}$	Internal Static Pressure
$P_{dishcagre}$	Discharge Pressure
P_{fan}	Fan Power Consumption
ΔP_T	Total Pressure Loss across Damper
P_V	Velocity Pressure
PSC	Permanent Split Capacitor
$\dot{Q}$	Air Volume Flow Rate
Q_{fan}	Fan Airflow
Q_{plenum}	Plenum Airflow
$Q_{primary}$	Primary Airflow
P_d or DP	Differential Pressure across Damper
RH	Relative Humidity
RPM	Round per Minute

THD	Total Harmonic Distortion
u	Velocity
V	Damper Control Voltage
VAC	Alternating Current Voltage
VAV	Variable Air Volume
VDC	Direct Current Voltage
VFD	Variable Frequency Drive
VSD	Variable Speed Drive
α	Damper Blade Angle
γ	Non-dimensional Damper Position
η	Non-dimensional ECM Setting
θ	Non-dimensional Inlet Area of Plenum Airflow
ρ	Air Density

TABLE OF CONTENTS

CHAPTER Page

LIST OF FIGURES

Page

Page

Page

Page

Page

Page

Page

Page

LIST OF TABLES

Page

Page

CHAPTER I

INTRODUCTION

Heating ventilation and air-conditioning (HVAC) systems are used in commercial and residential buildings to maintain thermal comfort and indoor air quality. Variable air volume (VAV) systems are a type of systems commonly applied in commercial buildings. VAV systems are designed to vary the amount of conditioned air to the zone to maintain the preset temperature and relative humidity. Energy is saved in VAV systems because the fan is working at part load. Two main benefits are offered. One is that the temperatures in occupied zones can be controlled rapidly to provide greater occupant comfort. Second, good energy efficiency can be realized with minimal simultaneous heating and cooling. Because of the two benefits, the VAV systems have increased their popularity in commercial buildings.

A typical VAV system is shown in Figure 1-1. Air is delivered to the VAV terminal unit from the supply fan. A VAV terminal unit is a zone-level flow control device. In its most simple form, it is no more than a calibrated air damper with an automatic actuator.

This thesis follows the style of *HVAC&R Research*.

Some terminal units employ a fan to help draw air from the plenum space and compensate for the pressure loss caused by downstream flexible ducts and diffusers. A terminal unit with a fan in it is called fan-powered terminal units (FPTUs).

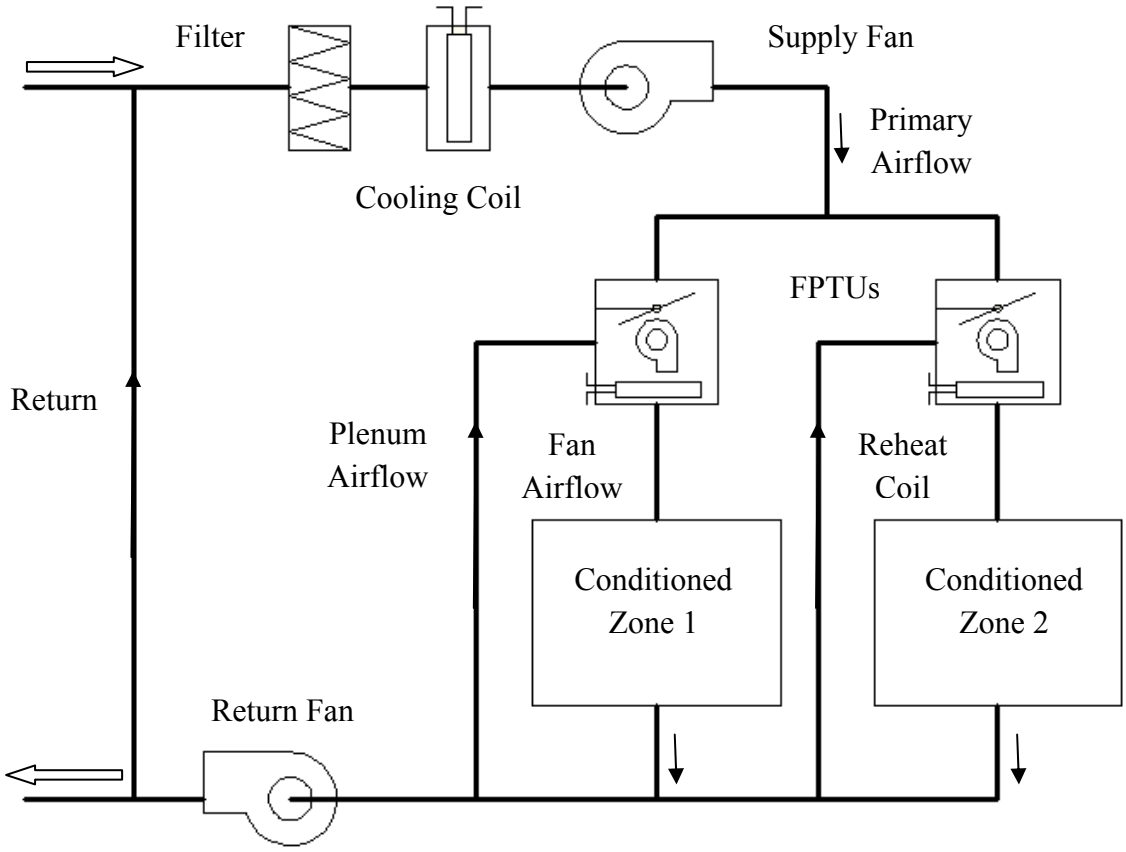

Fig. 1-1 Typical VAV System

Two configurations of FPTUs have been developed: series and parallel designs, which are shown in Figure 1-2. In a series design, the terminal unit fan is in series with the supply fan. Therefore, primary airflow from the supply fan always passes through the

terminal unit fan, which is required to operate continuously to supply a constant amount of air to the conditioned zone. As the zone's load decreases, the damper rotates and blocks some of the primary air. More air from plenum space is drawn and re-circulated into the conditioned zone. In a parallel design, the plenum air is drawn into the FPTU by a terminal unit fan that operates intermittently. When the maximum load in the zone is required, the fan is off. If the load decreases, the damper closes gradually to reduce the primary air entering the conditioned zone. When the primary air is below a specific amount, the fan is turned on. At this operating condition, the primary and plenum air are mixed within the terminal unit and delivered to the conditioned zone.

The ultimate goal of this study was to develop a semi-empirical model to characterize the airflow and power performance of the series FPTUs. To extend the applicability of this model, every component of the terminal unit was tested, including the primary inlet damper, the fan and the terminal unit frame. The experimental setups and procedures were developed and used in the different tests. Statistical analysis was conducted on the experimental data in order to build regression models. Models for the primary, plenum, and fan airflow and fan power consumption were generated and systematically combining these models, a series FPTU model was developed.

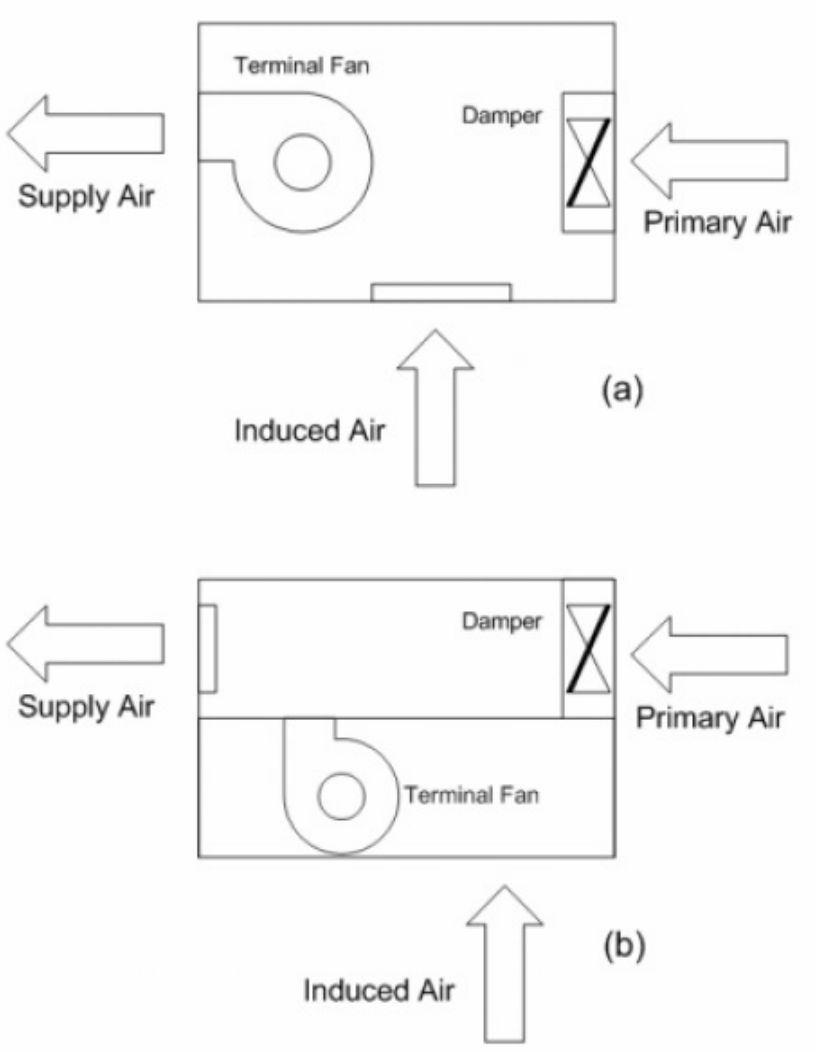

Fig. 1-2 Two Configurations of FPTUs (a) Series (b) Parallel

The model provides a way to evaluate the airflow and power performance of series FPTUs and therefore an engineer can choose series FPTUs wisely under various requirements by applying the model. Also, the model can be used to analyze the performance of a VAV system and set up the operation strategy.

Chapter II provides a literature review on VAV systems, terminal units and models developed in previous research. Chapter III and IV give detailed information on experimental instruments and procedures. Chapter V, VI and VII show the results of the experiments and provide regression modeling of primary, plenum and fan airflow. Chapter VIII describes the approach used to form a series FPTU model based on the models for primary, plenum, fan airflow and fan power consumption model. Also comparisons were made by using experimental and measured data to prove the validity of this model. Chapter IX summarizes the results and conclusions of this study.

CHAPTER II

LITERATURE REVIEW

Variable air volume (VAV) systems are widely applied in commercial and residential buildings because of their potential to reduce energy use. Studies have been conducted to exam this capability and optimize the performance of VAV systems.

Ardehali and Smith (1996) made comparisons of annual energy consumption and economic selection for both constant air volume (CAV) and VAV systems. Their simulations were performed with the TRACE program and based on a typical three-story office building and a typical residential building both located in Des Moines, Iowa. Their simulation results indicated that the energy consumed by CAV systems for heating and cooling were 60% higher than that of VAV systems. However, in their report, they did not point out which configuration of terminal units were chosen. It was important to characterize the difference of series and parallel terminal units so engineers can choose FPTUs properly.

In another study, Elleson (1993) introduced the differences in design of series and parallel terminal units. Field studies of cold air distribution systems were performed with both series and parallel terminal units in two separate buildings. Though this research mainly focused on the advantage of cold air distribution system, energy consumption of

both series and parallel terminal units was also mentioned. Simulation results showed that parallel terminal units could save 24% to 47% on fan energy compared to series terminal units in a regular system and 30% to 54% in a cold-air system. It was also reported that series terminal units required lower supply duct static pressure than parallel terminal units.

Khoo et al. (1998) tested three damper-only controlled terminal units and developed two non-linear models for pressure-dependent and pressure-independent terminal unit. This study concluded that the newly derived non-linear models were significantly more accurate than traditional damper-only models. Because many software packages use damper-only terminal unit models, the results of simulations may not be useful for fan-powered terminal unit applications. Mei and Levermore (2002) modeled each component in a VAV system including fan, duct and damper-only controlled terminal units by using an artificial neural network model on an HVACSIM+ platform. It was found that the simulation based on each component showed a good general agreement with the laboratory measurements.

Little work has been done on modeling fan-powered terminal units with electronically commuted motors (ECMs). Since 1985, when ECM motors were first applied in residential HVAC systems, engineers quickly realized their advantages: high efficiency, set-up versatility and better functionality. Abney et al. (2000) made a comparison between ECM and permanent split capacitor (PSC) motors. It was reported

that at lower speeds, ECM motors' efficiencies stayed above 60% even down to 400 rpm at 10% load. PSC motors' efficiencies were as little as 18% when they were running at their lowest operating point. Through experiments, Cramlet (2008) developed three models for fan airflow, primary airflow and power consumption of the fan-powered terminal unit. In his fan airflow analysis, he confirmed that variations of upstream static pressure, primary airflow and damper position had little effect on fan airflow performance which was consistent with Furr's (2006) research result. Cramlet's fan airflow model used ECM setting as the primary independent variable and inlet air velocity differential pressure as another variable. In his primary airflow analysis, Cramlet stated that the primary airflow of the terminal unit was proportional to the square root of the pressure differential across the terminal unit for a given damper setting. To keep the value inside the square root positive, an offset 0.27 was used in Cramlet's correlation, which took damper orientation as well as pressure differential across the terminal unit as two independent variables. In the power consumption analysis, Cramlet took both ECM setting and inlet air velocity differential pressure as independent variables. All of the three models had R^2 values above 0.99, which meant the correlations could give an accurate description of the function between the input and output. The models developed by Cramlet are listed in Table 2-1.

Table 2-1 Summary of Correlations Developed in Previous Research

Model	Expression	R^2
Fan airflow	$Q_{fan}=C_1+C_2\times V+C_3\times V^2+C_4\times P_{iav}$	0.997
Primary airflow	$Q_{Primary}=C_1\times(1+C_2\times S+C_3\times S^2)\times\sqrt{(DP+0.27)}$	0.997
Power Consumption	$P_{fan}=C_1+C_2\times V+C_3\times V^2+C_4\times P_{iav}$	0.998

Edmondson's (2009) research extended the work of Cramlet to seven series and seven parallel ECM controlled fan-powered terminal units. He used the same models developed by Cramlet to analyze the characteristics of terminal box performance. Also, he stated that the primary airflow model could be improved by using the internal static pressure to calculate the differential pressure across the damper instead of the pressure downstream of the fan.

It is possible to needs to develop a new model that can be used to predict Q_{fan}, Q_{plenum}, $Q_{primary}$ and power consumption without any offset based on previous research results. These predicted values can then be used to simulate energy use in HVAC systems. With accurate performance data, designers can then determine which series terminal units to install based on overall systems cost. In addition, FPTU model can be useful for network analysis to detect possible unbalanced conditions in the system and part load efficiency.

Both Cramlet and Edmondson treated the FPTU as a black box. They measured the primary airflow and fan airflow under varieties of upstream and downstream static pressures, and then correlated the measured data with different pressures and ECM settings. Though this method could simplify the modeling process, it has its disadvantages. For example, Cramlet and Edmondson's models were purely empirical and their models can only be applied to a specific FPTU which limits the applicability of their models.

If a FPTU model is based on the physical characteristics of components in a FPTU, then the model could be applied to a wider range of application than the purely empirical models used by Cramlet (2008) and Edmondson (2009). The goal of this research is to build up a FPTU model based on models of every component in the terminal unit, named primary airflow, plenum airflow and fan airflow and fan power consumption.

CHAPTER III

EXPERIMENTAL APPARATUS

This study can be divided into two stages: data collection and data analysis. Experimental data were taken and recorded in the first stage and data were categorized into two distinct groups, namely, airflow and power. Each group of data was collected by a separate data acquisition system and a single electronic data sheet was then used to summarize those two groups of data. In this chapter, the experimental setup was introduced, including airflow measurement equipment, series fan-powered VAV terminal units and power measurement devices, as well as the data acquisition system.

3.1. Airflow Equipment

3.1.1. Airflow Chambers with Blowers

Two airflow chambers were employed in the experiments to measure the airflow. Both chambers were built to the specifications in accordance to ANSI/ASHRAE Standard 51 (ASHRAE 2007). Figures 3-1 and 3-2 show the configuration of inlet and outlet flow chambers, respectively.

The inlet flow chamber was used to measure the primary airflow. A large capacity blower was connected at the entrance of the inlet airflow chamber to control the volume flow rate and the upstream static pressure. The purpose of the outlet flow chamber was to

quantify the fan airflow and simulate the plenum airflow. An assist blower was attached at the end of the outlet airflow chamber to control the discharge pressure as well as internal pressure of each terminal unit. Both the primary and assist blowers were equipped with the variable speed drives (VSD), which enabled the dynamical controlling of the blowers.

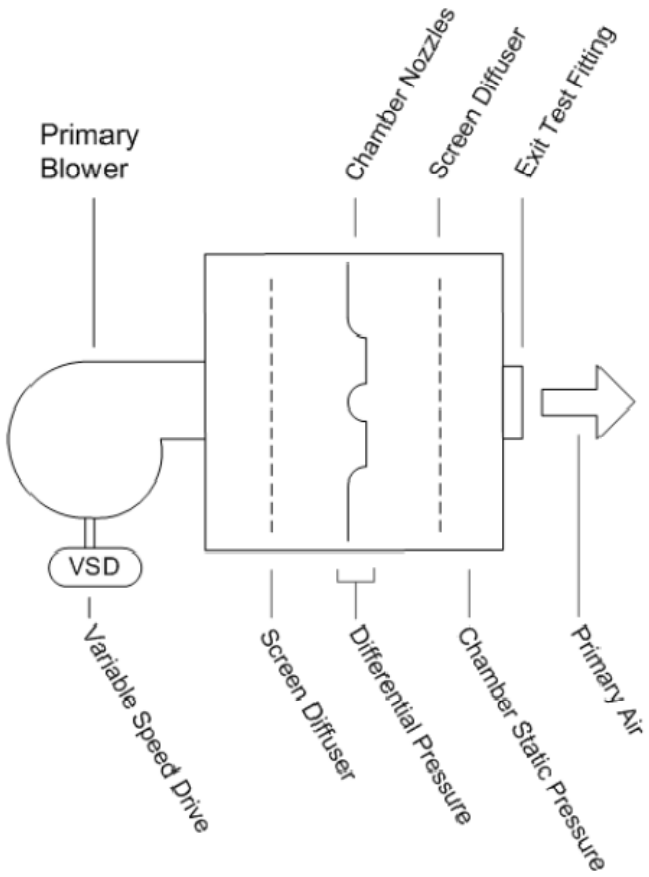

Fig. 3-1 Inlet Flow Chamber with Primary Blower

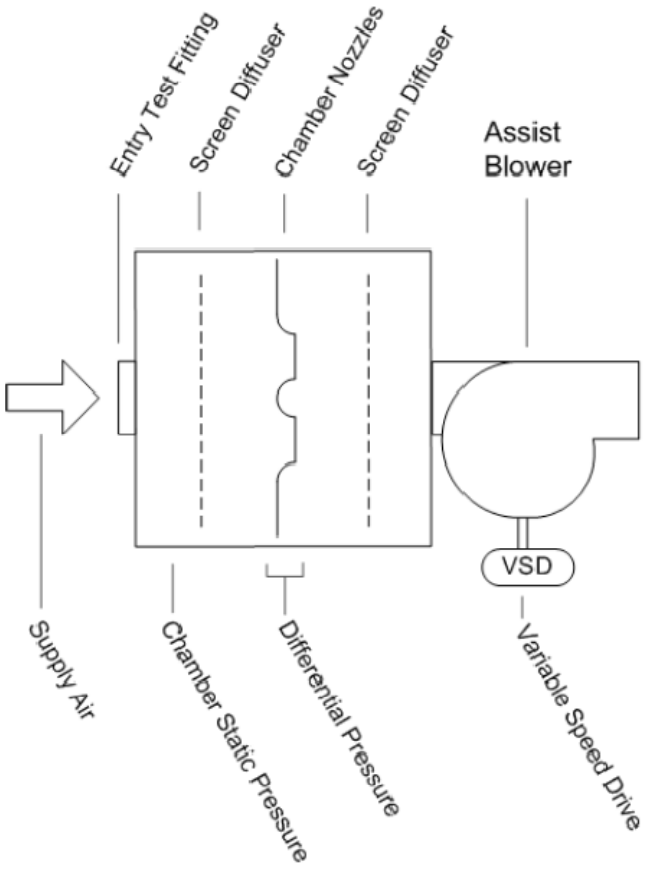

Fig. 3-2 Outlet Flow Chamber with Assist Blower

Two diffuser screens were installed at the entrance and exit of the nozzle bank in the inlet flow chamber to smooth the airflow through the chamber. The airflow area was controlled by covering or uncovering the outlet of individual nozzles. The airflow area, the differential pressure across the nozzles, and the static pressure inside the chamber were collected and used to calculate the volume flow rate. These data were converted to the corresponding values under standard temperature and pressure to eliminate the effects

of various environmental conditions in the lab during testing. A transition duct built to specification in ANSI/ASHRAE Standard 120 (ASHRAE 2008) was installed at the exit of the chamber.

The outlet flow chamber was similar to the inlet flow chamber, except the fan was installed at the exit. The assist blower was used to maintain a target discharge pressure in fan testing and internal pressure of the terminal unit in measurement of plenum airflow. The nozzles in this chamber were used to take the measurement of the fan airflow, which was composed of primary and plenum airflow.

Table 3-1 shows the particular characteristics of the two chambers used in the test. As shown, nozzle combinations were different for each chamber and could be selected by the operators depending on the specific need of the test. As the cumulative nozzle area was increased, less static pressure was required to provide the same amount of airflow. The complete procedure and equations are available in ANSI/ASHRAE Standard 120. Table 3-2 lists the fan motor power along with the control and motor characteristics of the two chambers.

Table 3-1 Chamber Airflow Characteristics

Type	Name	Maximum Airflow CFM (m^3/s)	Available Nozzles' Diameters inch (m)
Outlet	Silver	4000 (1.88)	1.5 (0.04), 3 (0.08), 5 (0.13), 5 (0.13), 5 (0.13)& 5 (0.13)
Inlet	Black	8000 (3.77)	3 (0.08), 3 (0.08), 4 (0.1), 4 (0.1), 6 (0.15), 6 (0.15)& 7 (0.18)

Table 3-2 Chamber Power Characteristics

Type	Name	Fan Motor Power hp (kw)	Controller	Motor
Outlet	Silver	7.5 (5.6)	VSD	AC Induction
Inlet	Black	30 (22.4)		

Sheet metal duct was used to connect the airflow chambers to components from the FPTUs. The upstream duct was circular with the same diameter of the inlet on the terminal unit. The inlet flow chamber and the dampers to be tested were connected by the upstream duct. The downstream duct was used to connect the fan to the outlet flow chamber. This piece of metal duct was rectangular with dimension of 16"×15"

(0.41m×0.38m) which results in an equivalent diameter of 17" (0.43m).The length of duct and the locations of static pressure measurement points were determined according to the specification in ANSI/ASHRAE Standard 130 (ASHRAE 2008), which is shown in Figure 3-3. Holes were drilled into the sheet metal duct at those locations and covered by copper pressure taps with matching diameter. The copper taps were sealed with adhesive tape. Four holes were drilled, 90° apart, in order to measure the average static pressure inside the duct. Copper taps were connected by using plastic tubing with the same length. Figure 3-4 shows the sketch of copper pressure tap, and how it was attached to the metal duct. Figure 3-5 illustrates how the pressure taps connected to the plastic tubing to measure the static pressures.

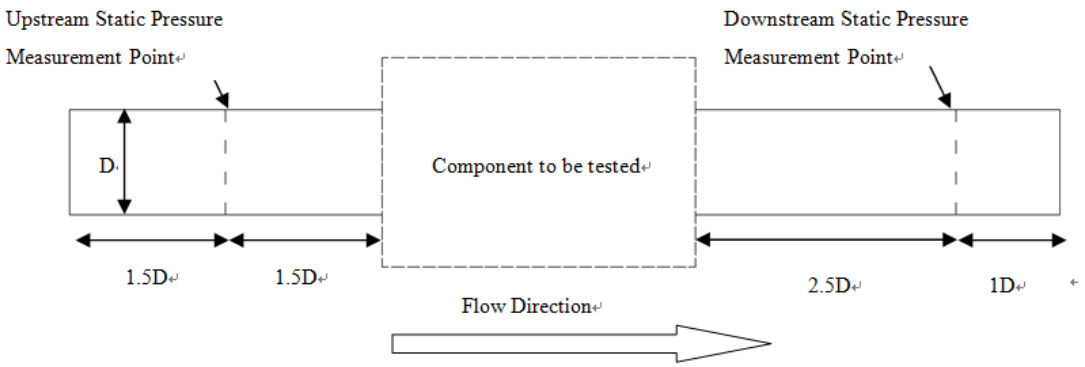

Fig. 3-3 Experimental Duct Setting

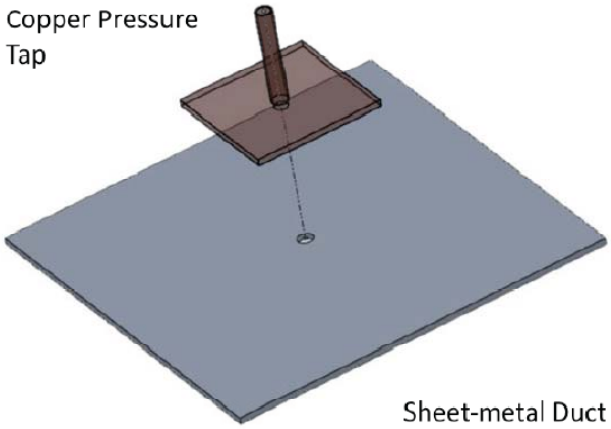

Fig. 3-4 Pressure Tap

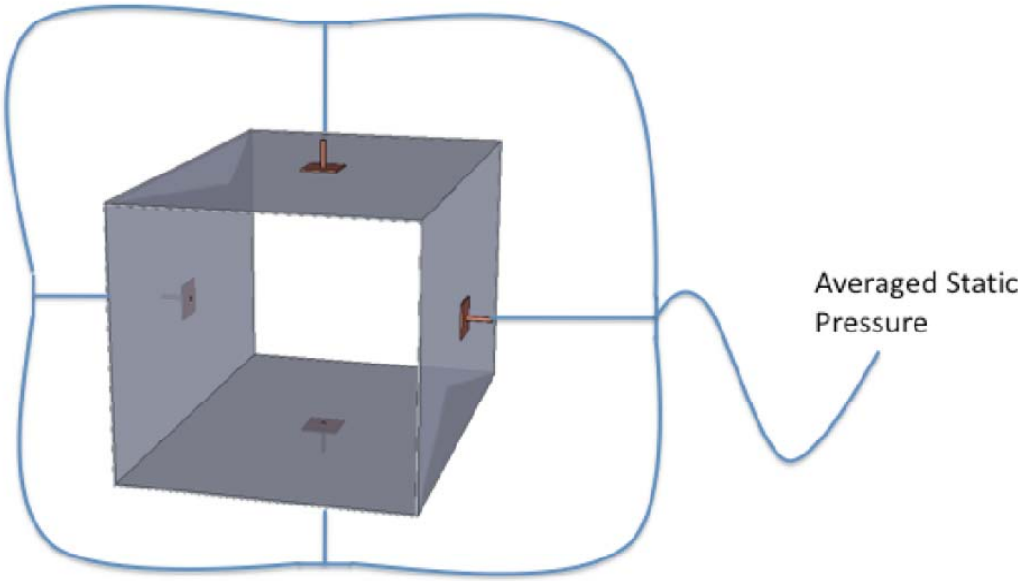

Fig. 3-5 Pressure Taps and Plastic Tubing

3.1.2. Variable Air Volume Fan-powered Terminal Unit

Terminal units with two sizes (8" and 12") of inlet diameters were evaluated in this study. All the terminal units came from three manufacturers, marked as A, B and C. The manufacturer C used two brands of motors in the FPTUs, named _M1 and _M2. Eight series FPTUs were used in this study and grouped by size (8" and 12"), manufacturers (A, B and C) and motor brands (_M1 and _M2). For example, S12C_M1 is the name of a 12'' series terminal unit from manufacturer C equipped with a brand 1 of the fan motor.

The terminal units from different manufacturers had slightly different designs. However, they all shared some general design elements and contained similar components. These similarities provided the idea that the performance of terminal units could be characterized based on the models for different individual components inside the FPTUs.

The incoming primary air entered the terminal unit through an inlet that was circular and it contained a differential pressure sensor to quantify the airflow delivered to the terminal unit. The sensors, shown in Figure 3-6, were designed to measure velocity pressure at several positions and average them to get a better representation of the average velocity pressure. Terminal units from different manufacturers had slight differences in inlet velocity sensor design. For example, the sensors from manufacturer A could measure inlet velocity pressure at twelve positions while sensors from manufacturer B and C could measure only four positions at a time. The outlet taps were connected to a pressure

transmitter via the plastic tubing and the differential pressure could be recorded by a data acquisition system.

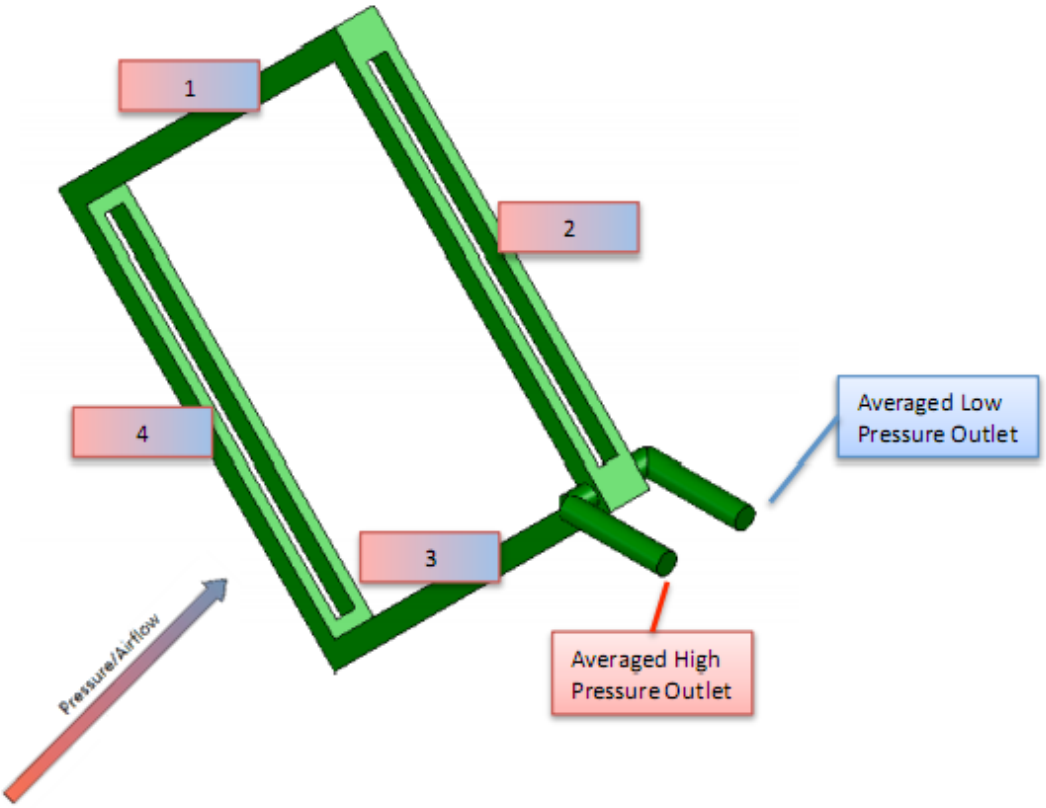

Fig. 3-6 Inlet Velocity Pressure Sensor

After the inlet velocity pressure sensor it was a mechanical damper. The damper was used to control the amount of primary air supplied to terminal unit. There were two types of dampers in the terminal units. The first type is the butterfly damper (Figure 3-7 (a)), which had an operating range from 0° (fully open) to 90° (fully closed). The other

type of damper was an opposed-blade damper (Figure 3-7 (b)), which had an operating range from 0° (fully open) to 45° (fully closed). Manufacturers A and B used butterfly dampers while manufacturer C employed the opposed-blade design. The damper was attached to a single rotational shaft that are shown in Figure 3-8, and a specific damper angle was achieved by using a damper actuator with 0-10 VDC control voltage.

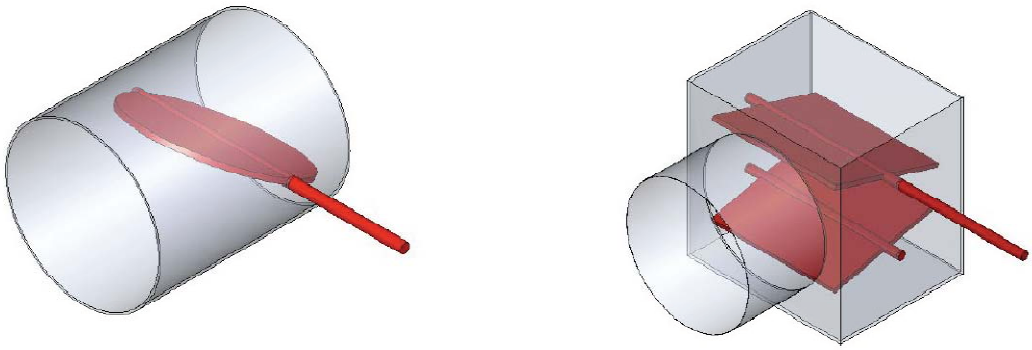

(a) (b)

Fig. 3-7 (a) Butterfly Damper (b) Opposed-blade Damper

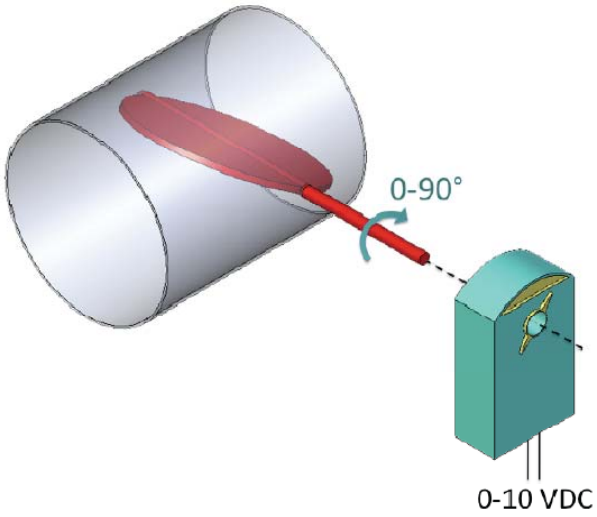

Fig. 3-8 Damper and Actuator

Manufacturer C installed a diffuser after the damper to smooth the airflow into the terminal unit. In this case, the diffuser was a piece of perforated sheet metal placed orthogonal to the inlet. The diffuser is shown in Figure 3-9.

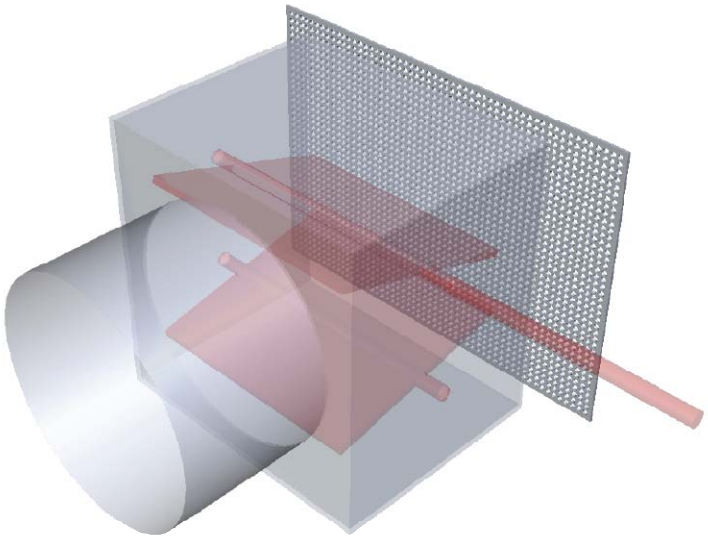

Fig. 3-9 Perforated Sheet Metal Diffuser

The key component of a FPTU was the fan inside the terminal unit. Typically, it was a single width centrifugal fan with forward curve blades, which is shown in Figure 3-10. Depending on the size and working range, the fan came with several capacities. All the fans in this study were supplied with single phase 277 VAC power. Table 3-3 shows the fan capacities of each terminal unit.

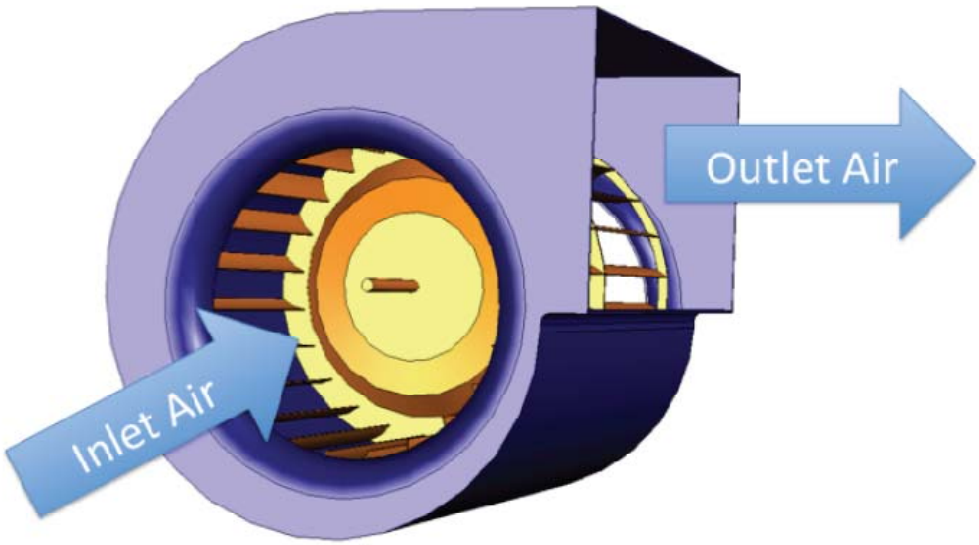

Fig. 3-10 Single Width, Forward Curve Centrifugal Fan

All the fans in this study were equipped with ECM motors, which were an ultra high efficiency programmable brushless DC motor utilizing a permanent magnet rotor and a built-in inverter. An internal microcontroller sequentially connected a DC current to magnets, causing the motor to turn. The timing, duration and firing order of these current pulses controlled the motor output and rotational direction. The ECM motor is illustrated in Figure 3-11.

Table 3-3 Summary of the Fan Power

FPTU	Rated Fan Power hp (kw)
S8A	1/2 (0.37)
S8B	1/2 (0.37)
S8C_M1	1/2 (0.37)
S8C_M2	1/2 (0.37)
S12A	1 (0.75)
S12B	1/2 (0.37)
S12C_M1	3/4 (0.56)
S12C_M2	3/4 (0.56)

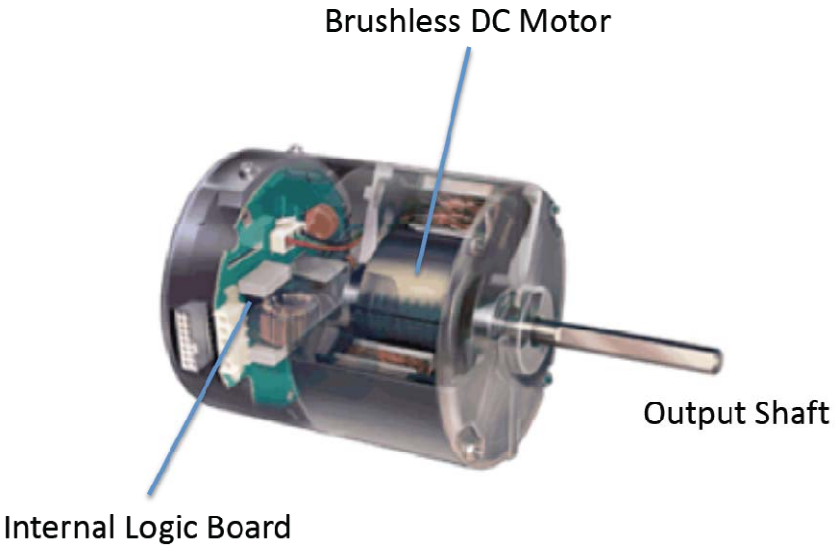

Fig. 3-11 ECM Motor

3.2. Data Acquisition

Measurements of several pressures were required, including upstream, downstream static pressure, discharge pressure, differential pressure as well as temperature and relative humidity (RH). All pressure measurements were made by using Dwyer 616 series differential pressure transmitter connected to pressure taps with plastic tubing. The transmitter features $\pm 0.25\%$ accuracy in several factories calibrated range. Because various pressure measurements in different ranges were required, several pressure transmitters with different ranges were used. Table 3-4 shows the operating range of the pressure transmitters.

The output of the pressure transmitters was a current that ranged from 4 to 20 mA, which was proportional to the measured pressure. Terminating resistors were employed to convert the output current into a voltage that could be measured by the data acquisition system. Temperature and RH were measured in a similar way. These measurements were made by using a dual purpose probe (Rotronic L-Series) with an accuracy of $\pm 0.9°F$ temperature and $\pm 3\%$ RH accuracy.

Table 3-4 Pressure Transmitter Operating Range

Pressure Location	Transmitter Model	Working Range inches w.g. (Pa)
Inlet flow chamber differential pressure	616-2	0-6 (0-1500)
Inlet flow chamber static pressure	616-3	0-10 (0-2500)
Upstream static pressure	616-0	0-2 (0-500)
Downstream static pressure	616-0	0-2 (0-500)
Outlet flow chamber differential pressure	616-2	0-6 (1500)
Outlet flow chamber static pressure	616-3	0-10 (2500)
Internal Pressure	616-0	0-2 (500)

The computer data acquisition system had two internal and two external DAQ boards from National Instruments. All pressure measurements, data were stored by using a 16-bit, 8-channel differential input NI-SC2040 external board connected to an NI-6034 internal PCI board. Temperature and RH were recorded by using an NI-6024E internal PCI board in conjunction with a CB-68LP external terminal block. This block allowed for

12-bit resolution on inputs and provided two 0-10 VDC analog outputs, which were used to control the primary and assist blowers connected to airflow chambers. A custom Visual Basic program was developed as the user interface for the National Instruments data acquisition (DAQ) equipment. This program was able to automatically collect data from all the tests and output those data into a single spreadsheet for ease of analysis.

3.3. Power Equipment

A Fluke 435 power quality analyzer was used to take the fan power measurements, including any internal component of the ECM motor setup and controller, which was powered by a main supply line using a transformer to convert the 277 VAC to 24 VAC. For those fans whose current was below 5A, the Fluke i5s current probes was used. However, if the current was above 5A but below 10A, the Fluke i1000s current probe was used. The simultaneous measured and recorded electrical data included voltage, current, real power, apparent power, power factor, THD, and up to the 25th harmonic of voltage, current, and power. Current probes were placed on the main power and neutral lines, while voltage probes were placed on the main, neutral, and ground lines. The data from several tests were stored in the analyzer's internal flash memory, and then downloaded to the computer via a USB interface. Fluke Power Log software was used to operate the USB interfaces. Figure 3-12 shows the power measurement system.

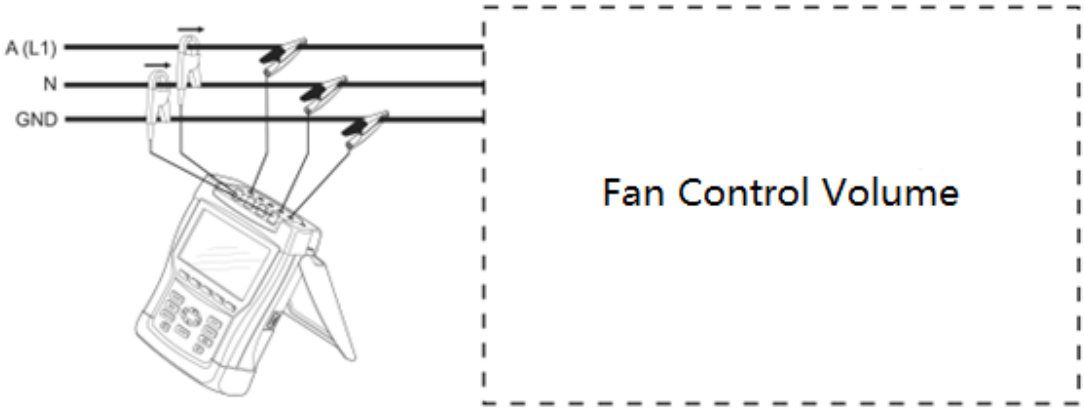

Fig. 3-12 Setup of Power Measurement

CHAPTER IV

EXPERIMENTAL PROCEDURE

Experimental data were collected from three different manufacturers for eight series fan-powered VAV terminal units with ECM motors. Both airflow and power measurements were made by using the equipment described in the previous chapter, the test procedures, data acquisition system and method of statistical data analysis applied to the raw data to get the semi-empirical models were explained in this chapter.

4.1. Method of Experimentation

This study modified the previous basic factorial test matrix used by Cramlet (2008) and Edmondson (2009) that simulated the performance of FPTUs in their designed working range. Several independent variables were chosen to characterize the performance of the terminal units. The ranges and levels were chosen to obtain an accurate representation of the performance for typical operating conditions in the field.

Two kinds of dampers were tested: the butterfly damper and the opposed-blade damper. Each damper was controlled by an actuator controlled by a 0-10 VDC control voltage, which was generated by a regulated DC power supply. This actuator changed its position from 0° (fully open) to fully closed position. The behavior of the actuator was a function of control voltage. The damper working range was equally divided into 11 test

points, and then the control voltage was also divided into 11 test points. The butterfly damper was fully open at 0 VDC and fully closed at 10 VDC. The opposed blade damper was fully open at 0 VDC and fully closed at 5 VDC. Table 4-1 shows a summary of damper settings.

Table 4-1 Summary of Damper Settings

Damper Type	Working Range (Degree)	Test Points	Corresponding Angle Increment (Degree)	Corresponding Voltage Increment (V)	Test Settings (V)
Butterfly	0-90	11	9	1	0, 1, 2, 3, 4, 5, 6, 7, 8, 9, 10
Opposed-blade	0-45	11	5	0.5	0, 0.5, 1, 1.5, 2, 2.5, 3, 3.5, 4, 4.5, 5

Each manufacturer used a different method to operate their ECM controller. These controllers were used to vary the speed and torque of the fan motor. Three types of controllers were provided. Manufacturer A provided a controller that was set to a value

between 0 and 100, so the settings of 20, 40, 60, 80 and 100 were used. Manufacture B provided a controller that was set using a 2-10 VDC signal, so the settings were 4 volts DC, 6 volts DC, 8 volts DC and 10 volts DC. Manufacturer C provided a controller that was set using 0-10 VDC signal, so settings were 2 VDC, 4 VDC, 6 VDC, 8 VDC and 10 VDC. For series units, testing without fan operation was impractical because the fan had to keep working to supply air to the conditioned zones. It was noticed that some fan capacities under certain ECM settings were out of the recommended operating range from the manufacturers. Those data were not used in developing the model. Table 4-2 shows the summary of ECM settings.

Table 4-2 Summary of Control Methods for ECM Controllers

Manufacturer	Control Method	Test Point	ECM Settings
A	0-100	5	20, 40, 60, 80 and 100
B	2-10 VDC	4	4, 6, 8, 10 VDC
C	0-10 VDC	5	2, 4, 6, 8, 10 VDC

Both upstream and discharge static pressures depended on the conditions inside a building and they were collected due to their significant effect on the performance of terminal units. The upstream and the discharge static pressures were adjusted by varying the speed of the primary and assist blowers attached to the airflow chambers. Control of both blowers was facilitated by a Visual Basic data acquisition program. Upstream static pressure was varied from 0.25 inches w.g. (62 Pa) to 1.5 inches w.g. (373 Pa) for 8″ (0.2 m) terminal units. However, after evaluating the data recorded by Edmondson, it was found that some target points could not be reached for the 12″ (0.3 m) terminal unit at either the high upstream static pressure settings or at the wild open damper settings. As a result, another three upstream settings were added to the 12'' (0.3 m) terminal unit test matrix to allow the use of Edmondson's data to verify the validity of the model. Those three settings were 0.05, 0.1 and 0.2 inches w.g.. The test matrix of upstream static pressure is shown in Table 4-3.

Table 4-3 Summary of Upstream Static Pressure Settings

Terminal Type inches (m)	Independent Variable	Test Points	Test Settings inches w.g. (Pa)
12 (0.3048)	Upstream Static Pressure, $P_{upstream}$	9	0.05 (12), 0.1 (25), 0.2 (50), 0.25 (62), 0.5 (124), 0.75 (187), 1 (250), 1.25 (311) & 1.5 (373)
8 (0.2032)		6	0.25 (62), 0.5 (124), 0.75 (187), 1 (250), 1.25 (311) & 1.5 (373)

Internal pressure of the FPTU was a new independent variable in this study. Neither Cramlet (2008) nor Edmondson (2009) measured this pressure because of their approaches to model the FPTUs as a "black box" resulted in focus only on measurements at the periphery of the FPTUs. Further, a typical FPTU did not have pressure taps to allow measurement of the internal pressure. However, it was necessary to make the measurements of the internal pressure in order to eliminate the offset in previous primary airflow model. The target internal pressure was achieved by adjusting the assist blower and varied from 0.01 inches w.g. to 0.2 inches w.g.. Table 4-4 is a summary of internal pressure settings. Figure 4-1 shows the upstream, downstream and internal pressure measurement points.

Table 4-4 Summary of Internal Pressure Settings

Independent Variable	Test Points	Test Range inches w.g. (Pa)
Internal Pressure, $P_{internal}$	20	0.01-0.2 (2.5-50)

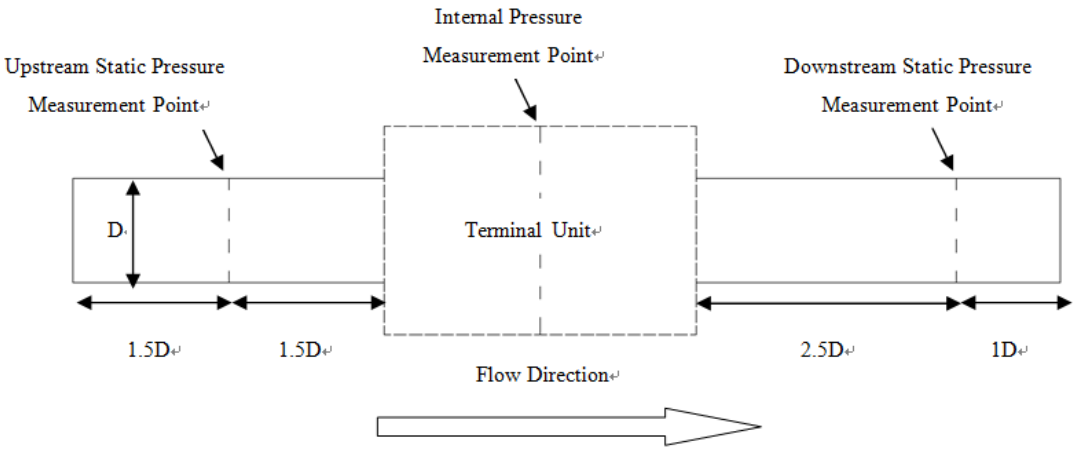

Fig. 4-1 Pressure Measurement Points Locations

The discharge pressure was determined by the fan operating range. Based on the information from each manufacturer, appropriate ranges of test settings were chosen. Table 4-5 shows the discharge pressure settings.

Table 4-5 Summary of Discharge Pressure Settings

Manufacture	Independent Variable	Test Points	Test Settings inches w.g. (Pa)
A	Discharge Pressure, $P_{discharge}$	6	0.1 (25), 0.2 (50), 0.3 (75), 0.4 (100), 0.5 (125) & 0.6 (150)
B		5	0.1 (25), 0.2 (50), 0.3 (75), 0.4 (100) & 0.5 (125)
C		6	0.0 (0), 0.1 (25), 0.2 (50), 0.3 (75), 0.4 (100), 0.5 (125)

4.2. Environmental Considerations

All the experimental data were collected in the Energy System Laboratory at the Riverside Campus of Texas A&M University. The test setup was in an open, high-bay laboratory which equipped with heating and cooling devices. Some of the tests were conducted during the time when either heating or cooling was required.

This study used unconditioned laboratory air instead of precisely controlled temperature air because the flow performance of the series FPTUs was the primary issue. Temperature and RH were recorded by using method described in the previous chapter. In addition, the assumption was made that the temperature and RH distribution was uniform throughout the test setup, even though a temperature rise as much as 5°F could be

generated when air went through the fans. However this temperature rise had little effect on the test results. For example, from the psychometric chart, the density of air at 70°F (21.1°C) and 60% RH is 0.0738lb/ft^3 (1.1822kg/m^3). While the density of air at 75°F (23.9°C) and 50% RH is 0.0731lb/ft^3 (1.1711 kg/m^3). This 5°F temperature rise results in a density difference of less than 1% which shows the effect of temperature rise because of fan operation can be ignored.

To provide measurement of the airflow temperature, RH and pressures were collected in the airflow chambers by using the ANSI/ASHRAE Standard 120. In order to compensate for the difference in air density due to various weather conditions on different test days and also to make it easier to do a direct comparison of test results, all of the volumetric airflow was adjusted to a standardized airflow with a reference air density at 0.075lb/ft^3 (1.2015 kg/m^3).

4.3. Statistical Analysis

SigmaStat software was used to provide statistical data analysis. The goal of the statistical analysis is to develop a simple, intuitive and accurate mathematical model of series fan-powered VAV terminal units to predict fan airflow, primary airflow, plenum airflow and fan power consumption.

Techniques used to generate models were the same as used in previous VAV research done by Cramlet (2008) and Edmondson (2009). Upstream and downstream

static pressure, discharge pressure, temperature, internal pressure, damper and ECM settings, as well as terminal unit dimension were collected to perform the linear and non-linear regressions.

The model's accuracy was quantified by R^2, which varies between 0 and 1. In order to provide a measurement of how well the statistical model represented the variance in the real data. Larger R^2 values (close to 1) indicated that the correlation was a good description of the relation between the independent and dependent variables. R^2 value of 1 meant that the models fit the data perfectly.

CHAPTER V

PRIMARY AIRFLOW MODEL

The purpose of the primary airflow model was to predict the amount of air through the damper at various differential pressures across the damper for different damper position. Experimental data were collected on four dampers. Two different types of damper were evaluated to develop a model to describe the characteristics of airflow and flow resistance through these damper. This chapter discusses the results of the experiments and the models developed for primary airflow and flow resistance through the dampers.

5.1. Primary Airflow Model

Primary airflow was modeled as a function of differential pressure across the damper and the damper position. In this study, the damper was taken out of the terminal unit and tested as an individual component. Four dampers were tested separately. They were grouped by size (8'' and 12'') and type (butterfly and opposed-blade). For example, BF8 was the name of a 8'' butterfly damper while OB12 represented an 12'' opposed-blade damper.

Dampers were connected to the inlet flow chamber via an upstream air duct. Airstream generated by the primary blower went through the inlet flow chamber and

dampers, and then was discharged freely into the environment. Volume flow rate, pressures and temperature were recorded. The upstream static pressure was used in conjunction with the environmental pressure to calculate the differential pressure P_d. Because the airstream was discharged freely into the environment, the environmental pressure was considered as zero. The test rig is illustrated in Figure 5-1.

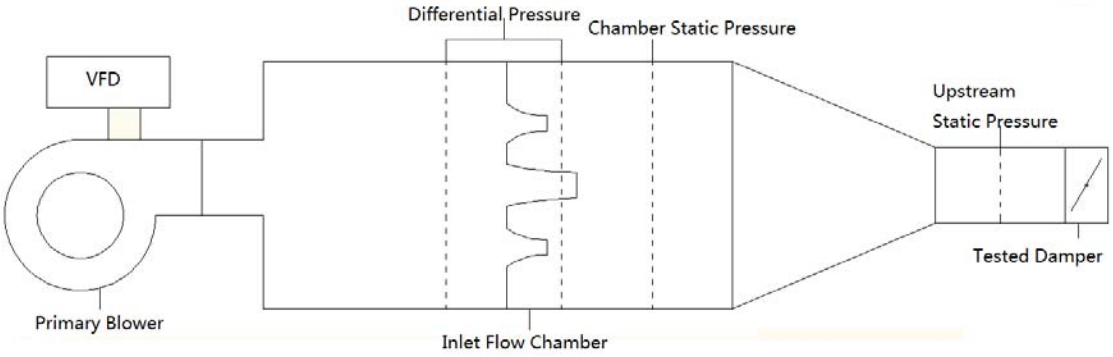

Fig. 5-1 Test Rig for Primary Airflow

There are two reasons for this test method. First, it was easier to reach the target differential pressure by controlling one static pressure, because the environmental pressure was set to zero all the time, then only upstream static pressure needed to be adjusted to reach the designed test condition. Second, taking the damper out of the terminal unit eliminated the effects from plenum and fan airflow on primary airflow.

Damper position was described by damper angle which was expressed in number of degrees from the fully open position. Different manufacturers used either butterfly or opposed-blade configurations. During the tests both types of dampers were set at 0, 10%, 20%, 30%, 40%, 50%, 60%, 70%, 80%, 90% and 100% open. Manufacturer C employed the opposed-blade design for both brands of motors and 0° being a fully open condition while 45° being a fully closed condition. Manufacturer A and B used a butterfly damper. In this case, 0° indicated a fully open condition while 90° represents the fully closed condition.

A 10 VDC signal was used to control damper angular movement with linear relationship existing between damper angle and control voltage. This relationship is shown by Equation (5-1). The variable α is the damper angle and variable V is the damper control voltage.

$$\alpha=9\times V \tag{5-1}$$

Each damper controlled the airflow rate by varying the area that airstream went through. The flow-through area at certain damper setting was considered as an important variable in developing a model applicable to all of the four dampers.

A non-dimensional variable γ was invented to describe this physical property for both types of dampers. The variable γ was defined in Equation (5-2). The variable A_d is the flow-through area of the damper at certain voltage and the variable A_{d0} is the flow-through area of the damper at fully open position.

$$\gamma=A_d/A_{d0} \tag{5-2}$$

The variable γ was a function of damper angle. For butterfly damper, it could be calculated according to Equation (5-3).

$$\gamma=1-\sin\alpha \tag{5-3}$$

For opposed-blade damper, it could be calculated by applying Equation (5-4)

$$\gamma=1-\sqrt{2}\times\sin\alpha \tag{5-4}$$

Tables 5-1 and 5-2 show the variations in γ against damper control voltage for butterfly and opposed-blade dampers, respectively. As control voltage increased, the damper angle increased linearly and γ decreased from 1 to 0.

Table 5-1 Damper Control Voltage vs. γ for Butterfly Damper

Control Voltage (V)	Damper Angle (Degree)	Variable γ
0	0	1
1	9	0.8436
2	18	0.6910
3	27	0.5460
4	36	0.4122
5	45	0.2929
6	54	0.1910
7	63	0.1090
8	72	0.0490
9	81	0.0123
10	90	0

Table 5-2 Damper Control Voltage vs. γ for Opposed-blade Damper

Control Voltage (V)	Damper Angle (Degree)	Variable γ
0	0	1
0.5	4.5	0.8890
1	9	0.7788
1.5	13.5	0.6699
2	18	0.5630
2.5	22.5	0.4588
3	27	0.3580
3.5	31.5	0.2611
4	36	0.1687
4.5	40.5	0.0815
5	45	0

Figures 5-2 to 5-5 show the primary airflow plotted against damper position for the BF8, OB8, BF12 and OB12, respectively. For the BF12 and OB12, some data were missing for the first two damper settings at higher differential pressure settings. The reason was that the blower was not capable of providing adequate amounts of air to reach the target static pressure settings, especially for the first two damper settings whose flow resistance was relatively small. The curves in those plots were generated by the model discussed later in this section. A full set of results were shown in the Appendix A.

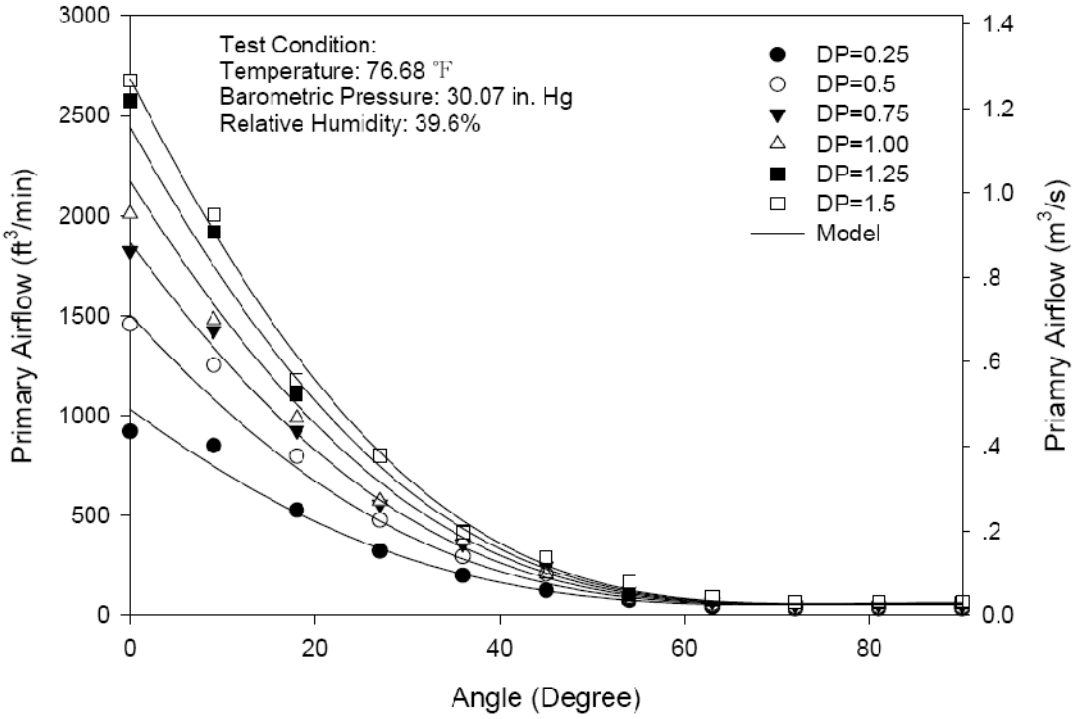

Fig. 5-2 Primary Airflow for BF8

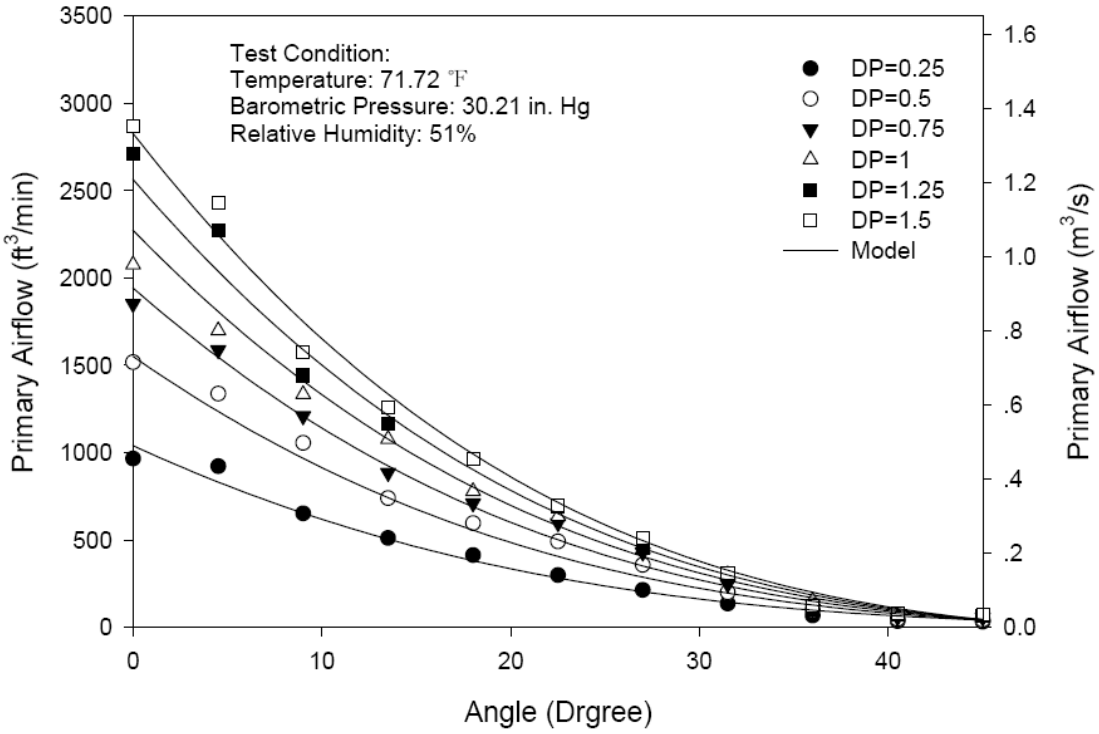

Fig. 5-3 Primary Airflow for OB8

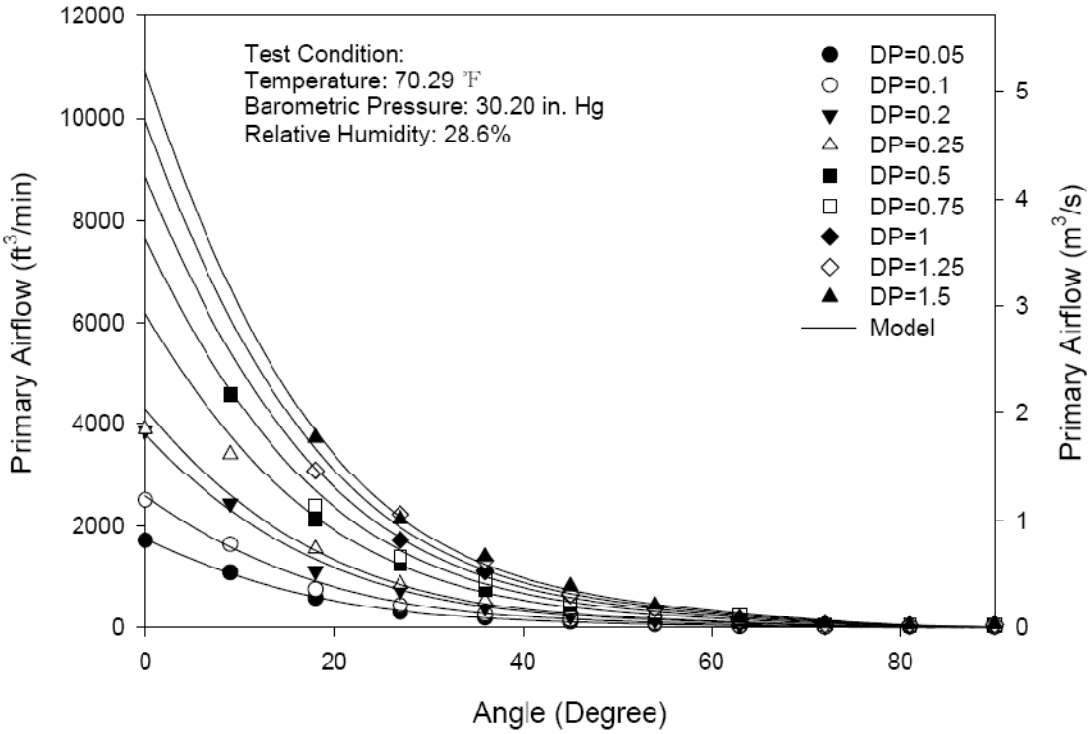

Fig. 5-4 Primary Airflow for BF12

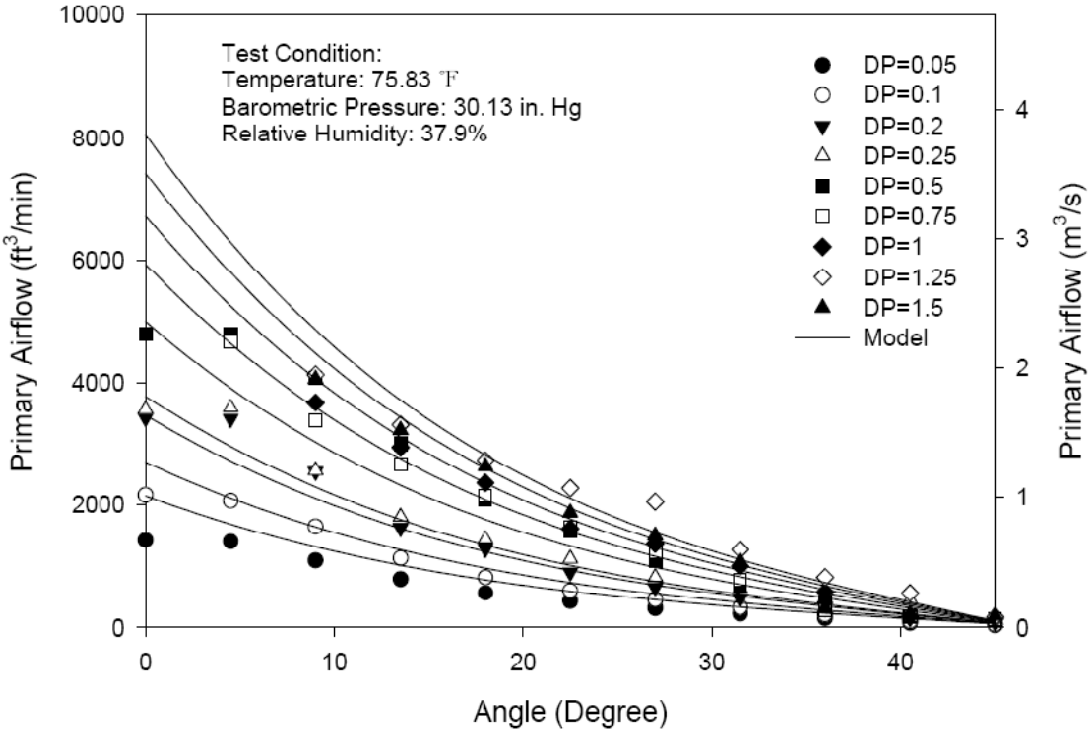

Fig. 5-5 Primary Airflow for OB12

The correlation fitted the experimental data was shown in Equation (5-5). This form was first developed by Furr (2006) who found that the primary airflow delivered to the terminal unit was proportional to the square root of the differential pressure across the terminal unit at given damper setting. Some necessary modifications were made to improve this model. First, the upstream and internal static pressures were used to calculate the differential pressure across the damper instead of using downstream static pressure to calculate the differential pressure across the terminal unit. One problem caused by using downstream static pressure was that an offset of 0.27 was required to maintain the term

positive under square root. By using internal pressure, this offset was no longer necessary. Second, the non-dimensional variable γ was employed to represent damper position. Since the operating ranges of butterfly and opposed-blade damper were different, it was convenient to a use non-dimensional variable to describe the performance of both types of dampers. The coefficients as well as R^2 value for this model are given in Table 5-3.

$$Q_{primary}=\left(a_1+b_1\times\sqrt{P_d}\right)\times(1+c_1\times\gamma+d_1\times\gamma^2+e_1\times\gamma^3)+f_1 \quad (5\text{-}5)$$

where P_d is the differential pressure across the damper.

Table 5-3 Summary of Coefficients and R^2Value for the Primary Airflow Model

Type	Diameter	a_1	b_1	c_1	d_1	e_1	f_1	R^2
BF	8''	-1.084	15.673	-14.111	172.316	-13.670	48.109	0.993
	12''	-0.634	19.091	130.158	-245.942	596.077	9.671	0.980
OB	8''	-1.728	19.886	29.873	59.815	33.041	28.665	0.990
	12''	5.394	41.282	66.313	-17.683	93.487	47.765	0.948

The lowest R^2 value was 0.948 for OB12. Several difficulties were met in developing this model. One was that some data were missing because the primary blower was not able to provide adequate airflow to maintain target pressures. Another difficulty was the large measurement error was generated when the damper setting was near the fully closed position. At those positions, only a small amount of air was allowed to go

through the chamber, and as a result the differential pressure generated by the airflow was too low to be accurately measured.

It was found that no damper was able to maintain a perfectly seal. Even the damper position was set at fully closed position there was still a small amount of air through the damper. This leakage was affected by the differential pressure across the damper. As the differential pressure increased, the leakage raised. The term $a_1+b_1\times\sqrt{P_d}+f_1$ was used to describe the air leakage for each damper used in this study.

5.2. Flow Resistance through Damper

In this study, a damper was used to control the primary airflow. An ideal damper would have no resistance to airflow when wide open, but would then supply a substantial amount of resistance upon partial closure, thus reducing the air flow rate. The pressure loss coefficient k was defined in Equations (5-6) and (5-7)

$$\Delta P_T=k\cdot P_V \tag{5-6}$$

$$\Delta P_T=k\rho u^2/2 \tag{5-7}$$

These equations can be related to volume flow rate entering the FPTUs by Equations (5-8) and (5-9)

$$u=\frac{\dot{Q}}{A} \tag{5-8}$$

$$\Delta P_T=\frac{\rho}{2}\cdot\left(\frac{\dot{Q}}{A}\right)^2 k \tag{5-9}$$

Total pressure was an appropriate parameter to use in this study, becauses a number of simulation programs, such as HVACSIM+ and TRNSYS, use total pressure difference as a key variable in ductwork design and friction loss calculations. To relate pressure loss coefficient to volume flow rate entering the terminal unit, the areas were calculated from the inlet diameters for primary airflow. Tests were conducted on four dampers grouped by sizes and types.

The total pressure drop across dampers was divided into static pressure and velocity pressure. The static pressure measurement point located close to the damper and was marked in Figure 5-1. The velocity pressure at the inlet was calculated on the basis of volume flow rate through the duct and the inlet area. The static pressure and velocity pressures were added to obtain the total pressure drop at the inlet.

The airflow was set at a face velocity of 3900fpm with damper fully open, and then the damper was closed in 9-degree increment until closed. Because the operating range of the pressure transmitter, which was used to measure the upstream static pressure, was from 0 to 2 in w.g., no accurate measurement could be made if the static pressure drop across the damper was out of this operating range. Therefore the test was terminated when the static pressure drop across the damper exceeded 2 in. w.g. The data collected were used to calculate flow resistances as well as pressure loss coefficients. Each of the tests

yielded an Excel spreadsheet of data and results. A sample data and result spreadsheet for OB8 was shown in Figure 5-6. The bold fonts indicated the input data.

5.2.1. Butterfly Damper

Figure 5-7 shows the percentage of airflow plotted against damper position of BF8 and BF12. It was noted that the primary airflow percentages did not go to zero in Figure 5-7. The reason for this was because the test was terminated when the pressure drop across the damper exceeded 2 inches w.g.

Two things can be concluded. First, it is obvious that both of them work in a non-linear way to control primary airflow. Though the damper varied from 100% to 90% open in the first damper setting, the airflow was maintained almost the same. When the damper dropped to 40% open, the decrease in airflow trended to be level. Only in a certain range is the behavior of butterfly damper approximately linear. Second, in the damper settings from 80% to 30% open, the percentage of airflow was sensitive to damper position. A 9-degree change in damper position could lead to a variation in airflow up to 15%.

OB8

Test Seting No.	Nozzle Combination (in)	Blower Setting (V)
4	3+4+6	6.00

Test Points (Damper Voltage)	Damper Angle α (Degree)	Damper Angle α (Radiant)	γ (non-dimensional)
0.00	0.00	0.00	1.00
0.50	4.50	0.08	0.89
1.00	9.00	0.16	0.78
1.50	13.50	0.24	0.67
2.00	18.00	0.31	0.56
2.50	22.50	0.39	0.46
3.00	27.00	0.47	0.36
3.50	31.50	0.55	0.26
4.00			
4.50			
5.00			

Test Points (Damper Voltage)	Volume Flow Rate Q (CFM)	Percent of Max Flow (%)
0.00	**1,384.10**	100.00
0.50	**1,381.70**	99.83
1.00	**1,348.60**	97.44
1.50	**1,258.70**	90.94
2.00	**1,177.00**	85.04
2.50	**1,121.20**	81.01
3.00	**980.10**	70.81
3.50	**888.80**	64.22
4.00		
4.50		
5.00		

Fig. 5-6 Sample Data and Results Spreadsheet for OB8

Test Points (Damper Voltage)	Density ρ (lbm/ft^3)	Area (ft^2)	Upstream Velocity V (ft/s)
0.00	0.07	**0.35**	66.09
0.50	0.07	**0.35**	65.97
1.00	0.07	**0.35**	64.39
1.50	0.07	**0.35**	60.10
2.00	0.07	**0.35**	56.20
2.50	0.07	**0.35**	53.53
3.00	0.07	**0.35**	46.80
3.50	0.07	**0.35**	42.44

Test Points (Damper Voltage)	Upstream Velocity Pressure P (in w.g.)	Upstream Static Pressure Ps (in w.g.)	Total Pressure Loss ΔPt (in w.g.)	Pressure Loss Coefficient k (non-dimensional)
0.00	0.98	**0.34**	1.32	1.35
0.50	0.98	**0.36**	1.33	1.37
1.00	0.93	**0.47**	1.40	1.51
1.50	0.81	**0.81**	1.62	1.99
2.00	0.71	**1.10**	1.81	2.56
2.50	0.64	**1.31**	1.95	3.04
3.00	0.49	**1.83**	2.32	4.72
3.50	0.40	**2.09**	2.49	6.17

Fig. 5-6 Continued

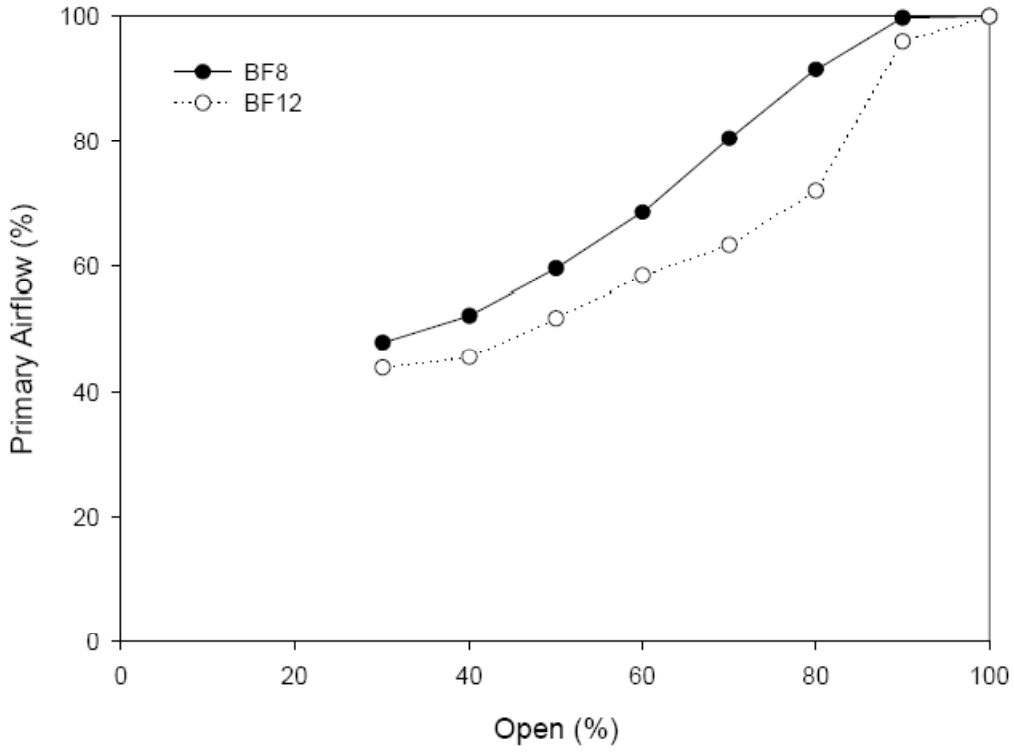

Fig. 5-7 Airflow Percentage for BF8 and BF12

Pressure loss coefficients shown in Figure 5-8 and 5-9 were calculated for both BF8 and BF12 by following the method mentioned above. As expected, when the damper varied from fully open to the fully closed position, the pressure loss coefficient continuously increased. The increment in pressure loss coefficient grew exponential instead of linearly. For the first two damper settings, the pressure loss coefficient did not change much. The same phenomenon was also observed at the last two damper settings. In the range of 18° to 63°, the pressure loss coefficient dramatically increased.

Correlations were developed by using the non-dimensional parameter γ as the main variable. Measured data were fitted by the exponential function shown in Equation (5-10). The coefficients and R^2 values for this model are summarized in Table 5-4 for BF8 and BF12.

$$k=a_5+b_5/(1+e^{\frac{\gamma-d_5}{c_5}}) \quad (5\text{-}10)$$

Table 5-4 Summary of Coefficients and R^2 Values for Butterfly Dampers

Type	Diameter	a_5	b_5	c_5	d_5	R^2
Butterfly	8"	1.2661	18.4167	-0.1587	0.2103	0.999
	12"	0.6124	24.7000	-0.2080	0.2401	0.987

The pressure loss characteristic data from the experiments is shown in Figures 5-8 and 5-9. Curves generated by the correlations in Equation (5-8) for the two dampers are also shown.

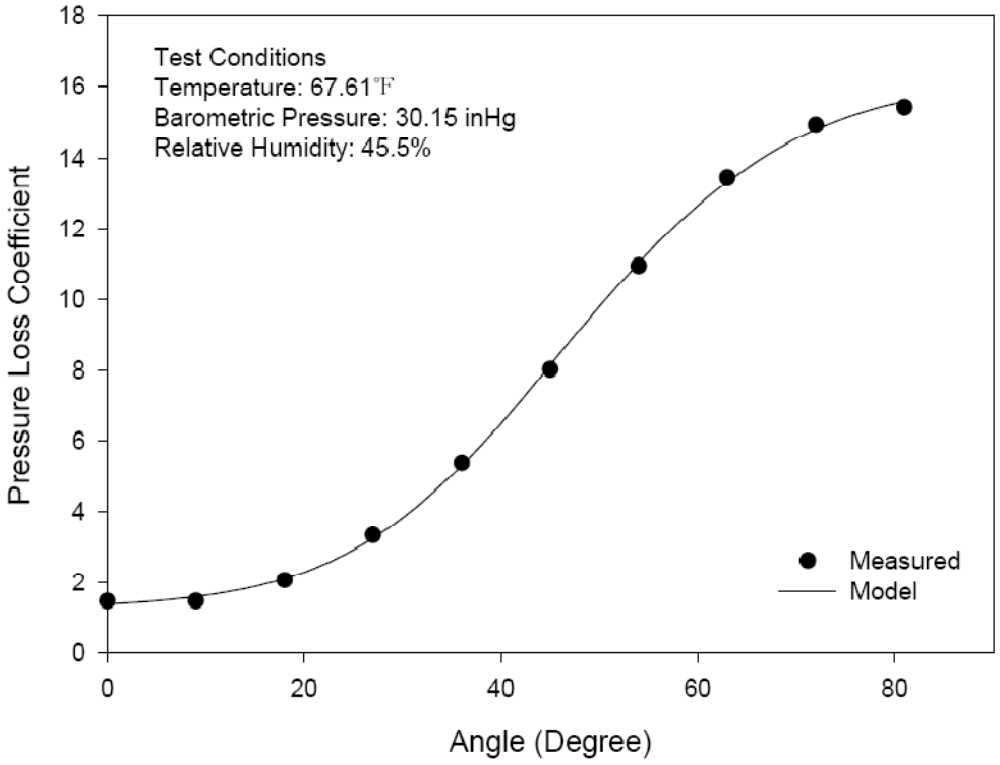

Fig. 5-8 Pressure Loss Coefficients for BF8

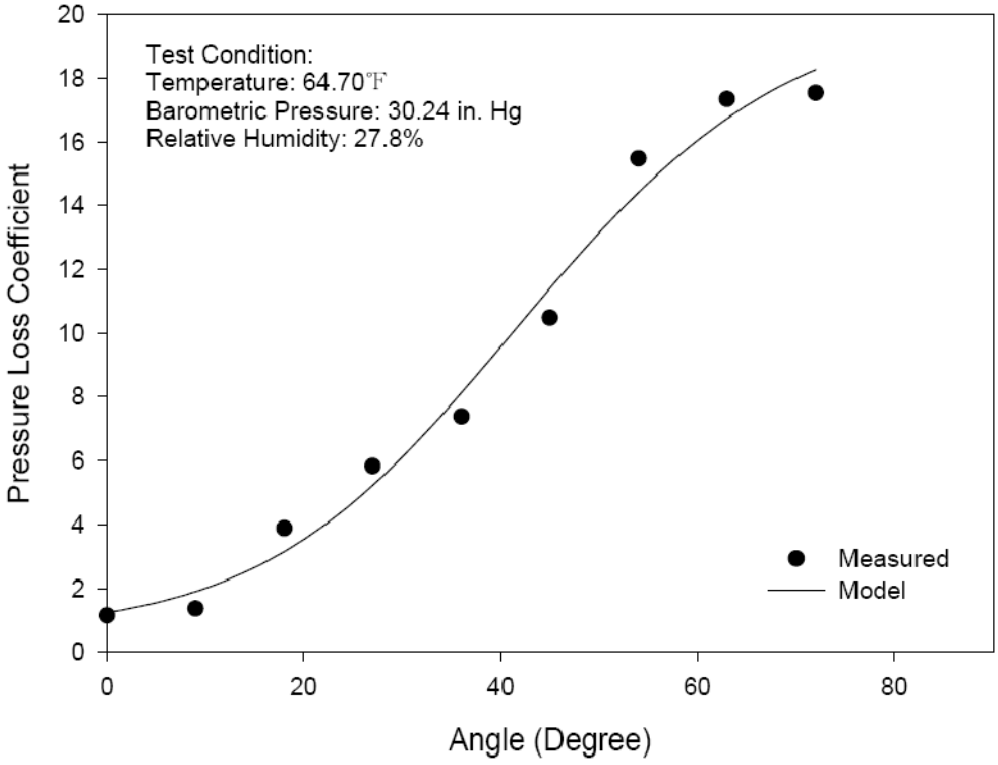

Fig. 5-9 Pressure Loss Coefficients for BF12

5.2.2. Opposed-blade Damper

The results for OB8 and OB12 are shown in Figure 5-10 which shows some common characteristics with BF8 and BF12. Both OB8 and OB12 worked in a non-linear way to control primary airflow. It can be observed that for the first three damper settings, the damper position varied from 100% open to 80% open, but the percentage of airflow was only reduced from 100% to 90%. For this range of damper setting, a big change in damper position would result in a smaller percentage change in airflow. In the range from 70% to 30% open, the airflow decreased rapidly from 90% to 60% for 8'' and 40% for

12’’. In this range a small change in damper position would cause a large change in airflow. Unlike butterfly dampers, the airflow rate continuously reduced and no level trend was observed when the opposed-blade damper was down to 30% open.

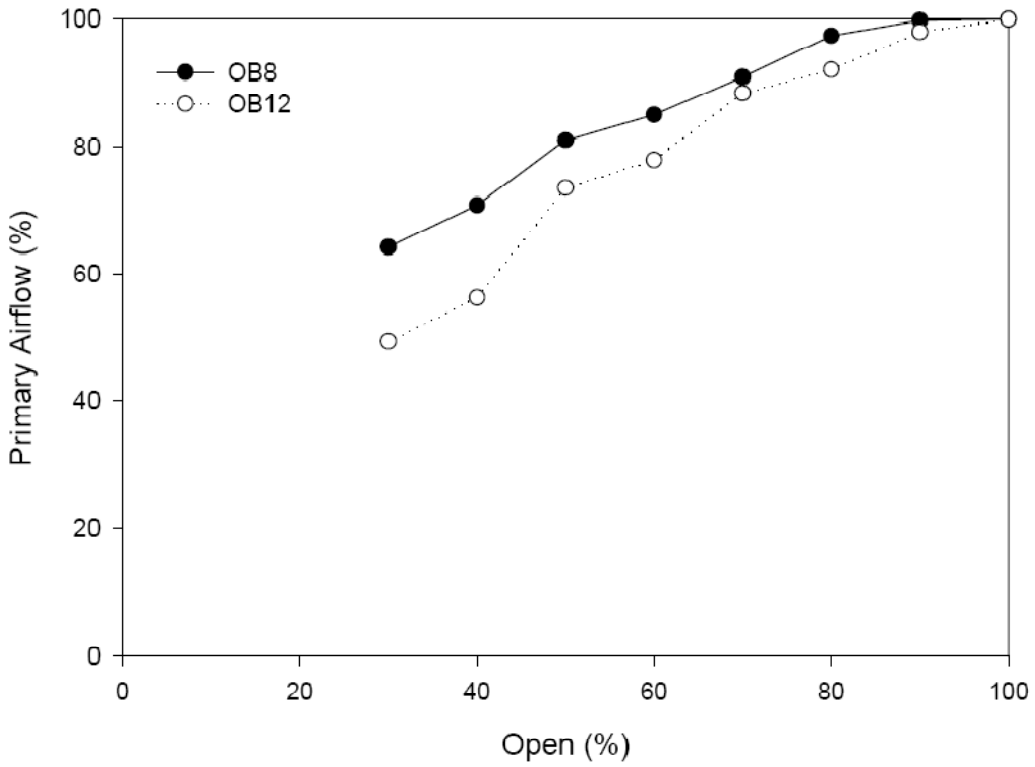

Fig. 5-10 Airflow Percentage for OB8 and OB12

Pressure loss coefficients calculated from experimental data are shown in Figure 5-11 and Figure 5-12 for OB8 and OB12, respectively. Experimental data were fitted into Equation (5-10). Coefficients and R^2 value were generated and are shown in Table 5-5.

Table 5-5 Summary of Coefficients and R^2 Value for Opposed-blade Damper

Type	Diameter	a_5	b_5	c_5	d_5	R^2
Oppose-blade	8''	1.2254	13.2726	-0.1681	0.1752	0.994
	12''	1.4726	15.6177	-0.0850	0.3379	0.992

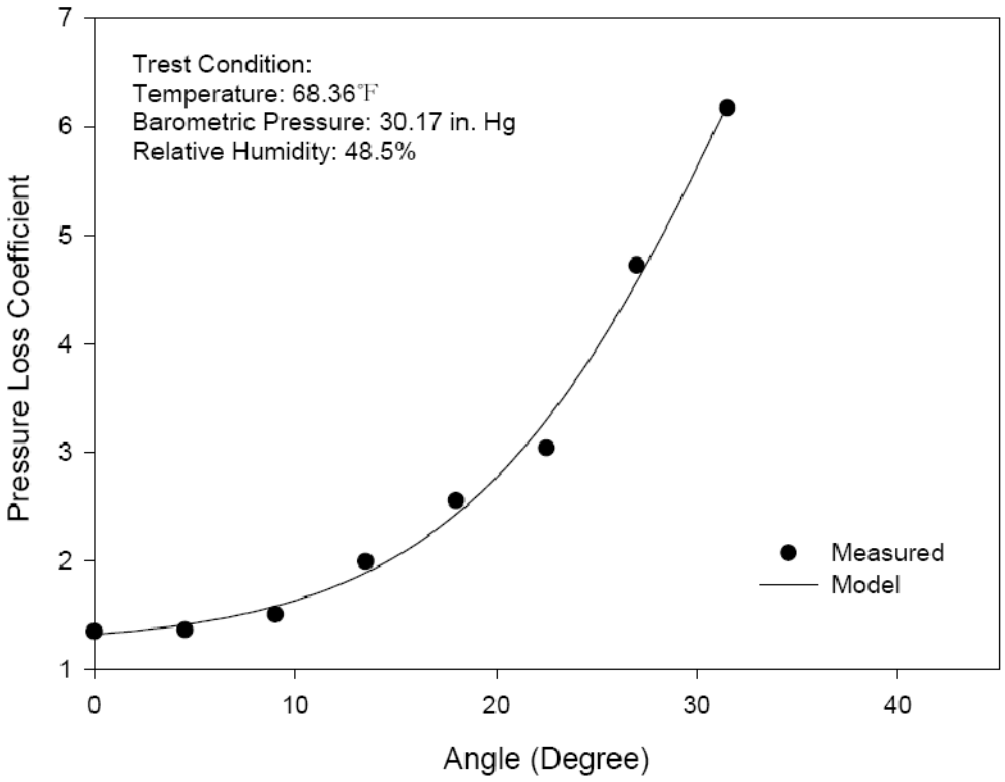

Fig. 5-11 Pressure Loss Coefficients for OB8

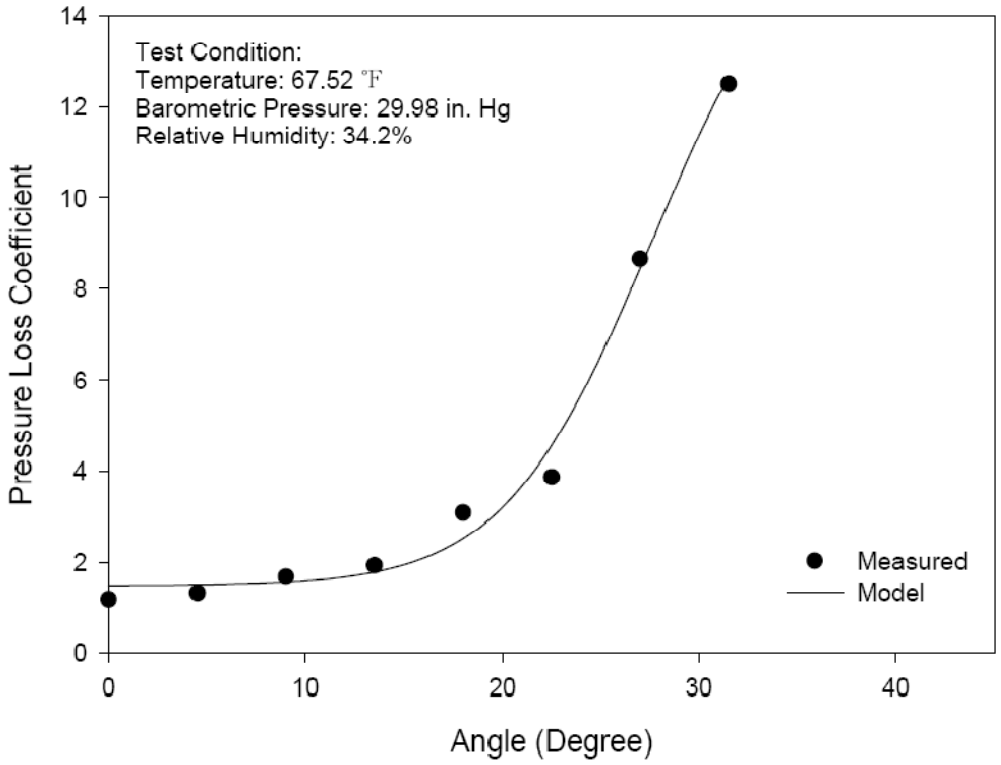

Fig. 5-12 Pressure Loss Coefficients for OB12

All of the four models developed above were applicable in the lower half of the damper's working range of angular movement, up to the first 50% (up to 45° for the butterfly damper and 22.5° for the opposed-blade damper). These models would provide inaccurate results if applied in the higher half of its working range due to the leakage and measurement error which were caused by the small apertures for flow through when the damper was almost fully closed. Further measurements were not easy to make and correlations could not be established for the nearly closed configuration. The dampers were not supposed to operate in the range of near fully closed because it was required by

ASHRAE Standard 62.1 (ASHRAE 2007) to provide a certain amount of fresh air to air-conditioning systems. The characteristics of the damper varied with damper type, size and airflow velocity. The approximately linear relationship of airflow rate to damper position could only be achieved over a part of the working range.

Given this fact, a minimum inlet static pressure was required to get air flowing into series terminal unit. Typically, this value ranged from 0.2 to 0.3 inches w.g. for series FPTUs and 0.5 to 0.6 inches w.g. for parallel FPTUs. Different design configurations in terminal units were responsible for differing requirements in minimum inlet static pressure. For series FPTUs, the fan generated a pressure rise before air entered the conditioned zone. This pressure rise could compensate for the pressure loss for air flow across the damper. While in parallel FPTUs, the fan was used to draw the air from the plenum space and no compensation for pressure loss caused by crossing the damper. The series terminal unit required a smaller inlet static pressure than the parallel design.

CHAPTER VI

FAN AIRFLOW AND POWER CONSUMPTION MODEL

A fan is the most important component in a FPTU. In a series terminal unit, the fan is arranged in line with the primary airstream. These terminal units require the fans to be operating continuously to supply air to the conditioned zone. A fan is the primary power consumption device in a FPTU, and as a result the performances of FPTUs were largely determined by the fans' behavior. In this study, fans were taken out of each terminal unit and tested separately, following the method described in ANSI/ASHRAE Standard 51. Fans were named after each fans corresponding terminal units, for example F_S8A was the fan from the terminal unit S8A, while F_S12C_M2 was the name of the fan from the terminal unit S12C_M2. Figure 6-1 shows the fan test rig used in this study. Pressure, airflow and power data were collected, and then models of airflow and power consumption were developed.

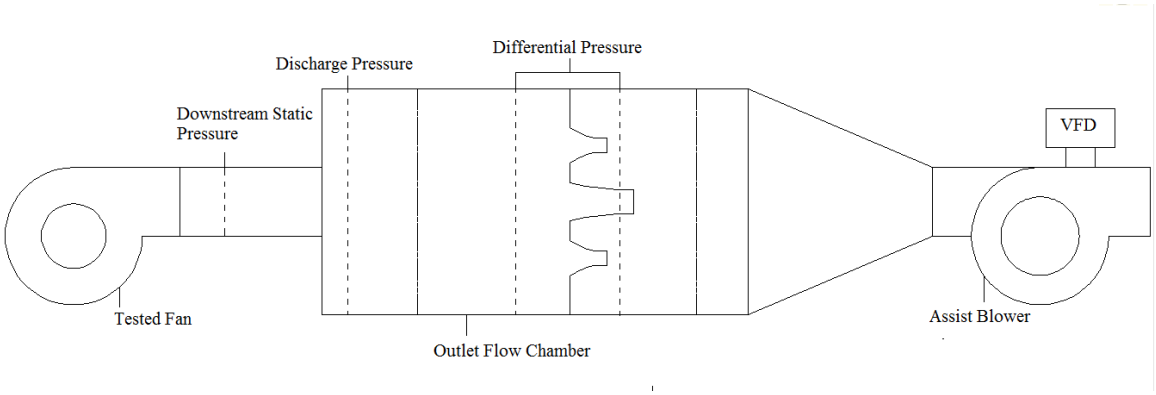

Fig. 6-1 Fan Test Rig

6.1. Fan Airflow

All the tested terminal units were equipped with ECM motors. One distinguishing feature of the ECM motor is that the airflow provided was independent of discharge pressure over a range. A typical PSC fan curve was shown in Figure 6-2 (a) with shaded space representing the valid operation range of the fan. As the discharge pressure increases, the overall airflow decreases. Figure 6-2 (b) shows a typical fan curve for an ECM motor fan with shaded area representing all valid operation points. It can be observed that, unlike a PSC motor, at higher discharge pressures the maximum and minimum airflows maintained the same values as at lower discharge pressures which means the airflow could be set to operate on a horizontal performance line for any points in the shaded area.

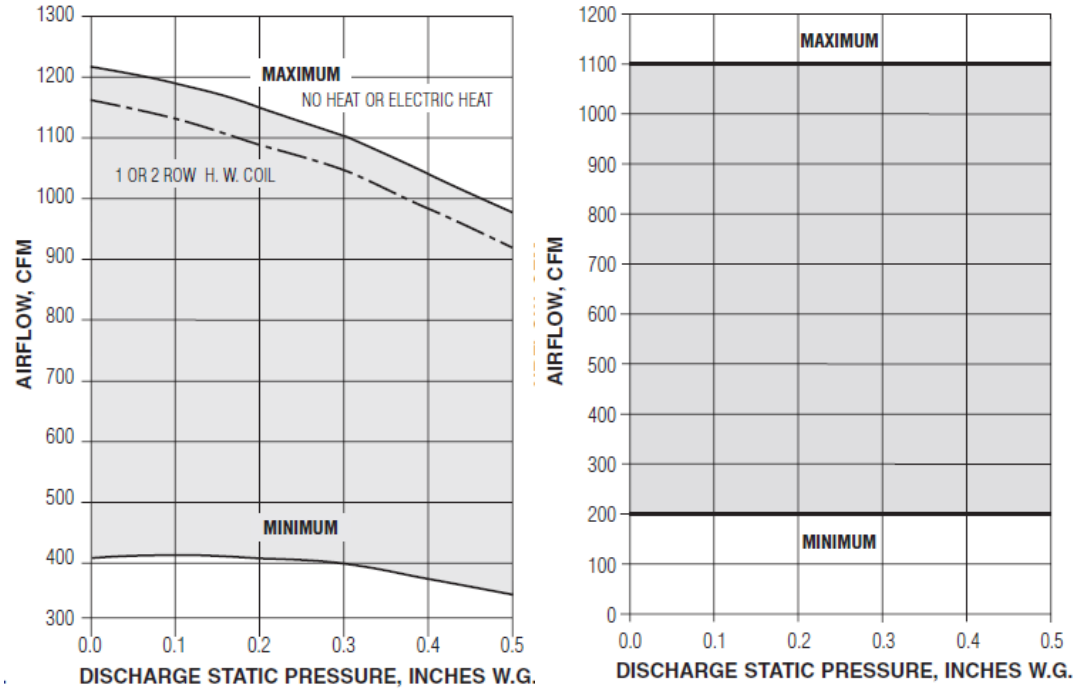

(a) (b)

Fig. 6-2 (a) PSC Fan Curve (b) ECM Fan Curve (Fan airflow capacity plotted against discharge static pressure. Adapted from Nailor Catalog)

In previous studies, Cramlet (2008) and Edmondson (2009) modeled the fan airflow as a function of ECM setting and inlet air velocity pressure of the terminal unit. However, in this study, the fan was taken out of the terminal unit and tested as an individual component and as a result the inlet air velocity pressure of the terminal unit was no longer available as variables. After plotting and analyzing the experimental data, it was found that the fan capacity was mainly a function of ECM settings. This result was similar to the conclusion stated by Cramlet (2008) and Edmondson (2009). One reason for this

similarity was the design of series terminal unit. If the primary airflow was lower than the air being supplied by the terminal unit, additional air would be drawn into the terminal unit from the plenum space. Another reason was that the ECM motor was designed to provide a constant volume flow rate at factory set points. The ECM motor could compensate for any changes in operating conditions, such as variations in external static pressure or induced air conditions. Figure 6-3 shows fan airflow for the F_S8A versus ECM setting. Full results are available in Appendix B.

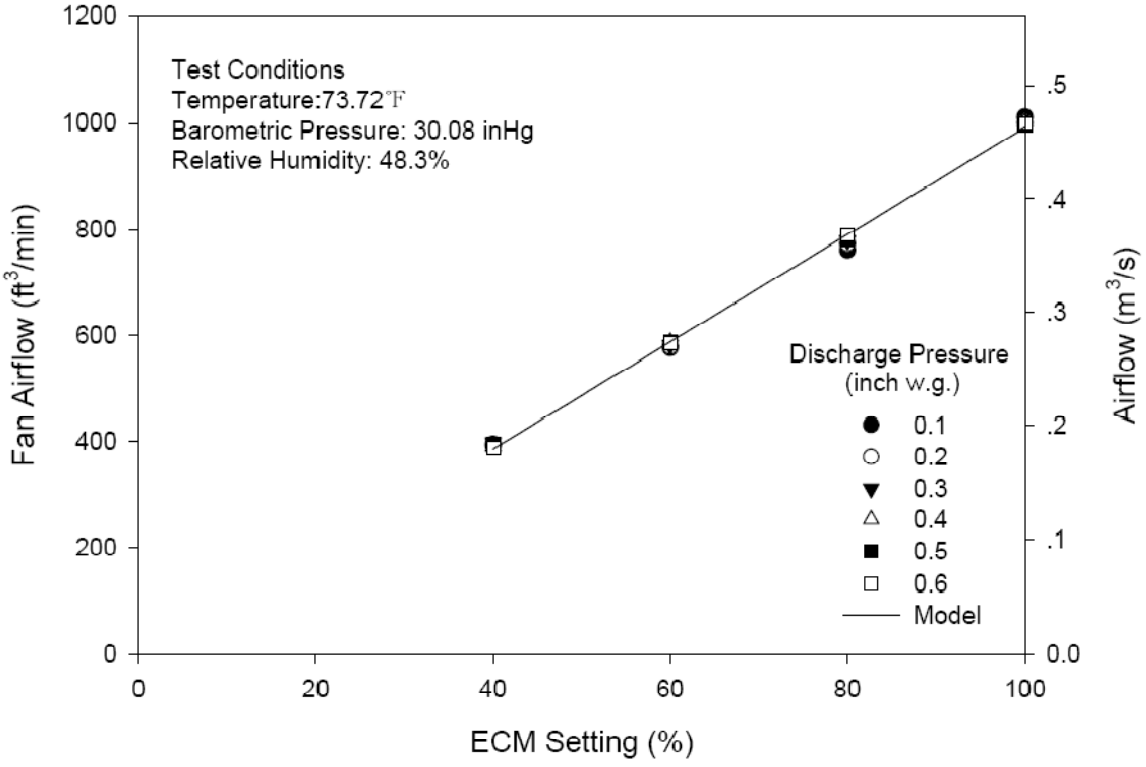

Fig. 6-3 Fan Airflow for F_S8A

It was also observed that the fan airflow showed a slight dependence on discharge static pressure. Figure 6-4 shows fan airflow for F_S12B versus ECM settings. The small variation in data was caused by the variations in discharge pressure.

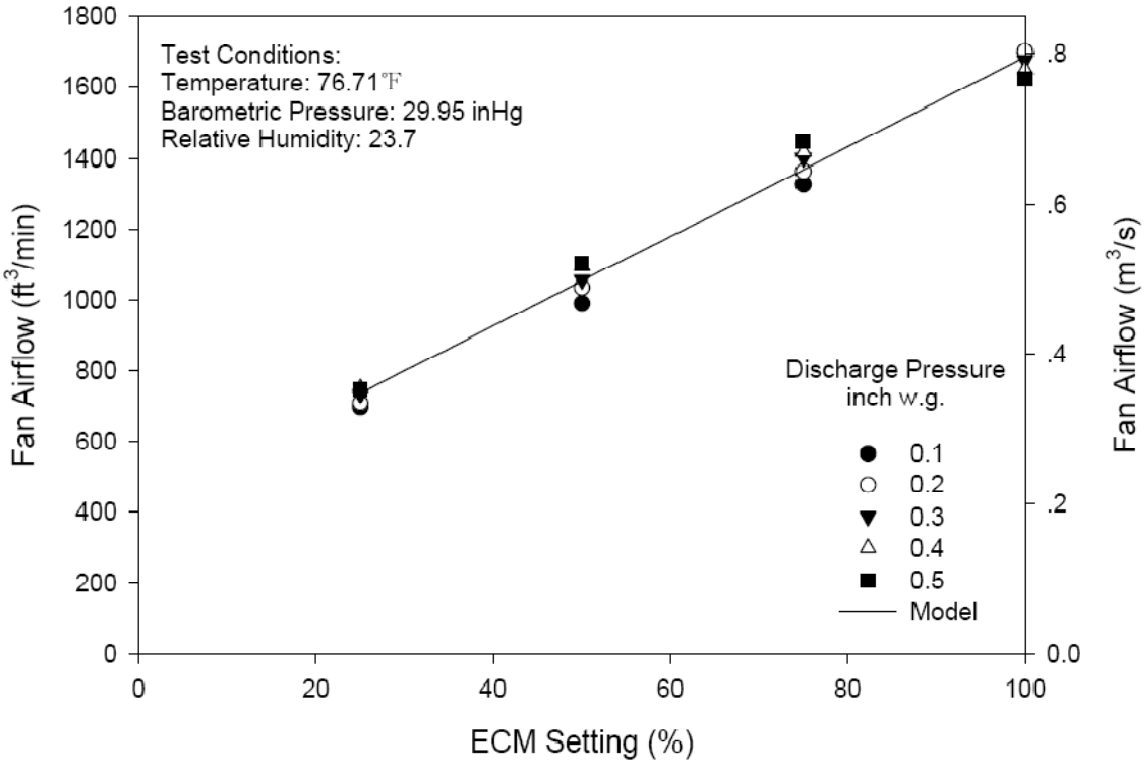

Fig. 6-4 Fan Airflow for F_S12B

The main difference between an ECM controller and SCR controller is the dependence of airflow on the fan settings. For an ECM controller, the fan airflow varied approximately linearly with the change in ECM settings. For example, if the ECM settings doubled, the airflow approximately doubled. However, for a SCR controller, the

dependence does not exist (Edmondson 2009). Since the ECM fan has characteristics of constant airflow and linear dependence on ECM settings, a linear model was used to describe the relationship between fan airflow and ECM settings. Because each manufacturer has its own method to operate the ECM controllers, it was necessary to use a non-dimensional variable in the model. A non-dimensional variable η was developed, which represented a percentage of the voltage over the whole operating range. The model used to fit the data is shown in Equation (6-1) with the coefficients shown in Table 6-1. The summary of ECM settings was shown in Table 6-2.

$$Q_{fan}=a_2+b_2\times\eta \tag{6-1}$$

Table 6-1 Summary of the Coefficients and R^2 Value for Fan Airflow Model

Fan	a_2	b_2	R^2
F_S8A	-19.258	10.111	0.998
F_S12A	73.093	22.607	0.996
F_S8B	60.233	15.119	0.987
F_S12B	420.260	12.639	0.989
F_S8C_M1	70.961	14.810	0.998
F_S8C_M2	61.043	12.704	0.937
F_S12C_M1	530.788	16.029	0.987
F_S12C_M2	32.695	21.458	0.995

Table 6-2 Summary of ECM Settings

Manufacturers	ECM Settings				
A	20	40	60	80	100
B	4 VDC	6 VDC	8 VDC	10 VDC	
C	2 VDC	4 VDC	6 VDC	8 VDC	10 VDC

This model correlated with the measured data well. All of the R^2 values are above 0.93 while the lowest value is 0.937 for S8C_M2. The relatively large fluctuations on fan airflow resulted in a lower R^2 value. It should be noted that even though all the fans were tested following the designed ECM settings, those data that were out of the nominal operating range were not used in developing the model, meaning the model generated was only applied to those points within operating range.

6.2. Power Performance

Cramlet (2008) and Edmondson (2009) modeled the power consumption of a FPTU as a function of ECM settings and inlet air velocity pressure. Since the fans were taken out of the terminal units and tested separately, discharge static pressure was used instead of inlet air velocity pressure. Fan power consumption was mainly dependent on the amount of air the fan provided. Because the fan airflow was a function of ECM setting, so the ECM setting was used as a variable rather than the fan airflow. Previous experiments were conducted at a fixed discharge pressure, so that it was not considered as a variable in the model. However, the ECM motor was able to sense a change in discharge static pressure. This ability allowed the motors to compensate for increased or decreased load, which resulted in variations in power consumption. In addition, based on the results of fan tests, downstream static pressure affected the power consumption.

Figure 6-5 shows the fan power consumption plotted against discharge pressure for F_S8A and Figures 6-6 shows these data for F_ S12B. The model fitted experimental data is shown in Equation (6-2)

$$P_{fan}=a_3\times\eta+b_3\times\eta^2+c_3\times\eta^3+d_3\times P_{discharge} \quad (6\text{-}2)$$

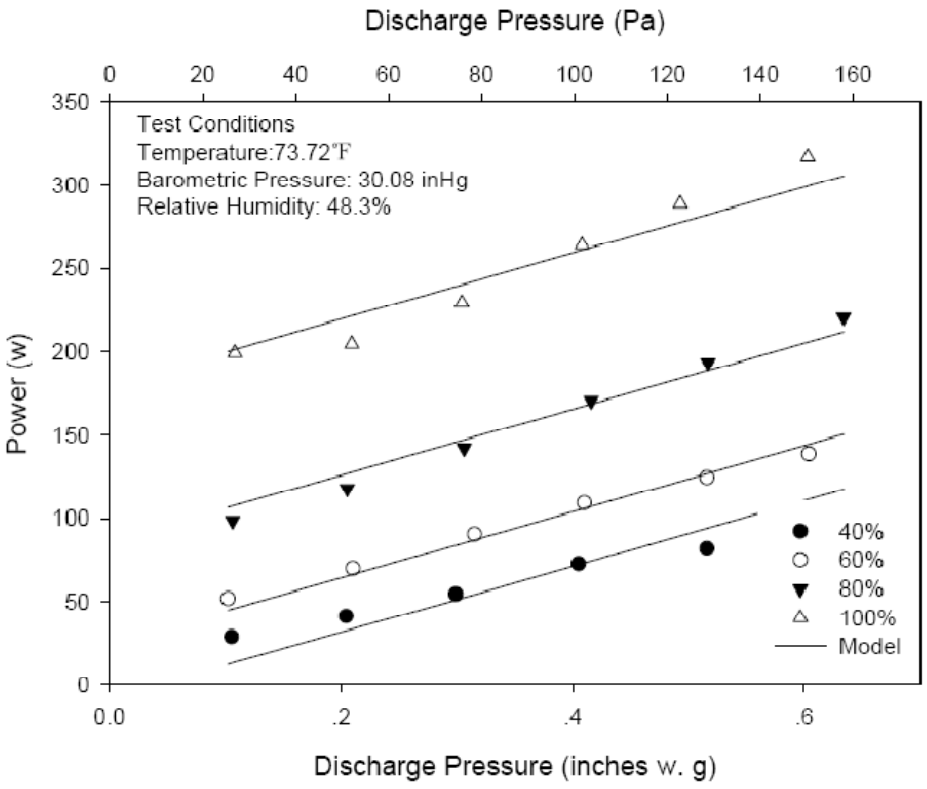

Fig. 6-5 Power Consumption for F_S8A

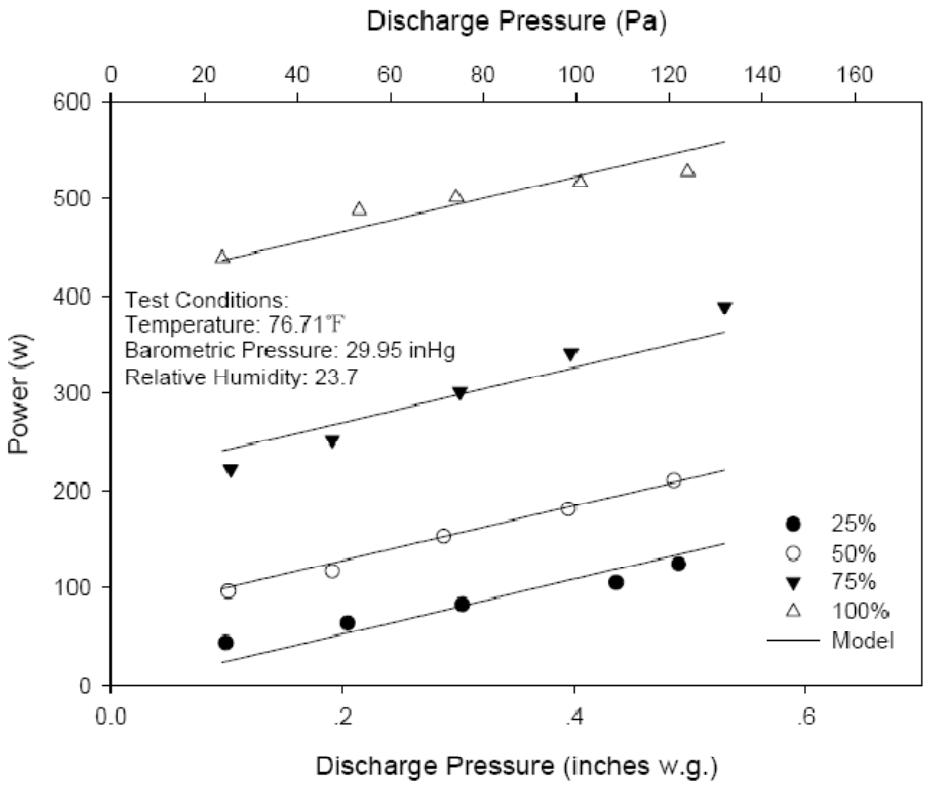

Fig. 6-6 Power Consumption for F_S12B

The form of the model was similar to those of Cramlet's (2008) and Edmondson's result (2009). However it differed in that discharge pressure was used instead of inlet air velocity pressure. The power consumption predicted by the model was consistent with measured data. The lowest R^2 was 0.986, which meant the model fitted the measured data well. Generally speaking, this model was able to provide satisfactory predictions of motor power consumption by using two individual variables without much complexity. Table 6-3 shows the coefficients and R^2 values for these series terminal units.

Table 6-3 Summary of Coefficients and R^2 for the Fan Power Consumption Model

Fan	a_2	b_2	c_2	d_2	R^2
F_S8A	-1.263	0.0239	0.0000672	197.817	0.986
F_S12A	-2.038	0.0479	0.000693	375.109	0.998
F_S8B	-3.065	0.0821	-0.00000424	275.617	0.990
F_S12B	-1.941	0.0744	-0.00014	281.860	0.994
F_S8C_M1	-1.068	0.0745	0.000331	158.116	0.996
F_S8C_M2	-0.386	0.0507	-0.000176	101.070	0.993
F_S12C_M1	-0.00981	0.0554	0.000252	263.585	0.993
F_S12C_M2	0.703	-0.0231	0.00101	258.869	0.990

It should be noted that all the data were collected within the nominal fan operating range specified by the manufacturers of the terminal units. The model should provide good results in the appropriate range for both airflow and power consumption. Table 6-4 shows the recommended operating range for each fan in the FPTU. Both fan airflow and power consumption models should be applied in this range.

Table 6-4 Summary of Recommended Operating Range

Fan	Recommended Operating Range	
	Discharge Pressure in w.g. (Pa)	Fan Capacity CFM (m^3/s)
F_S8A	0.1-0.5 (25-125)	300-1050 (0.14-0.5)
F_S12A	0.1-0.5(25-125)	700-2500 (0.33-1.18)
F_S8B	0.1-0.6 (25-150)	200-900 (0.09-0.42)
F_S12B	0.1-0.6 (25-150)	400-1600 (0.19-0.75)
F_S8C_M1	0-0.5 (0-125)	200-1100 (0.09-0.52)
F_S8C_M2	0-0.5 (0-125)	200-1100 (0.09-0.52)
F_S12C_M1	0-0.5 (0-125)	500-2025 (0.23-0.97)
F_S12C_M2	0-0.5 (0-125)	500-2025 (0.23-0.97)

It was observed that fans from manufacture B pulsed and operated on and off if it was set to be operating close to the designed maximum fan capacity. This created several difficulties in measurements. First an equilibrium test condition was hard to achieve. The discontinuous operation of F_S8B and F_S12B made discharge pressure fluctuated in a large range. A measurement could only be taken in this range near the target point. Second, airflow and power measurements were not made synchronously. It was possible that the airflow was measured at peak while power was measured at minimum value or in the

oppose way. Difficulty in measurement made the fan airflow models should be strictly applied in the designed operation range.

CHAPTER VII

PLENUM AIRFLOW MODEL

Air from the plenum space in a building was drawn into the terminal unit and mixed with the primary air provided by the main supply fan, and then the mixture is delivered to conditioned zone. Plenum airflow has two main functions. First, warm air from the conditioned zone was used to maintain a preset zone temperature when the cold primary air dropped to the minimum setting or other preset values at summer cooling part-load operation. Second, low-temperature primary air was mixed with warm plenum air to prevent the possible surface condensation in the cold air distribution system.

For series FPTUs, when the fan was operating then a negative pressure formed inside the terminal units while the outside pressure maintained constant. The plenum airflow was driven by the pressure difference between the inside and outside of the terminal unit. Due to the difficulty in the measurement, previous students, Furr (2006), Cramlet (2008) and Edmondson (2009), did not develop a model to simulate plenum airflow. In this study, tests were designed to simulate the plenum airflow and a model was developed. The results were discussed later in this chapter.

Plenum airflow was modeled as a function of the differential pressure between the inside and outside of the terminal unit as well as the dimension of the inlet area of the

plenum airflow. The differential pressure was the driving force of the plenum airflow. However, there was no pressure taps designed for measuring internal static pressure on the FPTUs. The method of measuring static pressures was used to take an average measurement of internal static pressure at four locations. Four holes were drilled in the top, bottom, left and right walls of the terminal units. Those holes were located in the intersection of two diagonals. Copper pressure taps with the same diameter as the holes were covered and sealed by using adhesive tape. Plastic tubing was then used to connect pressure taps to a pressure transmitter. Because the environmental pressure was zero, the differential pressure was simply the value of the measured static pressure. Figure 7-1 shows the experimental setup for plenum test.

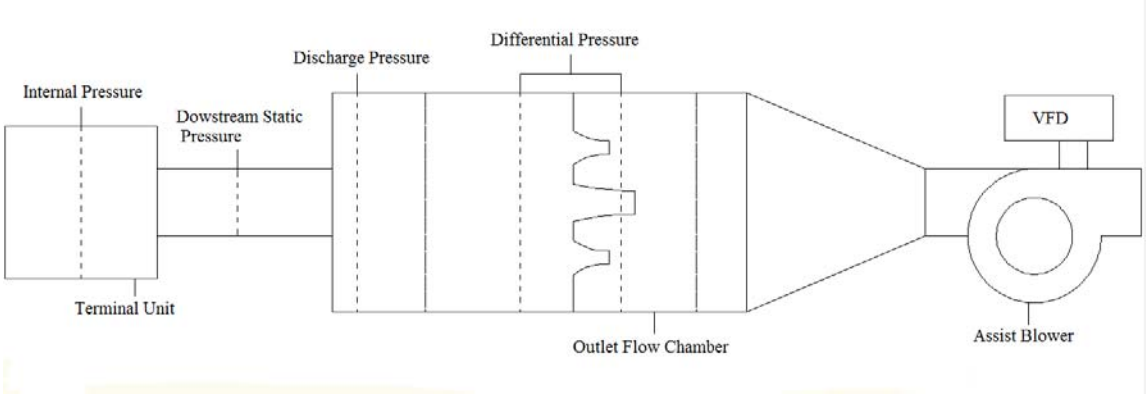

Fig. 7-1 Test Setup for Plenum Airflow

It was observed that there were two plenum airflow arrangements, which differed in flow directions. In arrangement A the direction of the plenum airflow was parallel to that of primary airflow, as shown in Figure 7-2. Manufacturers A and B employed this arrangement. In the other configuration, the direction of plenum airflow was perpendicular to that of primary airflow, which is illustrated in Figure 7-3. Manufacturer C adopted this design. It was difficult to use one single model to describe the plenum airflow for both configurations, so two correlations with different coefficients were generated.

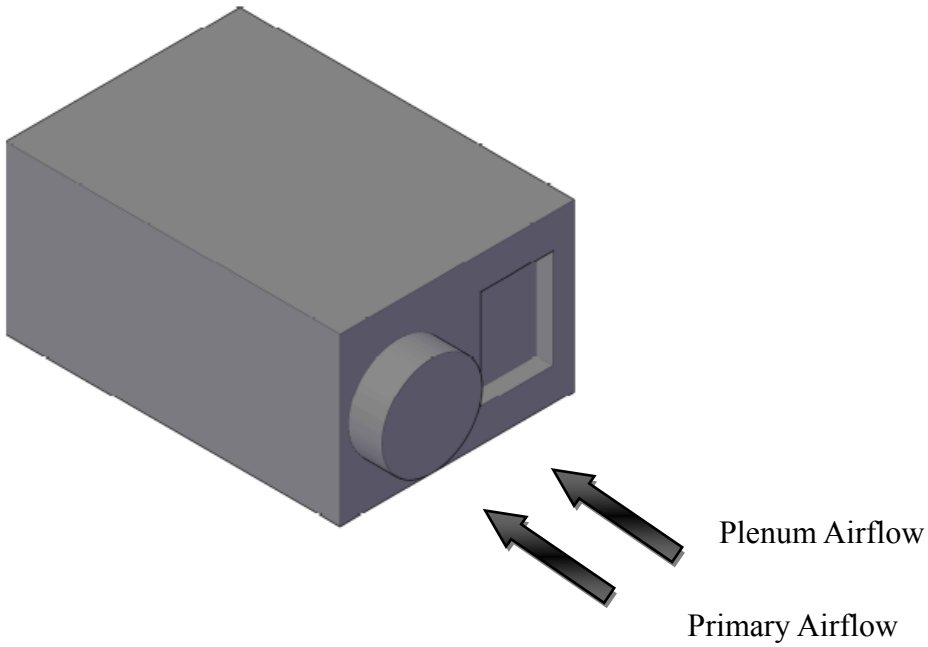

Fig. 7-2 Arrangement A for Plenum Airflow

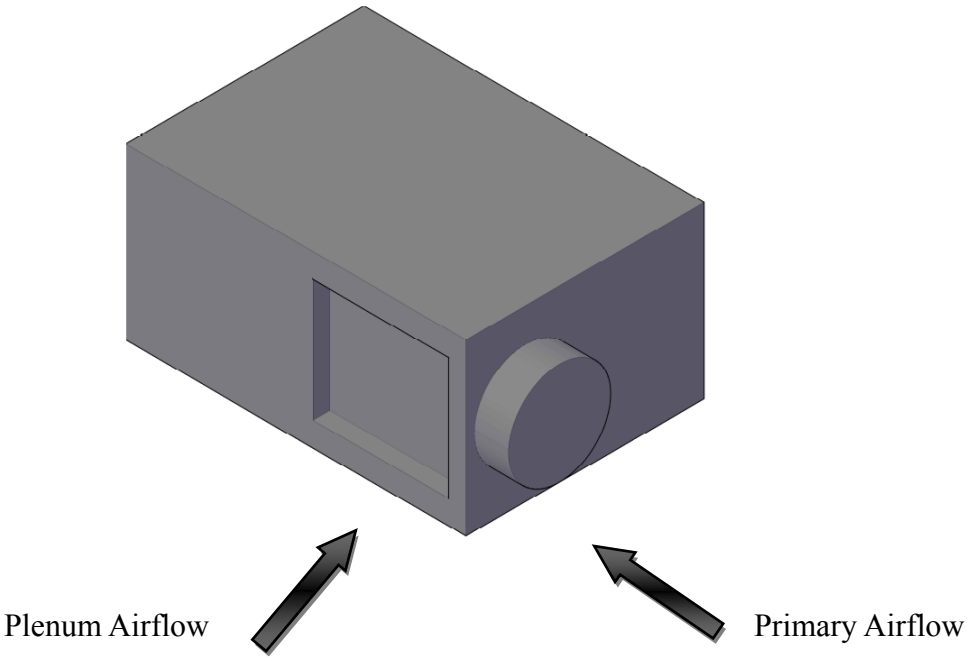

Fig. 7-3 Arrangement B for Plenum Airflow

The plenum airflow inlet was rectangular. Because terminal units from different manufactures were designed with various inlet areas, a non-dimensional variable θ was employed to describe this physical characteristic for various terminal units. The variable θ is defined in Equation (7-1). A_p is the inlet area of plenum flow and A_{p0} is a constant, $A_{p0}=14\times18=252$ in^2.

$$\theta=A_p/A_{p0} \tag{7-1}$$

The constant A_0 is the area of S12B's inlet. There are two reasons for choosing it as a standard area to calculate θ. One was that S12B was the first terminal unit being tested. Also, it had the largest inlet area among all the terminal units.

To measure plenum airflow accurately, the fan was taken out of the terminal unit, and the primary inlet damper was kept at a fully closed position with the primary inlet covered by adhesive tape to avoid air entering the terminal unit through the primary airflow inlet. The outlet flow chamber was connected to the terminal unit via a downstream air duct. The internal pressure varied from 0.01 inches w.g. to 0.2 inches w.g. and was controlled by adjusting the speed of the assist blower.

Mathematical models for different plenum airflow arrangements were in the same form with distinct constants. Equation (7-2) is the expression used to fit the experimental data.

$$Q_{plenum}=\left(a_4+b_4\times\sqrt{|P_{internal}|}\right)\times\left(1+c_4\times\theta+d_4\times\theta^2\right) \quad (7\text{-}2)$$

Coefficients for the arrangement A are listed in the Table 7-1 and coefficients for arrangement B (only S12C_M1 and S12C_M2) are listed in the Table 7-2.

Table 7-1 Coefficients and R^2 Value for Terminal Units with Arrangement A

a_4	b_4	c_4	d_4	R^2
3.304	1040.570	1.364	1.977	0.991

Table 7-2 Coefficients and R^2 Value for Terminal Units with Arrangement B

a_4	b_4	c_4	d_4	R^2
-0.671	151.084	71.901	-49.438	0.993

Figures 7-4 and 7-5 show the plenum airflow plotted against the differential pressure, and the curves were generated by the correlations in Table 7-1 and 7-2, respectively. The predicted values matched the measured data well, with the R^2 value above 0.99 for both cases. It could be concluded that the models were capable of characterizing the plenum airflow. Full results for the plenum airflow for eight series FPTUs are available in Appendix C.

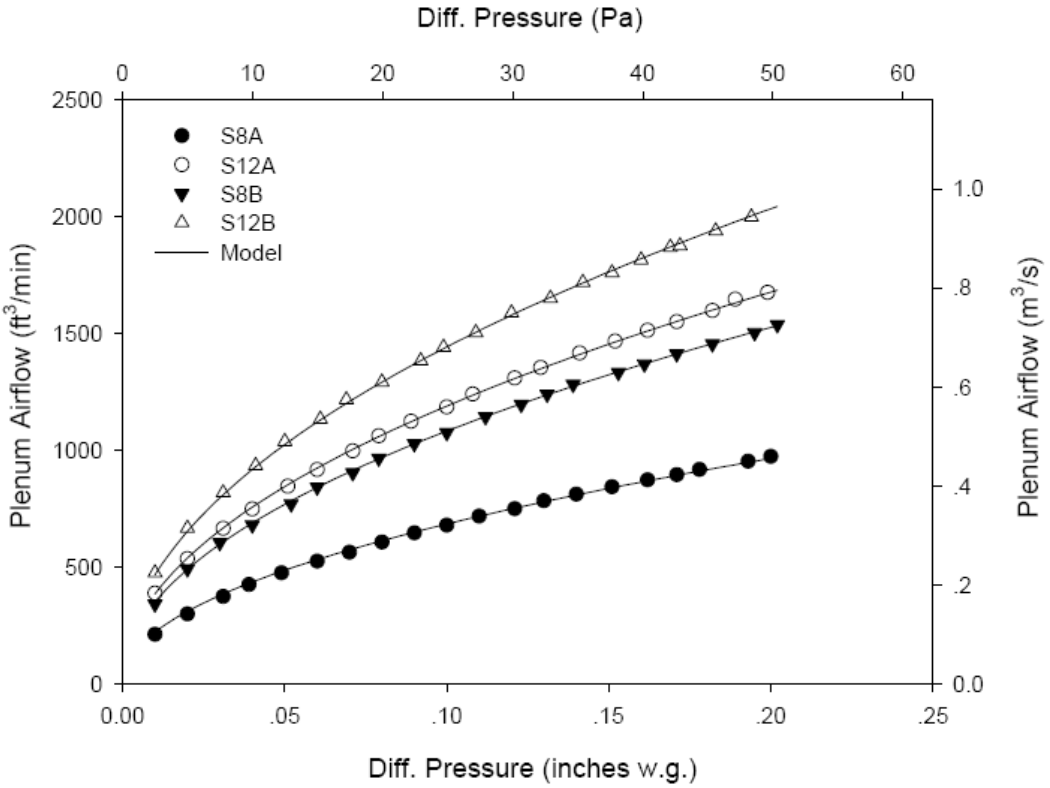

Fig. 7-4 Plenum Airflow for Terminal Units with Arrangement A

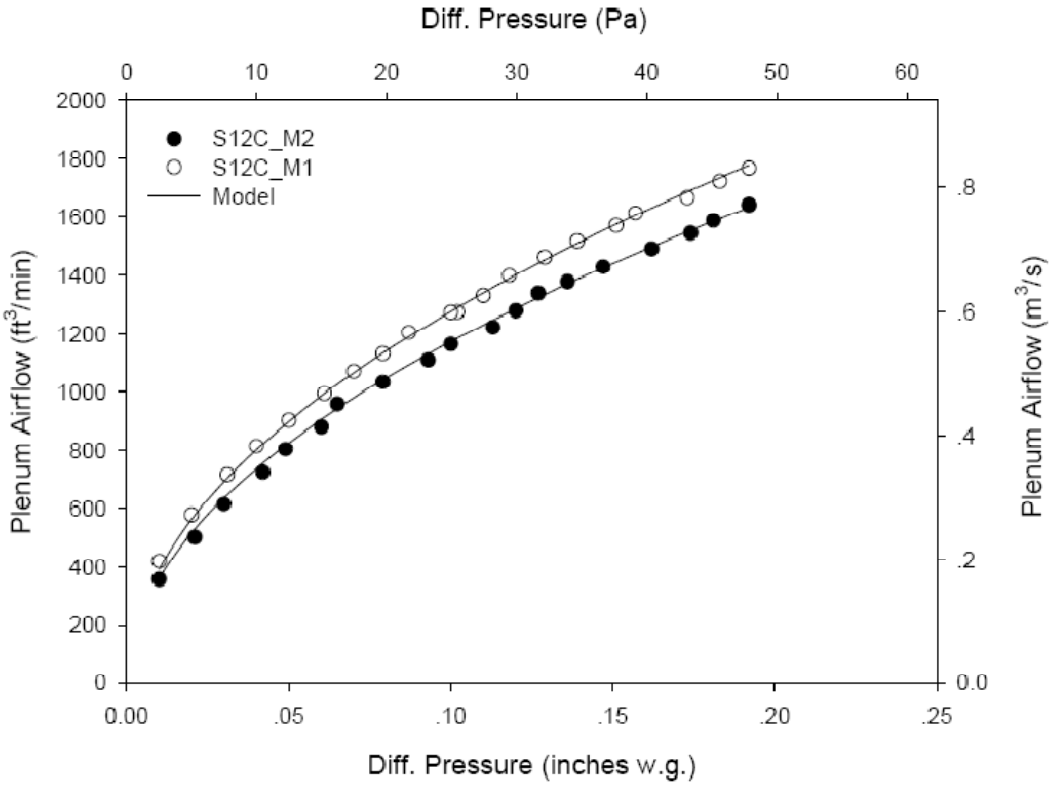

Fig. 7-5 Plenum Airflow for Terminal Units with Arrangement B

It was found that the behaviors of S8C_M1 and S8C_M2 were distinct from other terminal units (S12C_M1 and S12C_M2) provided by manufacturer C. After plotting and analyzing the experimental data it was found that the capability of plenum airflow for terminal unit S8C_M1 was too high to be considered to be in a reasonable range. Figure 7-6 shows the test result for S8C_M1 as well as S8C_M2 and S12C_M1.

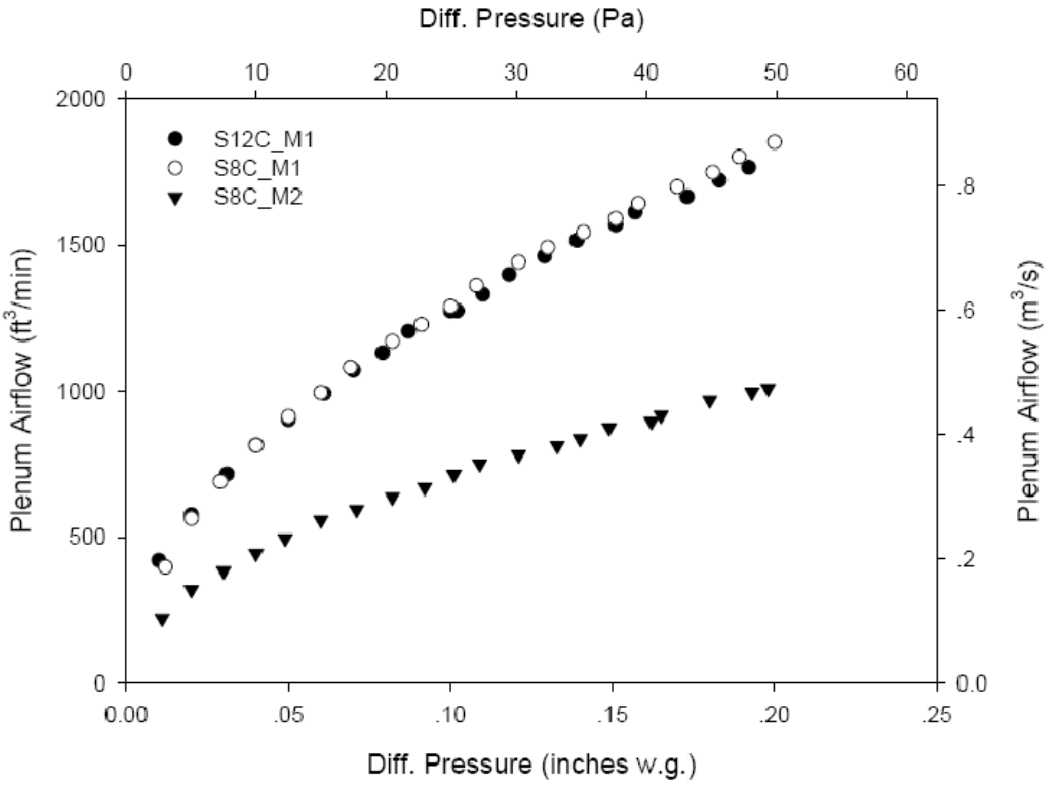

Fig. 7-6 Comparison of Plenum Airflow for S8C_M1, S8C_M2 and S12C_M1

The plenum airflow inlet areas of the two 8″ terminal units were almost the same (area of S8C_M1 is 168 in^2 and area of S8C_M2 is 170 in^2), but the S8C_M1 could induce as much as nearly twice the amount of air than S8C_M2. Since the primary airflow inlet was covered by adhesive tape and the damper was maintained at the fully closed position when the test was running, air could not enter the terminal unit through the primary airflow inlet. Therefore the possible reason for extremely high plenum airflow for S8C_M1 could be leakage. Small apertures were observed at the wall junctions of

S8C_M1. When the fan was working, air could go through those apertures which resulted in high plenum airflow. Figure 7-7 shows the plenum airflow plotted against the differential pressure across the terminal unit for S8C_M1. The coefficients and R^2 value for this terminal unit are shown in Table 7-3.

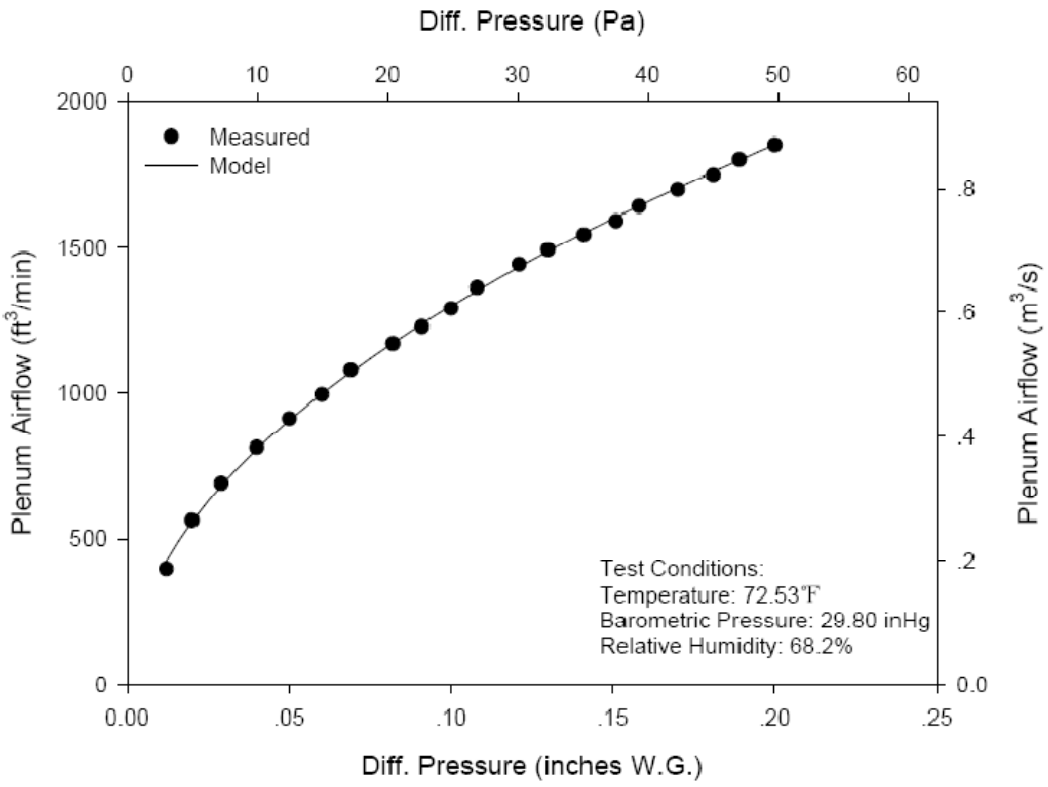

Fig. 7-7 Plenum Airflow for S8C_M1

Table 7-3 Coefficients and R^2 Value for Terminal Unit S8C_M1

a_4	b_4	c_4	d_4	R^2
-0.733	76.730	40.777	60.666	0.995

The data from S8C_M2 seemed reasonable. But it was found a single correlation could not be established to describe all the plenum airflow for S12C_M1, S12C_M2and S8C_M2. Another correlation which was only applied to S8C_M2 was generated. This correlation followed the form of Equation (7-2), and the coefficients are listed in Table 7-4.

Table 7-4 Coefficients and R^2 Value for Terminal Units S8C_M2

a_4	b_4	c_4	d_4	R^2
-0.323	56.057	29.680	43.514	0.990

The R^2 value is 0.99, meaning the model matched the measured data of plenum airflow well for S8C_M2. Figure 7-8 shows the experimental data plotted against differential pressure for S8C_M2. The model curve was generated by the correlation above.

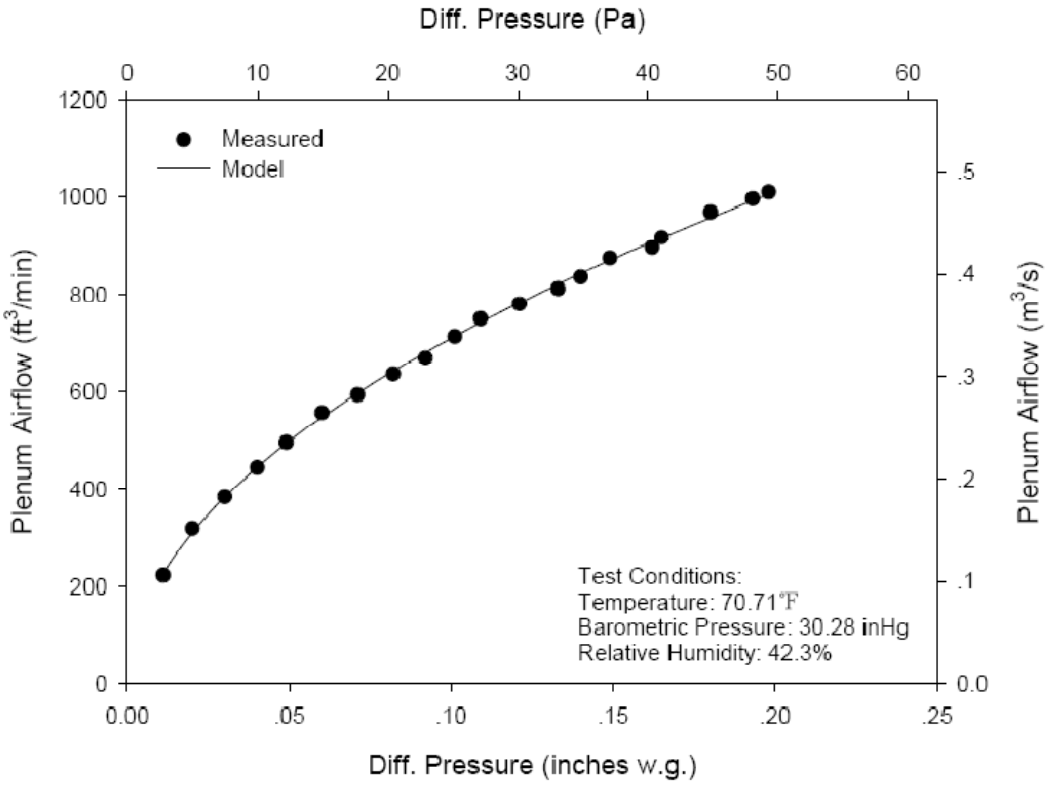

Fig. 7-8 Plenum Airflow for S8C_M2

CHAPTER VIII

TERMINAL UNIT MODELS

Models for FPTUs must be able to estimate primary, plenum and fan airflow and fan power based on pressures, ECM settings, damper settings as well as terminal unit physical dimensions were taken as individual variables. By solving the group of equations developed in the previous chapters simultaneously, airflows and fan power consumption were estimated. A comparison was made by using measured and predicted data to verify the model's accuracy.

This chapter describes the development of the FPTU model, which was built by using models developed in previous chapters. Comparisons with experimental data were made to demonstrate its ability to characterize the performance of FPTUs.

8.1. Model for FPTUs

Four streams of airflow, which are shown in Figure 8-1, enter or exit the series terminal units, namely primary, plenum and fan airflow, as well as leakage. The primary, plenum and fan airflows were discussed and models were generated separately in previous chapters. Though leakage might exist during a test, it was not taken into consideration for the series terminal units. One reason was that there was no effective and practical way to measure the amount of air coming into a series terminal unit by leakage.

More importantly, for a series FPTU, the fan always runs and creates a slightly negative pressure inside of the terminal unit. This negative pressure is used to induce air into the terminal unit from the plenum space. Because the leakage would also be induced from the plenum space, leakage in a series terminal unit has no negative consequences on the performance of the terminal unit. So the effect caused by a leakage can be ignored.

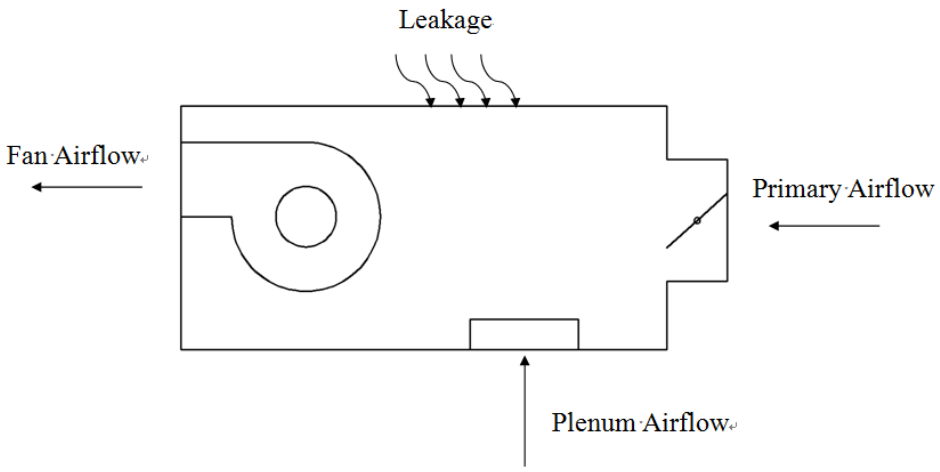

Fig. 8-1 Volumetric Balance for Series FPTU

To derive a simple model, several assumptions were made to simplify the mass conservation equation, Equation (8-1). First, all the airflow measurements were assumed to be made at steady state, which led to elimination of the transient term dm/dt, Equation (8-2). The mass of airflow was equal to volumetric flow multiplied by density (8-3). Second, the uniform unconditioned laboratory air was used in all tests and the temperature

rise across the fan was assumed to have a negligible effort on air density. Thus, the density of air was assumed to be constant. Because the mass flow rate was a product of volumetric flow and air density, Equation (8-3), this assumption implied the volumetric flow entering should be equal to the volumetric flow existing of the terminal unit, which was expressed in Equations (8-4) and (8-5).

$$dm/dt = \sum \dot{m}_{in} - \sum \dot{m}_{out} \quad (8\text{-}1)$$

$$\sum \dot{m}_{in} = \sum \dot{m}_{out} \quad (8\text{-}2)$$

$$\dot{m} = \dot{Q} \times \rho \quad (8\text{-}3)$$

$$\sum \dot{Q}_{in} = \sum \dot{Q}_{out} \quad (8\text{-}4)$$

$$\dot{Q}_{Primary} + \dot{Q}_{Plenum} = \dot{Q}_{Fan} \quad (8\text{-}5)$$

Models for primary, plenum and fan airflow were generated in previous chapters. However both primary and plenum airflow models used internal pressure as a variable to eliminate the necessary offset in Cramlet's (2008) and Edmondson's (2009) correlation. It was not practical to measure the pressure in field tests because no pressure taps are installed on the terminal units for this measurement. This pressure as well as the other three streams of airflow was determined by solving a group of equations simultaneously. The group of equations was formed by Equations (8-6), (8-7), (8-8) and (8-9) as listed below:

$$Q_{primary}=\left(a_1+b_1\times\sqrt{P_{upstream}-P_{internal}}\right)\times(1+c_1\times\gamma+d_1\times\gamma^2+e_1\times\gamma^3)+f_1 \quad (8\text{-}6)$$

$$Q_{fan}=a_2+b_2\times\eta \quad (8\text{-}7)$$

$$Q_{plenum}=\left(a_4+b_4\times\sqrt{|P_{internal}|}\right)\times\left(1+c_4\times\theta+d_4\times\theta^2\right) \quad (8\text{-}8)$$

$$Q_{fan}=Q_{plenum}+Q_{primary} \quad (8\text{-}9)$$

In this group of equations, the non-dimensional variables γ, η, θ and $P_{upstream}$ were known at a given operating condition. The variable γ could be calculated from the damper control voltage, η was available from ECM setting and θ was constant for a specific terminal unit. The upstream static pressure $P_{upstream}$ could be measured directly. $Q_{primary}$, Q_{fan}, Q_{plenum} and $P_{internal}$ were unknowns. Therefore the set of equations can be solved simultaneously for the unknowns.

The fan power consumption was a function of the ECM setting and discharge pressure, both of which could be measured directly. The model for power consumption is shown in Equation (8-10).

$$P_{fan}=a_3\times\eta+b_3\times\eta^2+c_3\times\eta^3+d_3\times P_{discharge} \quad (8\text{-}10)$$

An Excel spreadsheet was used to solve the group of equations with a sample shown in Figure 8-2. Airflow and power equations were entered into the spreadsheet and set as functions of input variables, which are in bold fonts. The input data included the ECM setting, the damper control voltage, the inlet area of plenum airflow and the upstream and downstream static pressure. Once the input data was available, the

non-dimensional variables could be calculated from the ECM setting, the damper control voltage and the inlet area of plenum airflow, respectively. Several intermediate variables were used to simplify the calculations. Table 8-1 shows the mathematical expressions of these intermediate variables. It should be noted that these intermediate variables were developed only for simplification of the calculation and had no significant physical meanings.

By eliminating the common variables, a quadratic equation with internal pressure $P_{internal}$ was derived. This equation is shown in Equation (8-11). The capital letters in this equation are the intermediate variables shown in Table 8-1.

$$\left(E^2-D^2\right)^2\times P_{internal}^2+\left[2\times F\times\left(E^2-D^2\right)+4\times C^2\times E^2\right]\times P_{internal}+F^2=0 \quad (8\text{-}11)$$

The internal pressure $P_{internal}$ could be solved through Equation (8-12)

$$P_{internal}= -\left(2\times F\times\left(E^2-D^2\right)+4\times C^2\times E^2\right)+\sqrt{\left[2\times F\times\left(E^2-D^2\right)+4\times C^2\times E^2\right]^2-4\times\left(E^2-D^2\right)^2\times F^2}\Big/ 2\times\left(E^2-D^2\right)^2 \quad (8\text{-}12)$$

After solving Equation (8-12), the internal pressure $P_{internal}$ was available, and then put it into Equation (8-6) and (8-8) to calculate the primary and plenum airflow. The fan power consumption equation could be solved directly if the specific operating condition and the terminal unit were given. The complete calculation process is available in Appendix G.

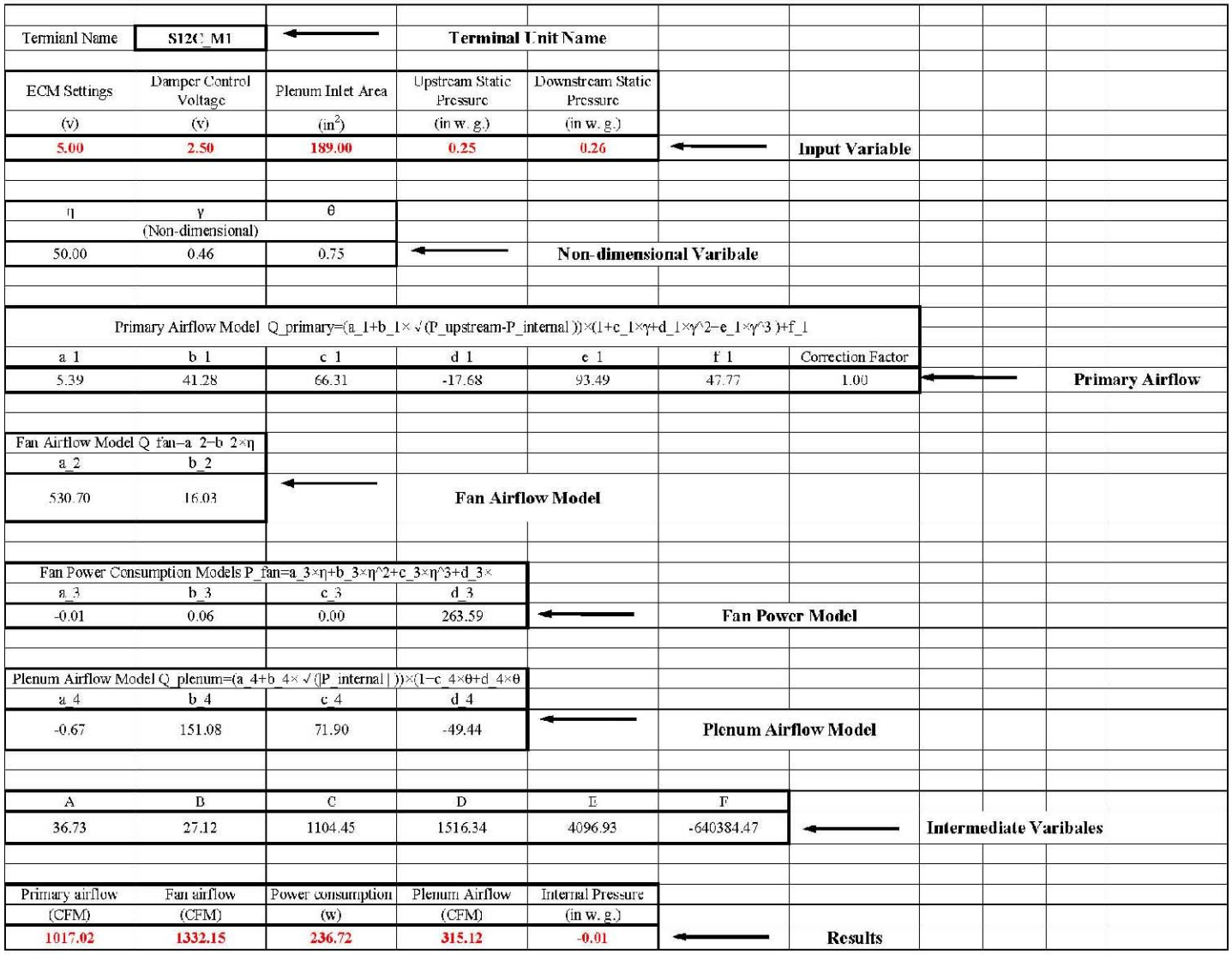

Fig. 8-2 Sample Data and Results Spreadsheet for S12C_M1

Table 8-1 Summary of Intermediate Variables

Intermediate Variables	Mathematical Expressions
A	$1+c_1\times\gamma+d_1\times\gamma^2+e_1\times\gamma^3$
B	$1+c_4\times\theta+d_4\times\theta^2$
C	$Q_{fan}-f_1-a_1\times A-a_4\times B$
D	$b_1\times A$
E	$b_4\times B$
F	$D^2\times P_{upstream}$

8.2. Verification of Model for FPTUs

The values predicted by the model for series FPTUs were compared with measured data. All the eight series FPTUs had been tested in previous studies (Cramlet 2008 and Edmondson 2009). For the same upstream and downstream pressures, and ECM and damper settings, airflow and power values were predicted by the models. The predictions from the model were plotted and compared to experimental data.

After the comparison, it was found that when the damper setting was in the higher half of its working range, over 45° for the butterfly damper and over 22.5° for the opposed-blade damper, the predictions of primary airflow for BF8, BF12 and OB8 from the model were below the measured data. The comparisons of primary airflow for

terminal units S8A, S12B and S8C_M2 are shown in Figures 8-3, 8-4 and 8-5, respectively. There were three reasons for these differences. First, no dampers were perfectly airtight during the tests. When the damper settings approached the fully closed position, there were still many small apertures for flow, which allowed leakage crossed the damper. Second, when damper setting was near the fully closed range, it allowed only a little air went through the airflow chamber and the damper. This small amount of air generated a low differential pressure in the airflow chamber. Even using the nozzle with the smallest diameter, this differential pressure was too low to be accurately measured. A large measurement error resulted in the difference between the prediction and measurement. Another reason is the system effects. The system effects were attributable to installed conditions that were different in any ways from those used in the laboratory tests. The series FPTUs model was established based on the models of primary, plenum and fan airflow and fan power consumption models, while those sub-models were developed from the separate tests on each component of the series FPTUs which included the primary inlet damper, the fan and the terminal unit frame. When putting all the sub-models together to form the series FPTUs model, the differences between the laboratory test conditions and the installed conditions might cause the inconsistency between the prediction and the measurement in primary airflow at higher damper settings. In measurement of the primary airflow through the damper, the effects brought

by plenum airflow and fan airflow were eliminated by testing the damper alone. So the primary airflow model did not take the effects brought by plenum and fan airflow. However the plenum airflow arrangement and fan configuration would affect the flow pattern within the series FPTUs and result in the difference between the prediction and the measurement.

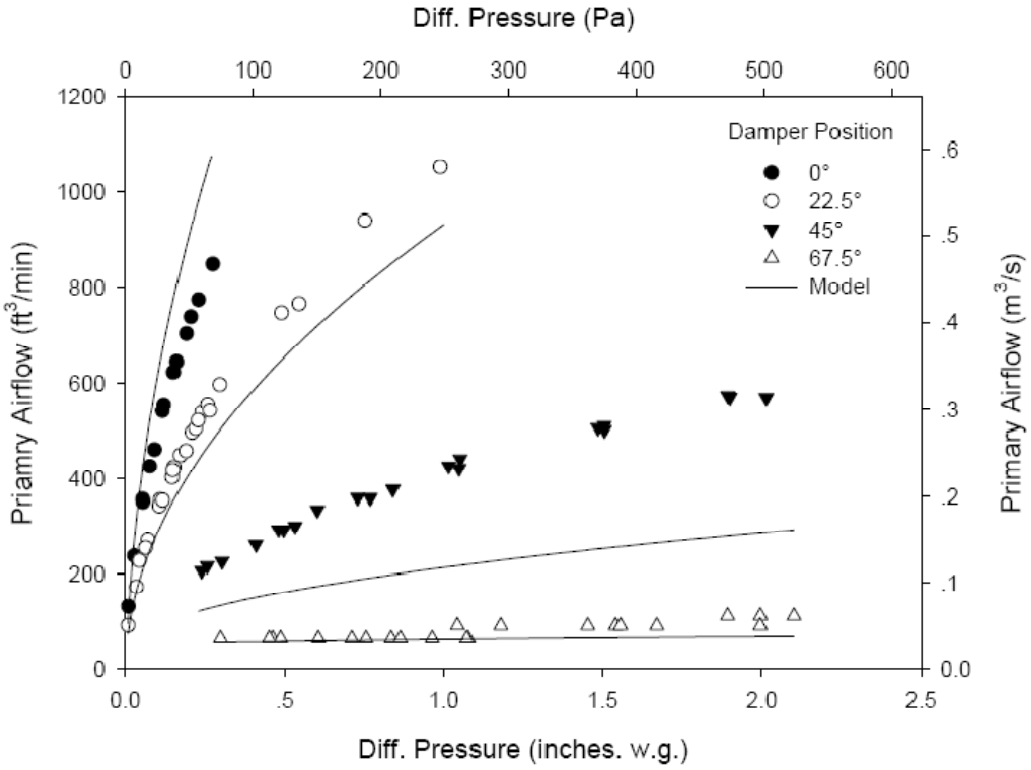

Fig. 8-3 Comparison in Primary Airflow for S8A without Correction Factor

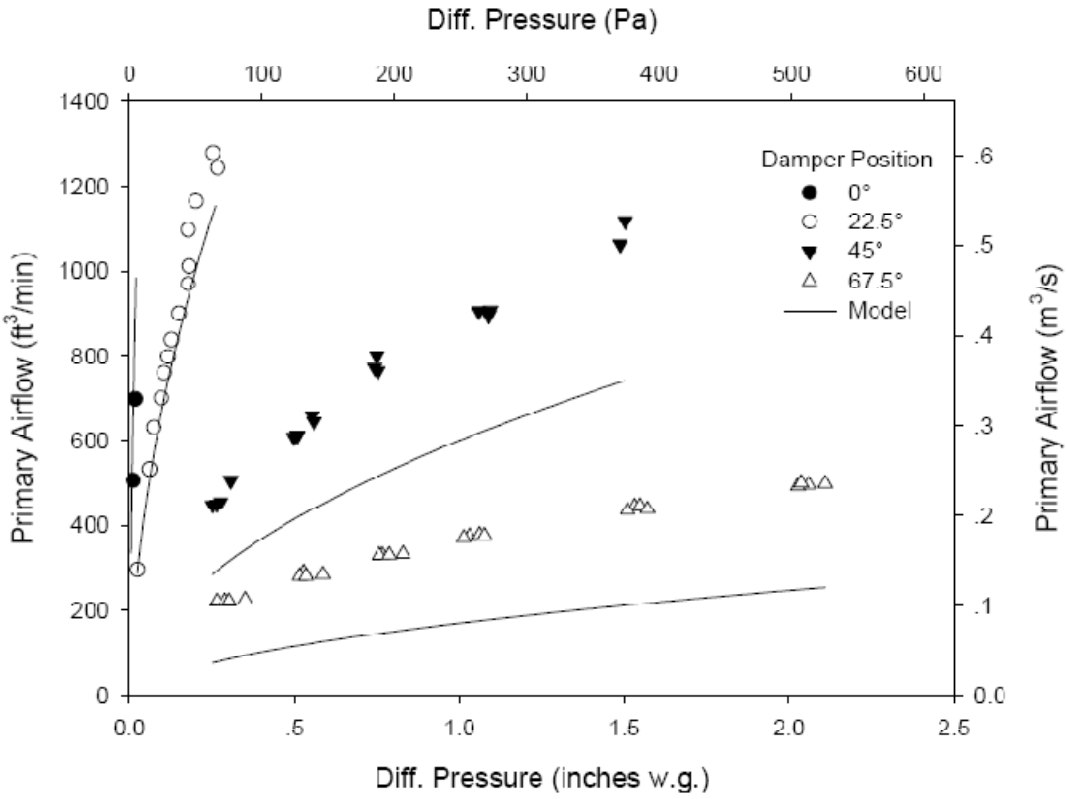

Fig. 8-4 Comparison in Primary Airflow for S12B without Correction Factor

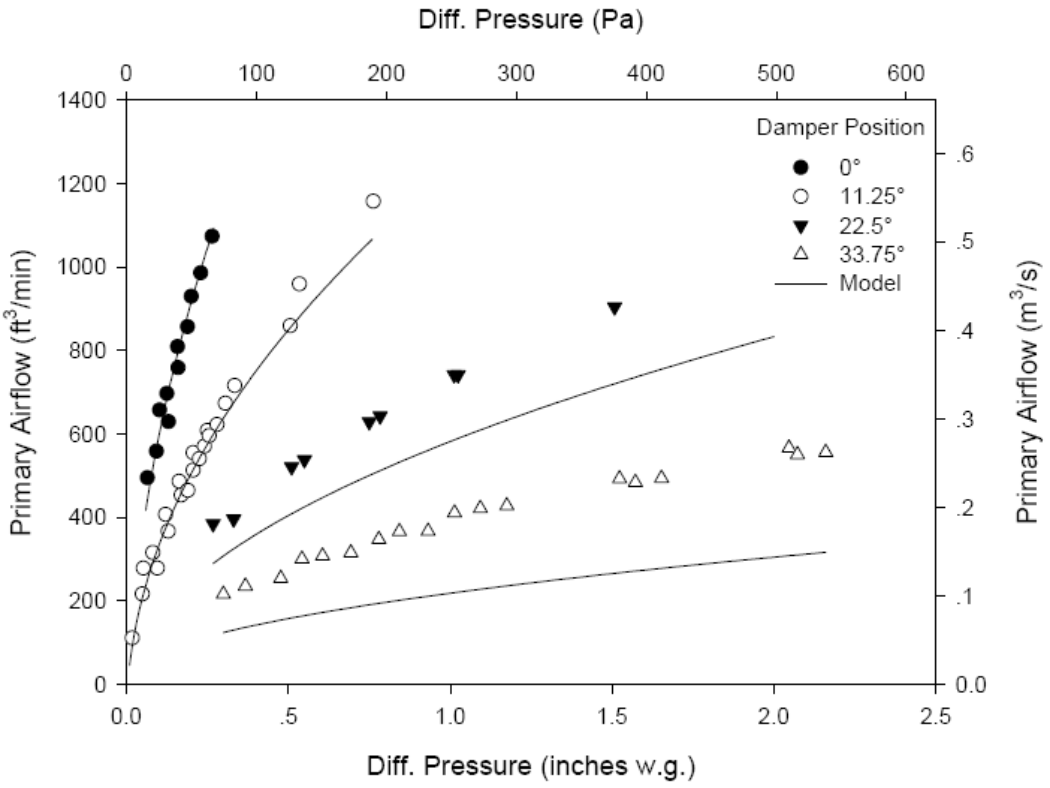

Fig. 8-5 Comparison in Primary Airflow for S8C_M2 without Correction Factor

Because the primary, plenum and fan airflows were connected to each other, an inaccurate prediction of primary airflow would risk the reliability of the whole series FPTUs model. To reduce the difference between the prediction and measurement, correction factors were added in the calculation process for primary airflow. The primary airflow model was multiplied by a correction factor and then in conjunction with the models of plenum, fan airflows and mass balance equation to calculate the internal pressure of the terminal unit. By using the internal pressure, the corrected primary and

plenum airflow were determined. Figure 8-6 shows the calculation process by using correction factor.

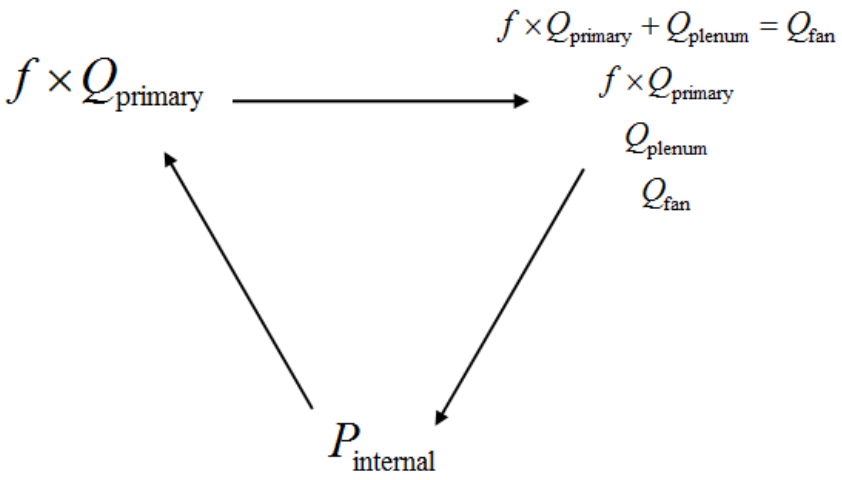

Fig. 8-6 Schematic Diagram of Calculation Process by Using Correction Factor

Employing correction factors was a way to compensate for the inaccurate measurement and the system effects generated when using the sub-models to form the FPTU model. Correction factors were determined by comparing the predicted values to measured data. It was found these factors varied with damper settings, damper types as well as damper size. Correction factors and corresponding damper settings used in this study are listed in Tables 8-2, 8-3 and 8-4.

Table 8-2 Correction Factors for BF12

Type	Size	Damper Angle	Correction Factor
Butterfly	12’’	0 °	N/A
		22.5 °	
		45 °	2
		67.5 °	

Table 8-3 Correction Factors for BF8

Type	Size	Damper Angle	Correction Factor
Butterfly	8’’	0 °	N/A
		22.5 °	
		45 °	1.5
		67.5 °	

Table 8-4 Correction Factors for OB8

Type	Size	Damper Angle	Correction Factor
Opposed-blade	8’’	0 °	N/A
		11.25 °	
		22.5 °	1.4
		33.75 °	

Figures 8-7, 8-8 and 8-9 show the prediction of primary airflow with correction factors for S8A, S12B and S8C_M2. After using the correction factors, the differences between the predictions from the model and the experimental measurements were reduced. In addition, the new model totally eliminated the offset, which was required in the previous model developed by Cramlet (2008) and Edmondson (2009).

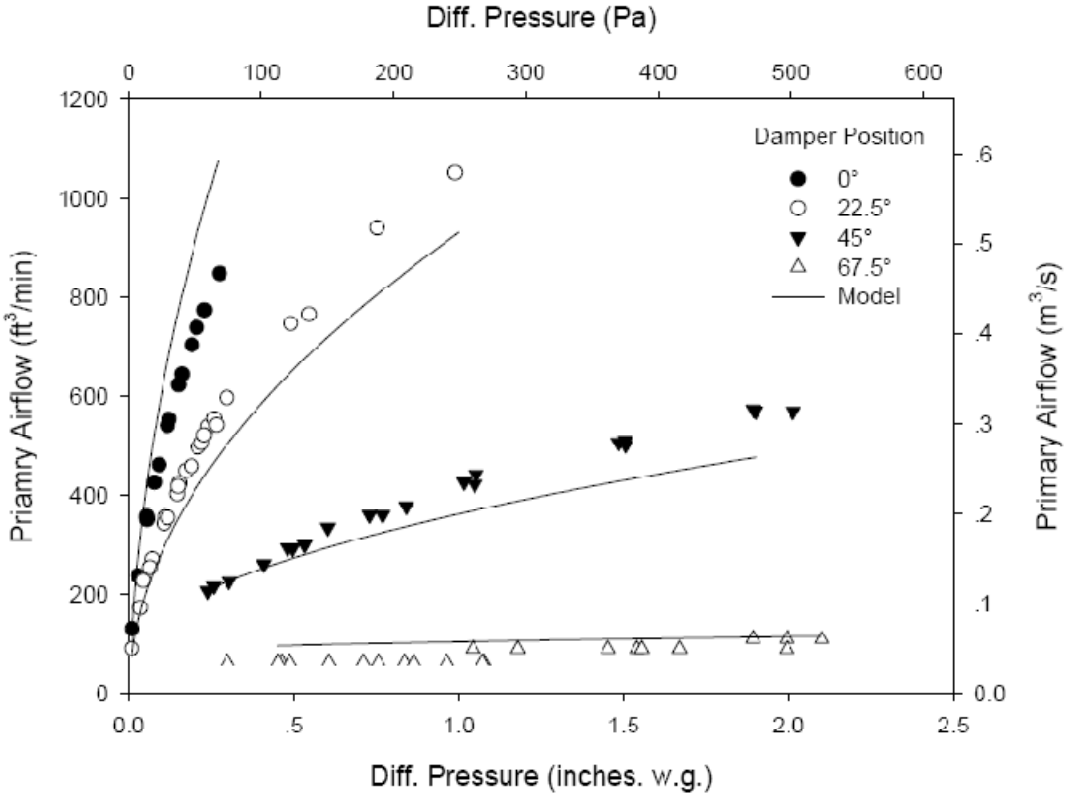

Fig. 8-7 Comparison in Primary Airflow with Correction Factor for S8A

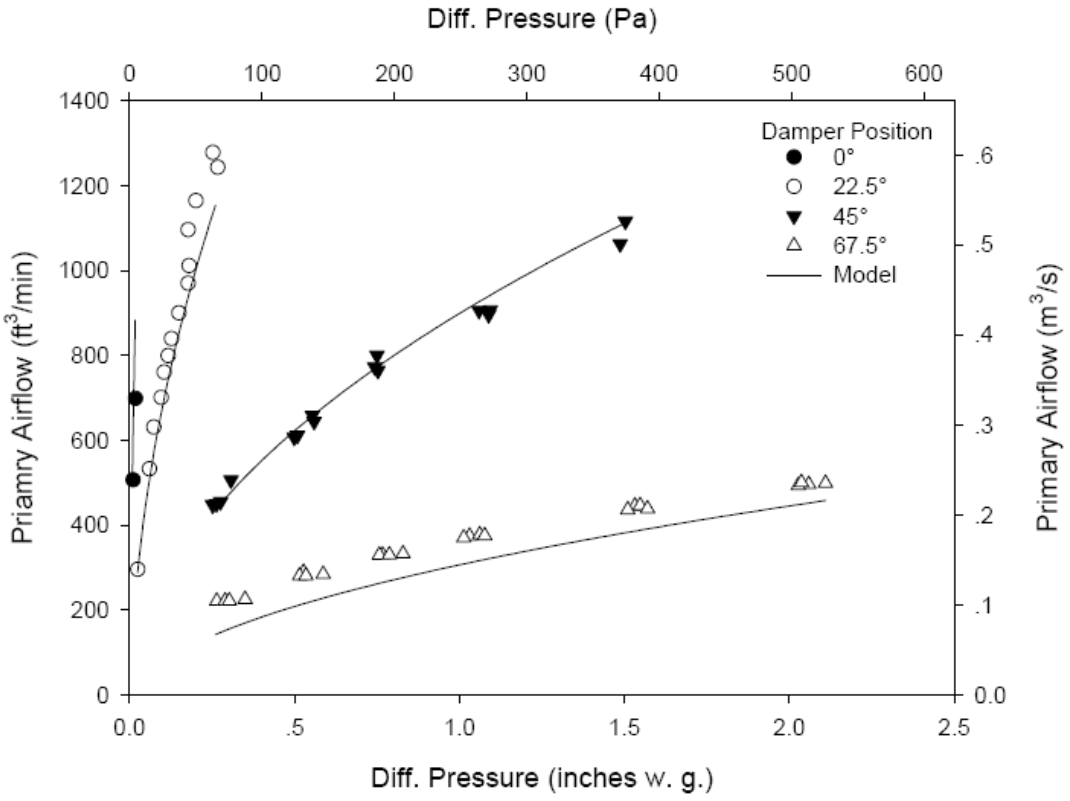

Fig. 8-8 Comparison in Primary Airflow with Correction Factor for S12B

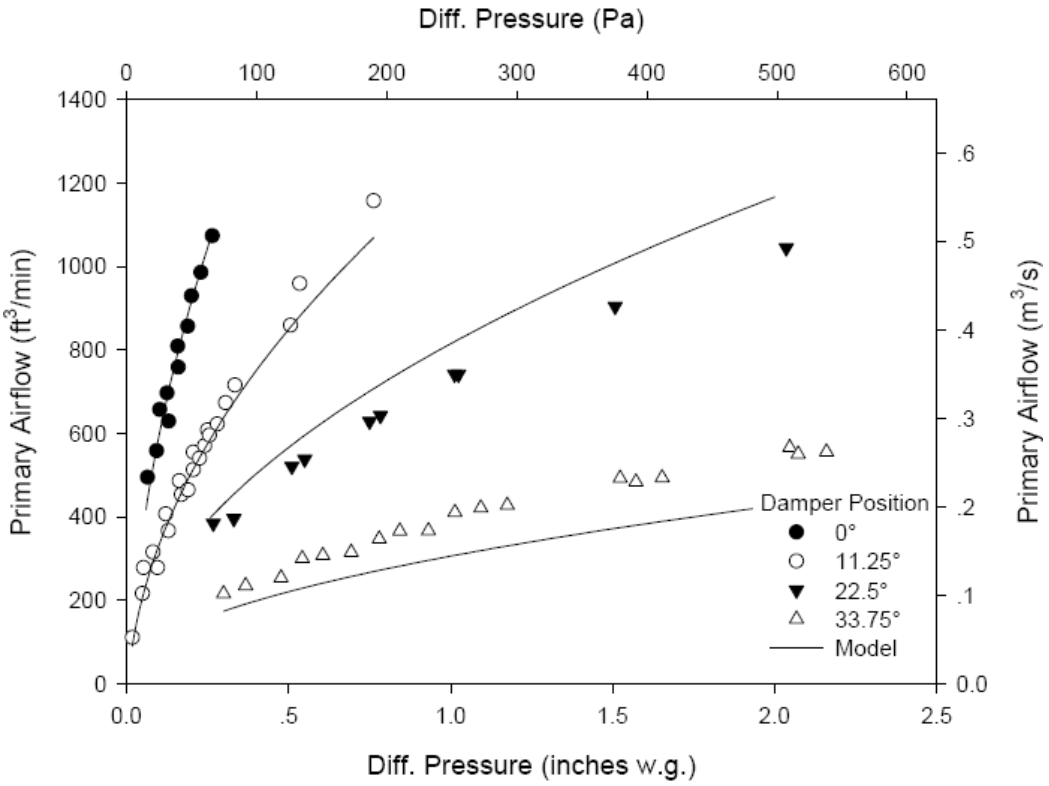

Fig. 8-9 Comparison in Primary Airflow with Correction Factor for S8C_M2

Figure 8-10, 8-11 and 8-12 show the measured and predicted data of plenum airflow for S8A, S12B and S8C_M1. As shown the model was able to predict the trend of plenum airflow. Since the data of plenum airflow was calculated by subtracting primary airflow from fan airflow in the previous studies conducted by Cramlet (2008) and Edmondson (2009) instead of a direct measurement, it resulted in some negative numbers. Those data were deleted before generating the plots because negative plenum airflow was not allowed to happen in real engineering project.

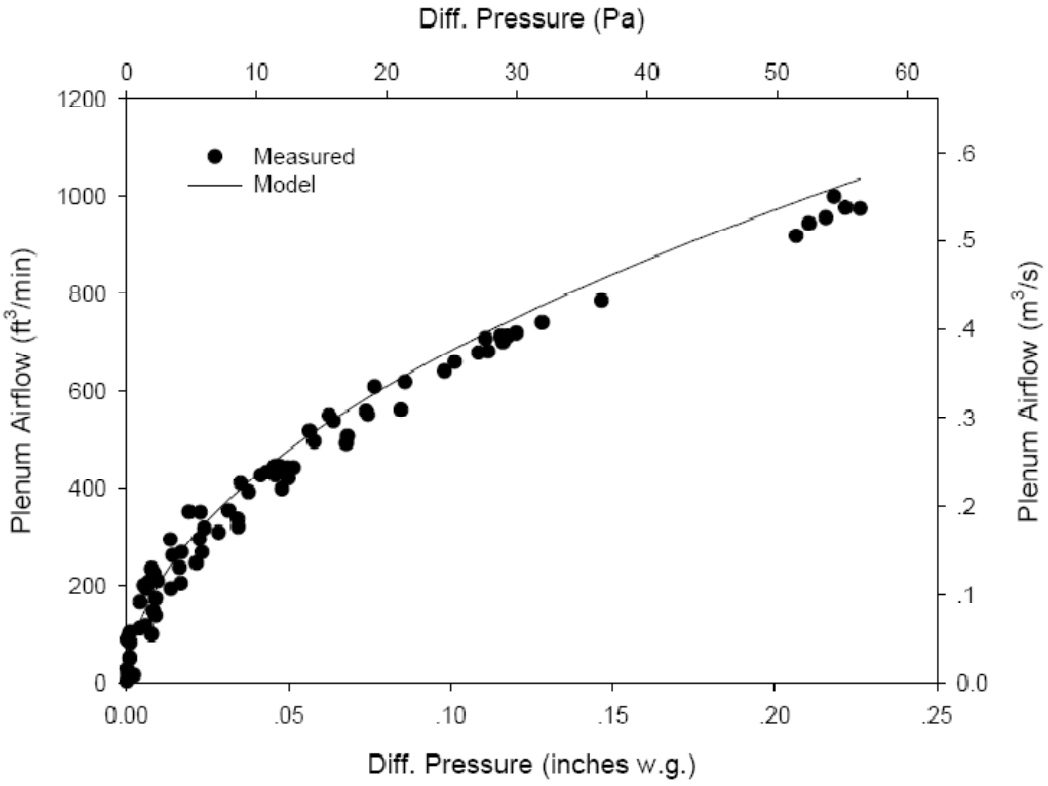

Fig. 8-10 Comparison in Plenum Airflow for Terminal Unit S8A

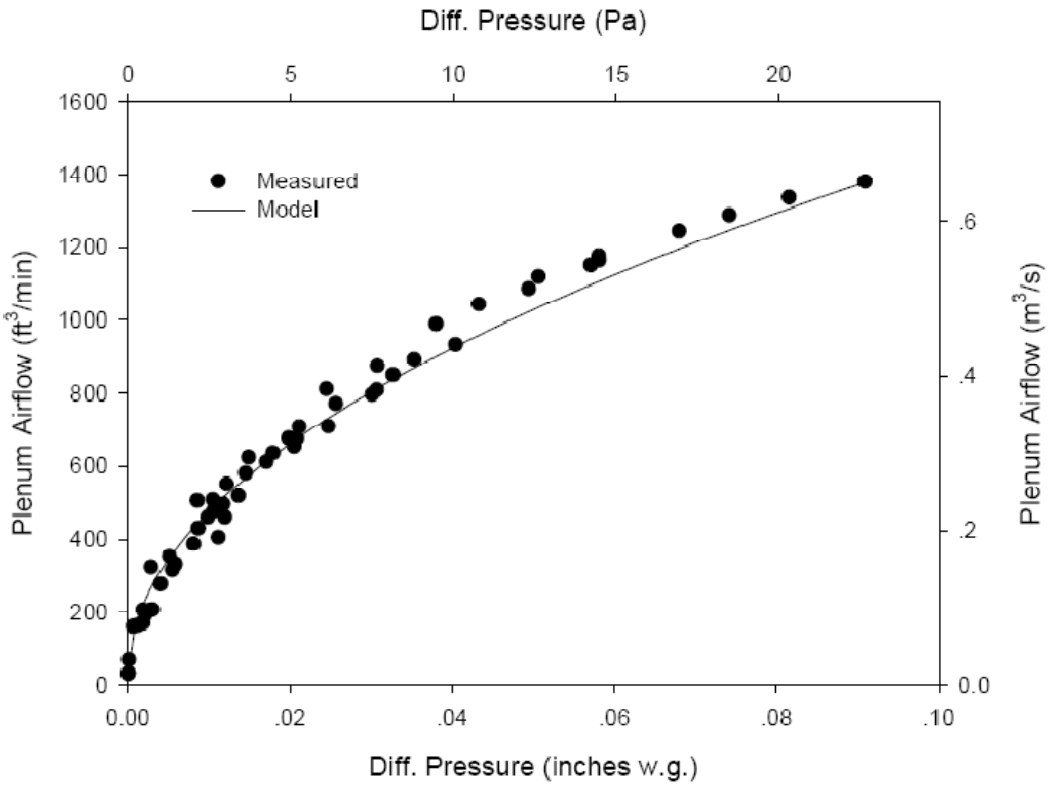

Fig. 8-11 Comparison in Plenum Airflow for Terminal Unit S12B

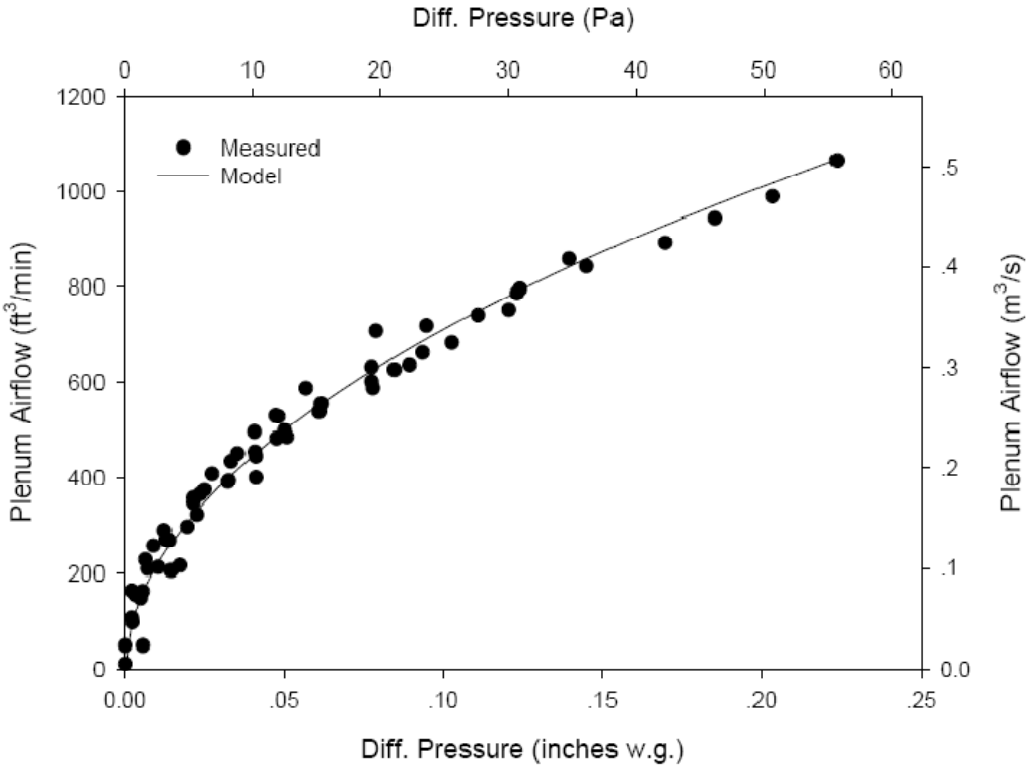

Fig. 8-12 Comparison in Plenum Airflow for Terminal Unit S8C_M2

The measured and predicted data of fan airflow for S8A, S12B and S8C_M2 are shown in Figure 8-13, 8-14 and 8-15. Unlike traditional PSC motors, the ECM motors could compensate for any changes in static pressures, thus providing constant airflow even though the external static pressure or induced air conditions varied. This feature is shown by the horizontal lines that represent the predicted fan airflow. The prediction of fan airflow was consistent with the measurement in previous studies, which proved the validity of the model.

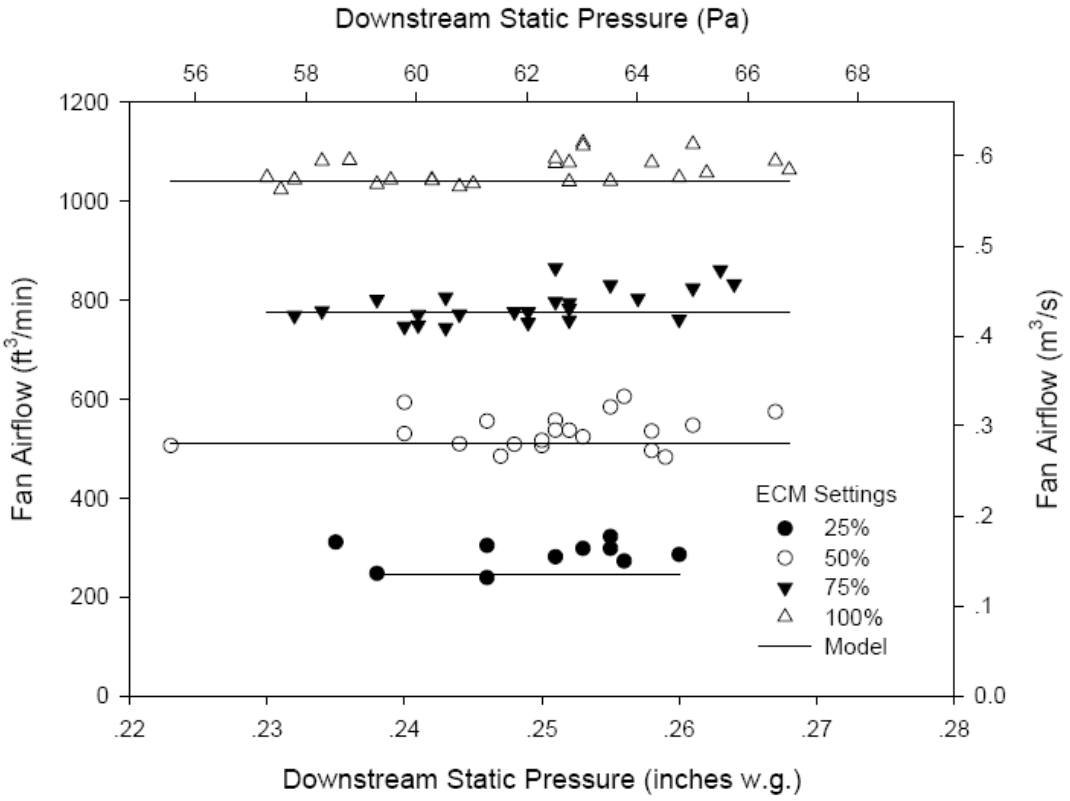

Fig. 8-13 Comparison in Fan Airflow for Terminal Unit S8A

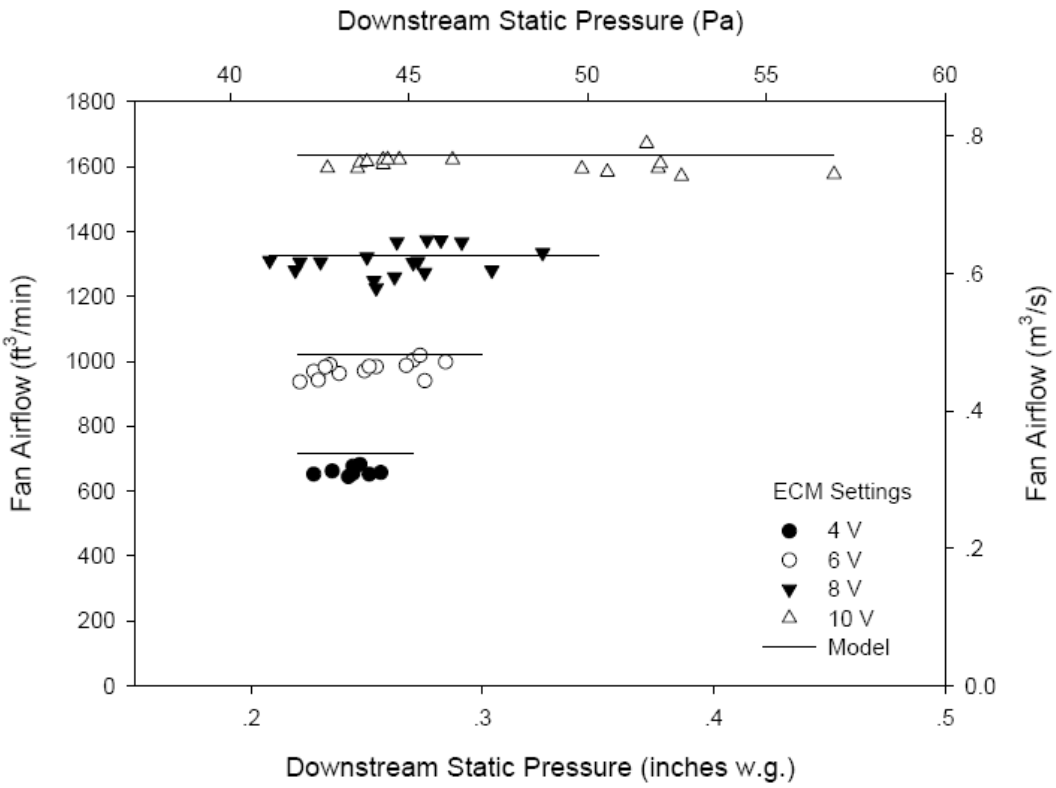

Fig. 8-14 Comparison in Fan Airflow for Terminal Unit S12B

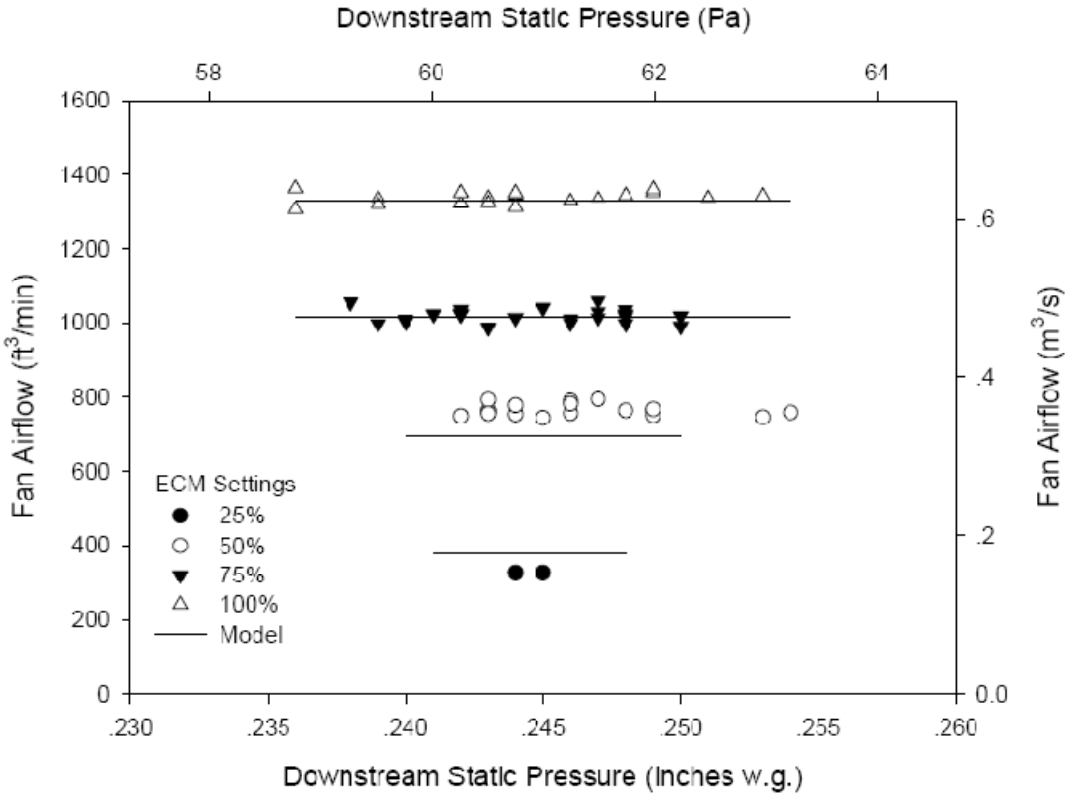

Fig. 8-15 Comparison in Fan Airflow for Terminal Unit S8C_M2

Figure 8-16, 8-17 and 8-18 show the fan power consumption plotted against discharge pressure for the fans in terminal units S8A, S12B and S8C_M2. It was found that the model could provide satisfactory predictions of fan power consumptions in the series FPTUs except for the fan in S8C_M1. For this fan, the prediction did not match the measurement, with one reason for this inconsistency being that the original ECM controller for F_S8C_M1 was missing. An alternative ECM controller had been used

during the tests, and if the original ECM controller for this terminal unit was available, the fan power consumption model could be improved.

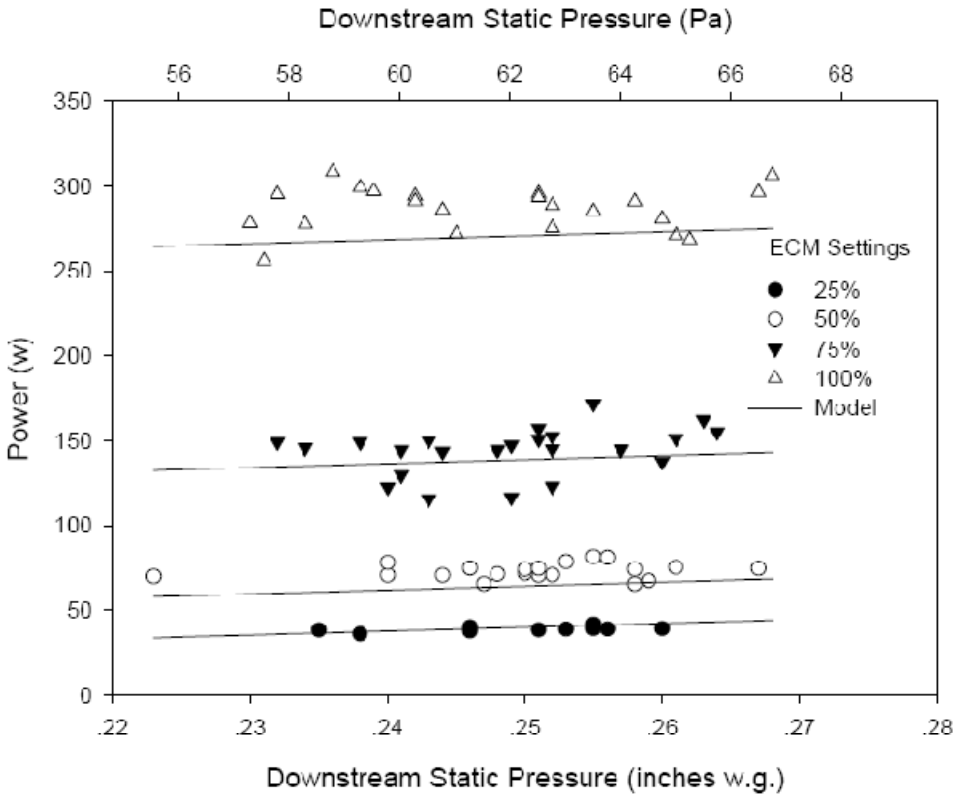

Fig. 8-16 Comparison in Power Consumption for Terminal Unit S8A

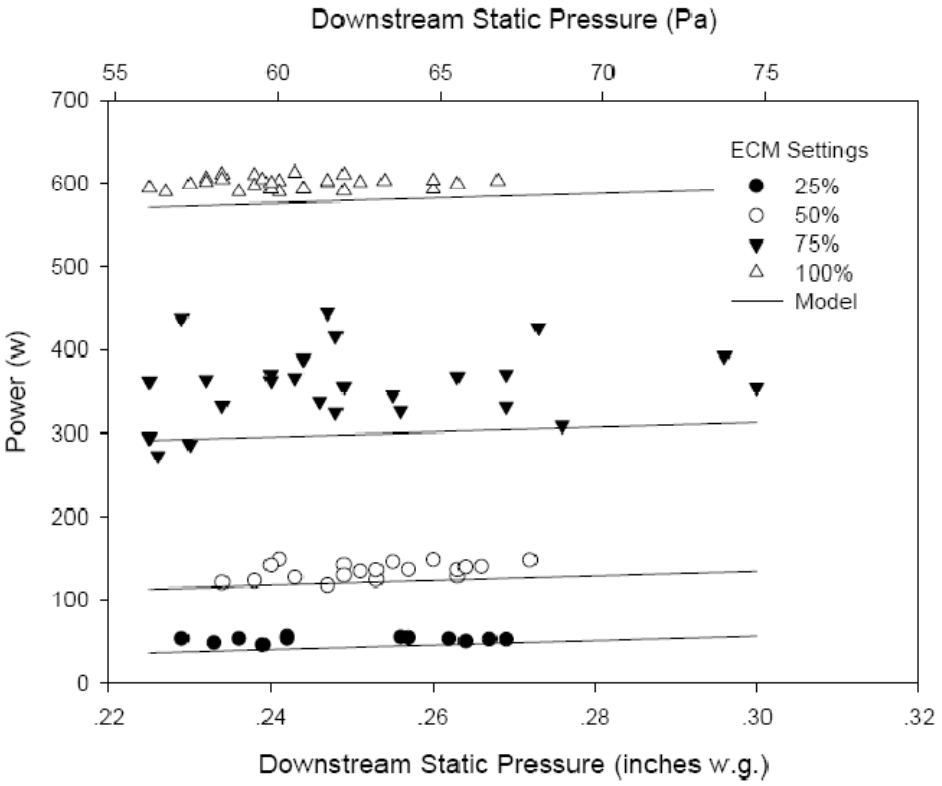

Fig. 8-17 Comparison in Power Consumption for Terminal Unit S12B

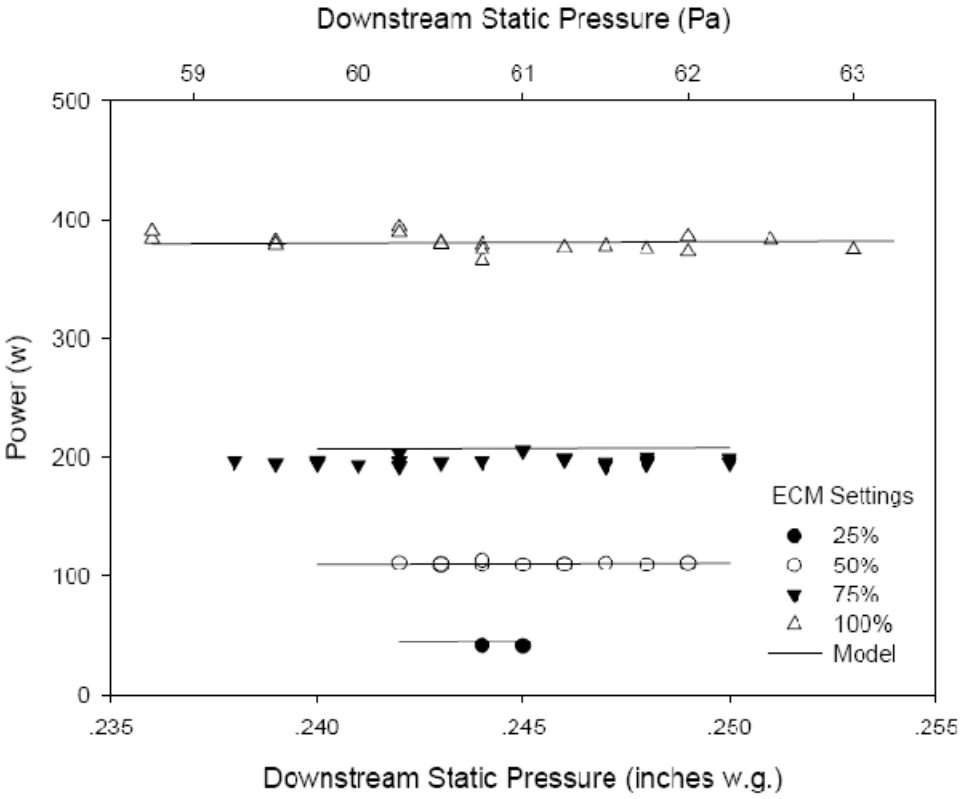

Fig. 8-18 Comparison in Power Consumption for Terminal Unit S8C_M2

Overall, the FPTU model developed from models of primary, fan and plenum airflow was quite able to characterize the airflow and power performance of the FPTUs, and the values predicted by the model showed high consistent with measured data. However, like other models, this model has its own limit in that the models of primary, fan and plenum airflow, as well as power, were only valid in the designed operation range. If inappropriate settings are input into this model, either no results or an inaccurate would be generated.

CHAPTER IX

SUMMARY AND CONCLUSIONS

Previous studies have shown that the VAV systems are more energy efficient than the traditional CAV system. The fan-powered VAV terminal units are the zone-level control devices in a VAV system. And they come either in parallel or series configurations. One difference between the two configurations is that the fan on the series terminal unit requires continuous operation while the fan on the parallel terminal unit can operate intermittently. Furr (2006) developed several models for FPTUs with PSC motors to characterize the airflow performance and power consumption.

Because of its potential to save energy, some FPTUs are starting to equip with ECM motors. Cramlet (2008) conducted some experiments and generated a preliminary model for one parallel and one series terminal units with ECM motors. Edmondson (2009) extended the work of Cramlet to seven series and seven parallel FPTUs with ECM motors. Models of the same form used by Furr (2006) were applied in the Cramlet (2008) and Edmondson's (2009) studies to characterize the various performances of terminal units with ECM motors.

To develop the semi-empirical models of series FPTUs and extend their applicability, every component was taken out of the series FPTUs and tested seperately in

this study. Some necessary modifications were made to the model and test matrix used in previous studies. In addition, four models were generated to characterize the performance of series FPTUs with ECM motors.

The first was the primary airflow model, which used the damper setting as well as the differential pressure across the damper as two individual variables. Four correlations following the same form were generated for various types and sizes of dampers. This model had a R^2 value the ranged from 0.948 to 0.993. Some data were missing because the primary blower was unable to provide adequate airflow to reach the target differential pressure. This model could be improved if these missing test points were available. In addition, large measurement errors in the lower half of the damper operating range was another problem that needed to be solved.

The second model was the fan airflow model, which only depended on the ECM setting. Since ECM motor could compensate for any variation in static pressure, the fan airflow should be independent of the upstream or discharge static pressure. The R^2 value of this model varied from 0.937 to 0.998. The low R^2 value for some fans suggested that the discharge pressure could still affect the fan airflow, but this influence was not as strong as for the PSC motor. Also, it was found that the fan airflow was difficult to predict if the fan was working outside of its designed range. In this situation the fan airflow was greatly

influenced by the discharge pressure, and the fan could not provide a constant volume flow rate.

The third model was plenum airflow, which was a newly established model. Due to the difficultly measuring in plenum airflow, model had not been developed in previous studies. The plenum airflow could be expressed as a function of inlet area and differential pressure, which was calculated from the internal and environmental pressures. Two correlations were generated for the two different arrangements of plenum airflow. With the exception of one terminal unit, which did not behave like others, both of the models had the same form for different configurations. This model had R^2 values above 0.99. Because of the difficulty in direct measurement of plenum airflow, it was calculated from primary and fan airflow. If more accurate data were acquired, it was possible to modify and improve the model by comparing the measured and predicted data.

The last model was for fan power consumption. The ECM setting and discharge pressure were considered as two variables in this model. The lowest R^2 value of this model was 0.986 and highest one was 0.998, which correlated the measured data well. The power consumption model was of great importance. It can be used to predict the potential power needed for the terminal unit operating with the ECM motor, and compare the power consumption at different operating condition.

In the primary airflow model, internal pressure was used instead of downstream static pressure. This modification totally eliminated the offset that was generated in previous study. By solving a group of equations formed by primary, plenum, fan airflow models as well as mass conservation equations, the airflow performance of FPTUs was characterized.

Verification was made to prove the FPTU model's validity by comparing the measured and predicted data of airflow and power consumption. Correction factors were employed in the primary airflow model to compensate for the difference caused by large measurement errors in the damper's higher half of operating range and the system effects by using the sub-models to form the FPTU model. The predicted values were consistent with measurements and no offset was needed in the primary airflow model. Generally, the newly established models were able to describe the airflow performance as well as power consumption of series FPTUs without adding complexity.

From the comparison between the prediction and measurement, it was concluded that the series FPTUs model was not a simple combination of sub-models of primary, plenum and fan airflow. The system effects caused by the differences between the installed conditions and the ways used in the laboratory tests should be considered when building up the series FPTUs model.

In conjunction with the results from previous studies, these models can be used to investigate if FPTUs will have better performance than non-powered terminal units in different operating conditions. Also, by employing the models for the parallel terminal units, they can be used to determine which configuration is more energy efficient for different application and climate conditions. In addition, using the model for terminal unit with the PSC motor, a comparison between terminal units with different motors can be made and the benefit gained by using ECM motors can be determined. Based on the airflow and power consumption characteristics of the series FPTU provided by the models, it will be easier for engineers to choose the size and type of terminal units for specific application.

REFERENCES

Abney, J., D. Int-Hout, and G. Jones. 2000. ECM motors in series flow fan powered terminals and unit ventilators. White Paper. http://www.titus-hvac.com/resources/files/whiteecm.pdf

Ardehali, M.M., and T.F. Smith. 1996. Evaluation of variable volume and temperature HVAC system for commercial and residential buildings. *Energy Conversion Management* 37(9): 1469-1479

ASHRAE. 2007. ANSI/ASHRAE Standard 51-07. *Laboratory Methods of Testing Fans for Certified Aerodynamic Performance Rating*. Atlanta, GA: American Society of Heating, Refrigeration and Air-Conditioning Engineers, Inc.

ASHRAE. 2007. ANSI/ASHRAE Standard 62.1-2007. *Ventilation for Acceptable Indoor Air Quality*. Atlanta, GA: American Society of Heating, Refrigeration and Air-Conditioning Engineers, Inc.

ASHRAE. 2008. ANSI/ASHRAE Standard 120-2008. *Method of Testing to Determine Flow Resistance of HVAC Ducts*. Atlanta, GA: American Society of Heating, Refrigeration and Air-Conditioning Engineers, Inc.

ASHRAE. 2008. ANSI/ASHRAE Standard 130-2008. *Method of Testing for Rating Ducted Air Terminal Units*. Atlanta, GA: American Society of Heating, Refrigeration and Air-Conditioning Engineers, Inc.

Cramlet, A. 2008. Performance of ECM controlled VAV fan power terminal units. M.S. Thesis, Texas A&M University, College Station.

Edmondson, J.L. 2009. Modeling of ECM controlled fan-powered terminal units. M.S. Thesis, Texas A&M University, College Station.

Elleson, J.S. 1993. Energy use of fan-powered mixing boxes with cold air distribution. *ASHRAE Transactions* 99(1): 1394-1358

Furr, J.C. 2006. Development of models for series and parallel fan variable air volume terminal units. M.S. Thesis, Texas A&M University, College Station.

Khoo, I., G.J. Levermore, and K.M. Letherman. 1998. Variable-air-volume terminal units I: Steady-state models. *Building Services Engineering Research & Technology* 19(3): 155-162

Mei, L., and G.J. Levermore. 2002. Simulation and validation of a VAV system with an ANN fan model and a non-linear VAV box model. *Building and Environment* 37: 277-284

APPENDIX A

PRIMARY AIRFLOW

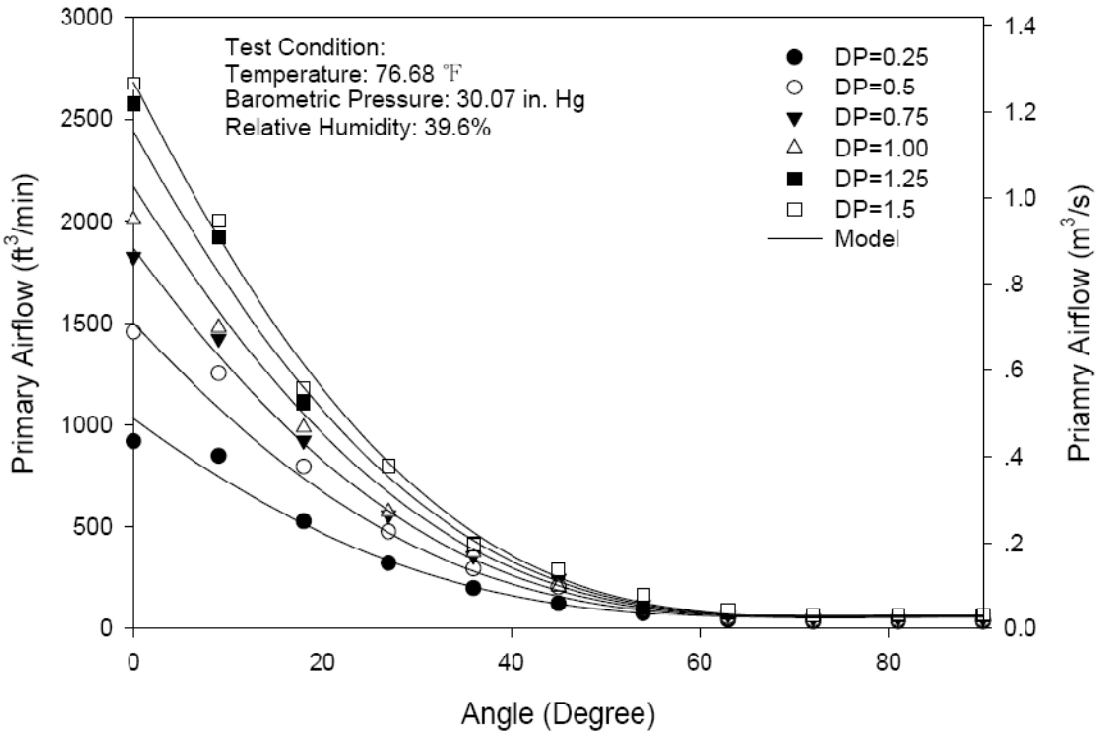

Fig. A-1 Primary Airflow vs. Damper Position for BF8

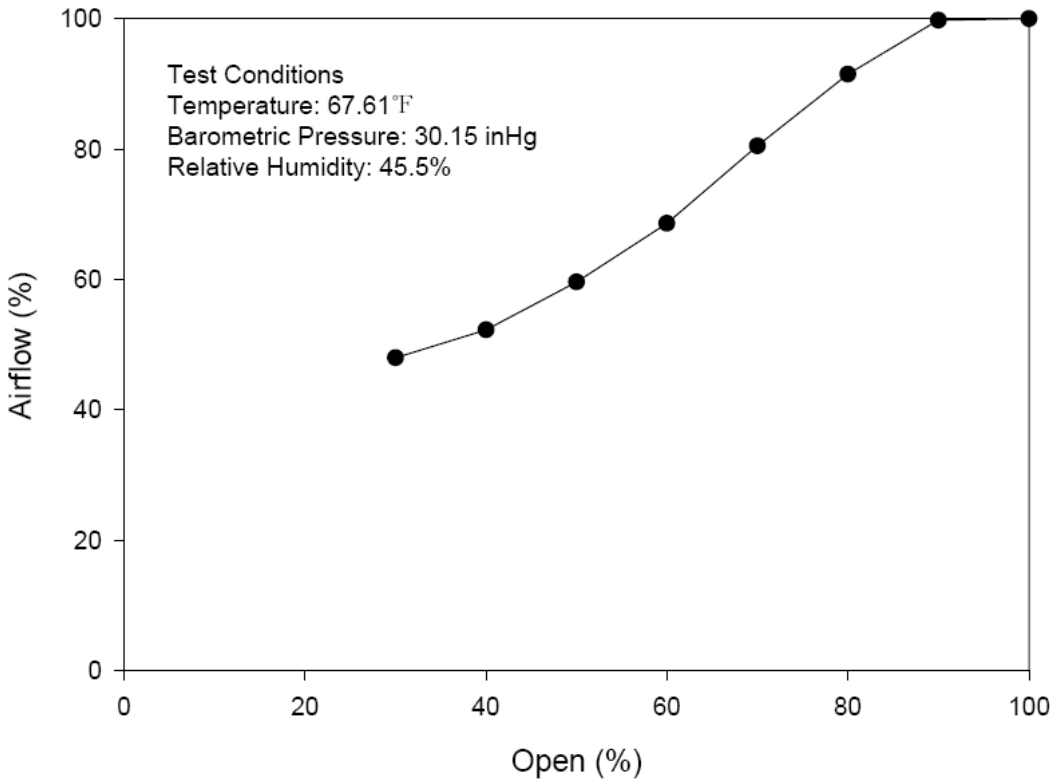

Fig. A-2 Primary Airflow Percentage vs. Damper Position for BF8

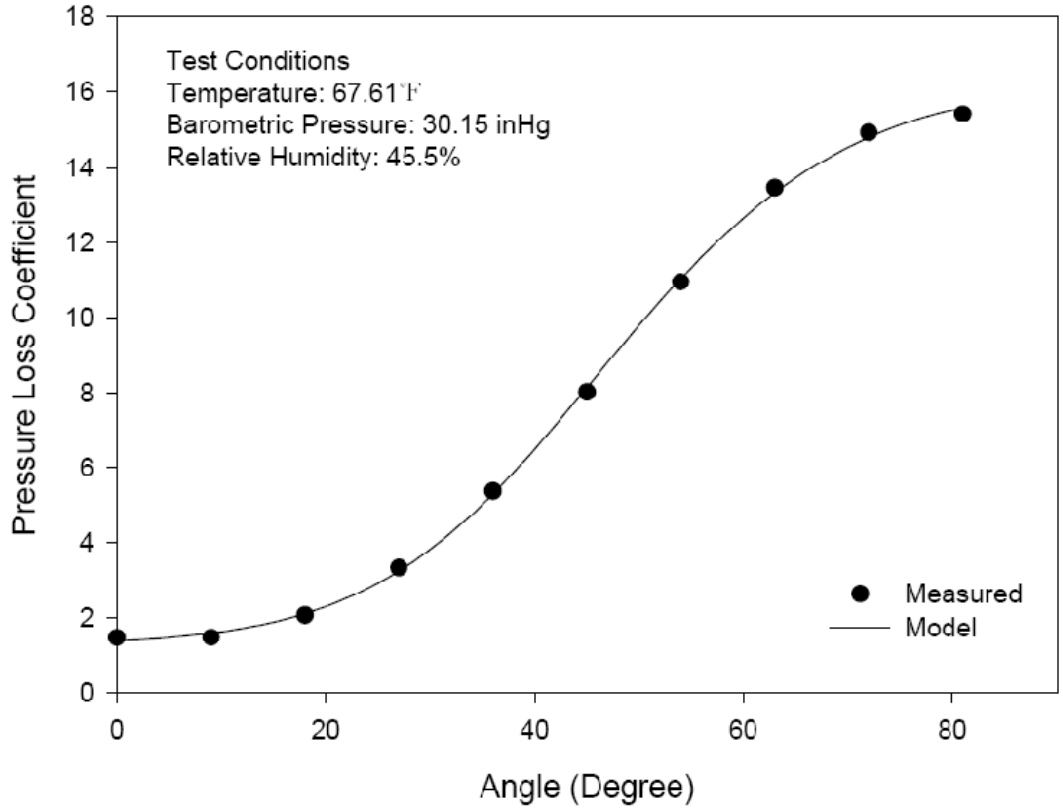

Fig. A-3 Pressure Loss Coefficient vs. Damper Position for BF8

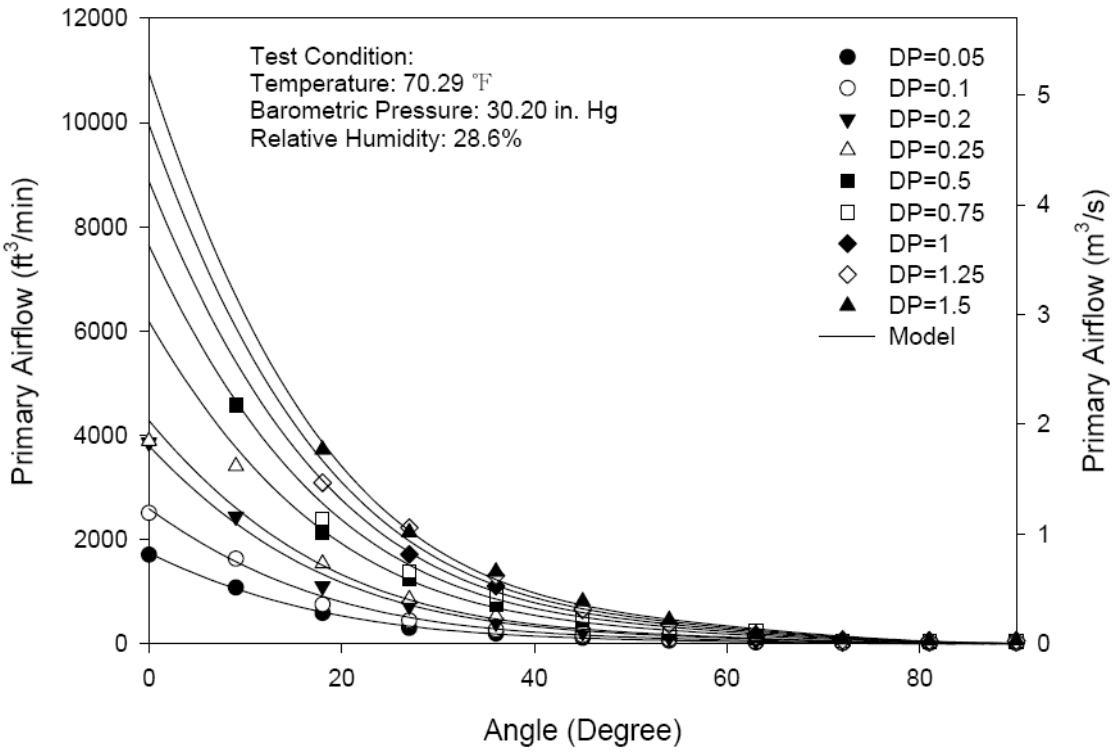

Fig. A-4 Primary Airflow vs. Damper Position for BF12

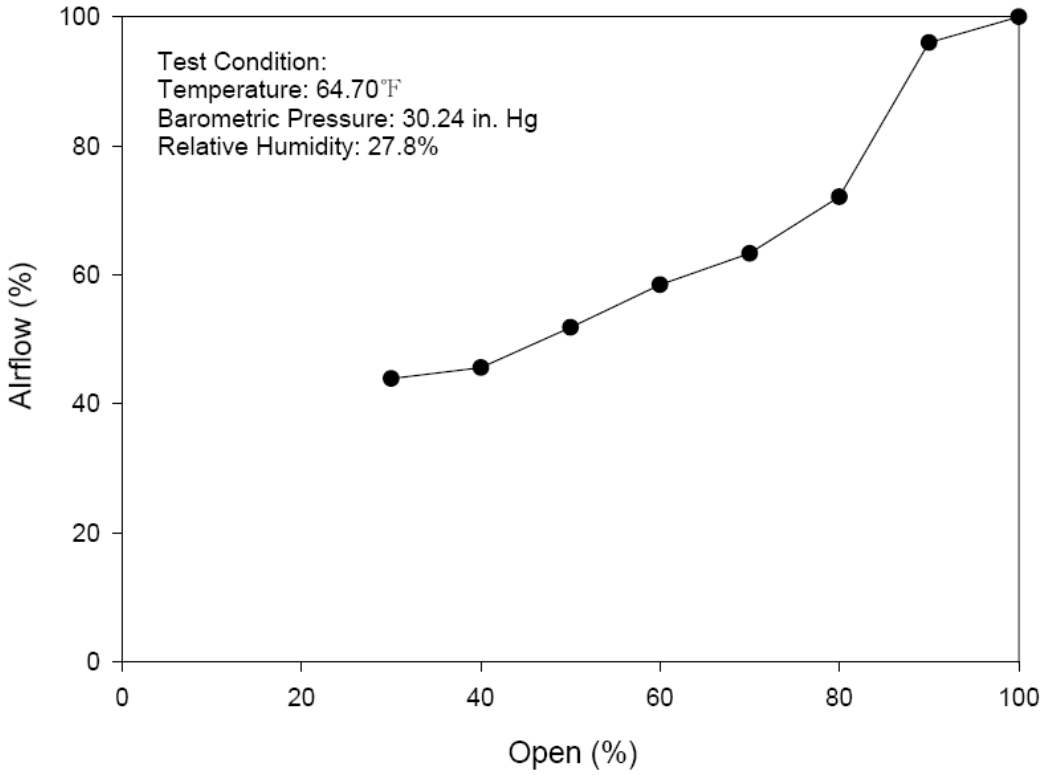

Fig. A-5 Primary Airflow Percentage vs. Damper Position for BF12

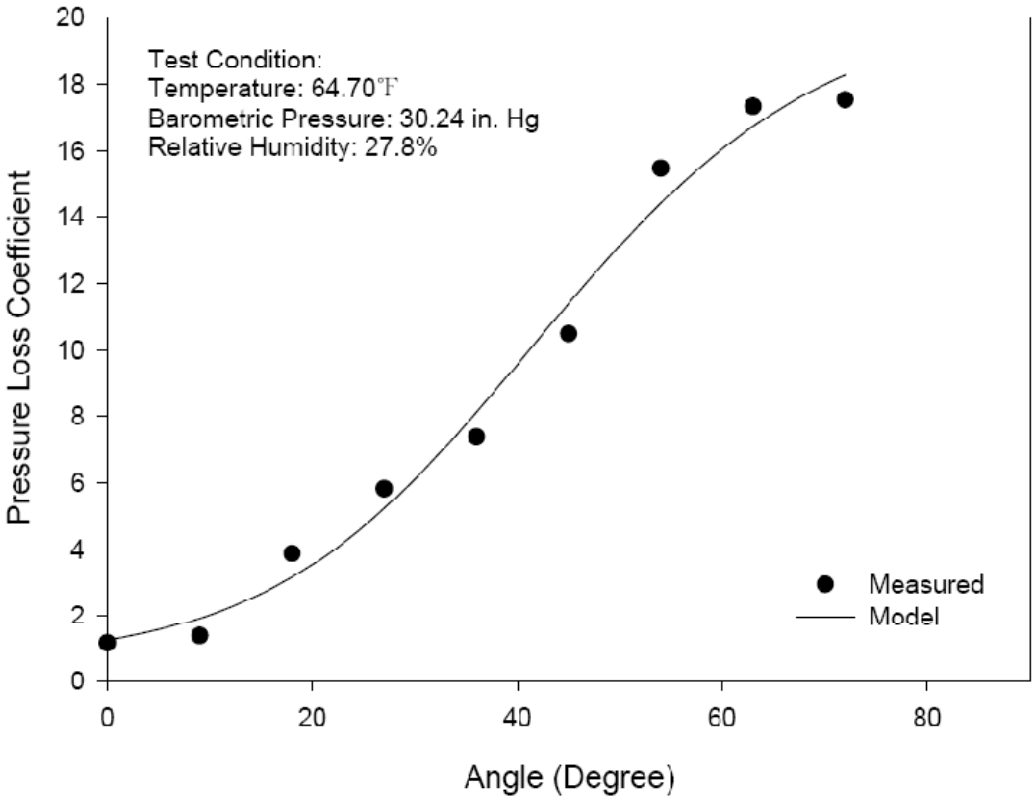

Fig. A-6 Pressure Loss Coefficient vs. Damper Position for BF12

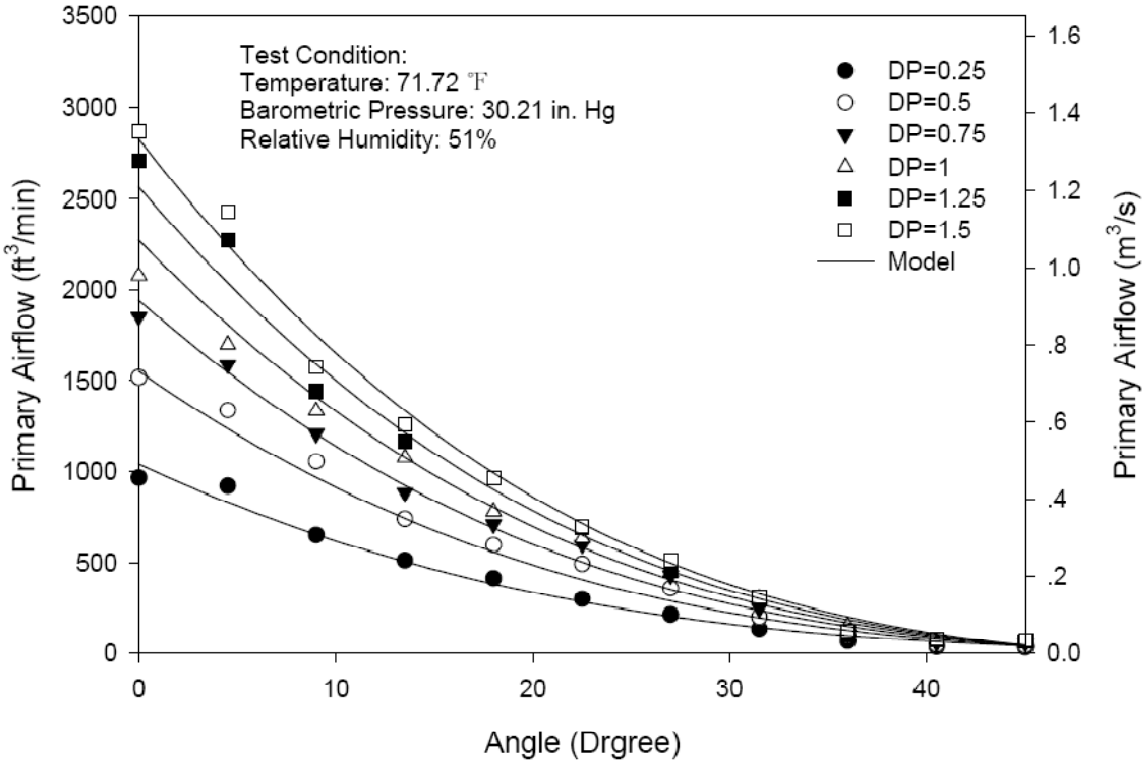

Fig. A-7 Primary Airflow vs. Damper Position for OB8

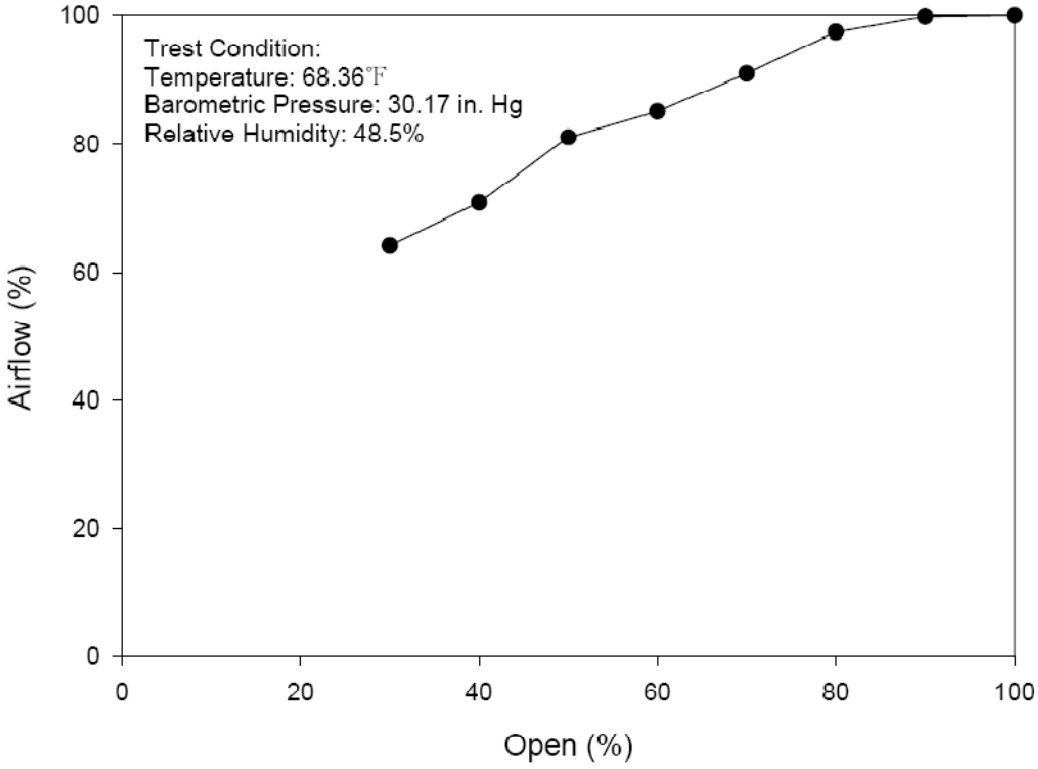

Fig. A-8 Primary Airflow Percentage vs. Damper Position for OB8

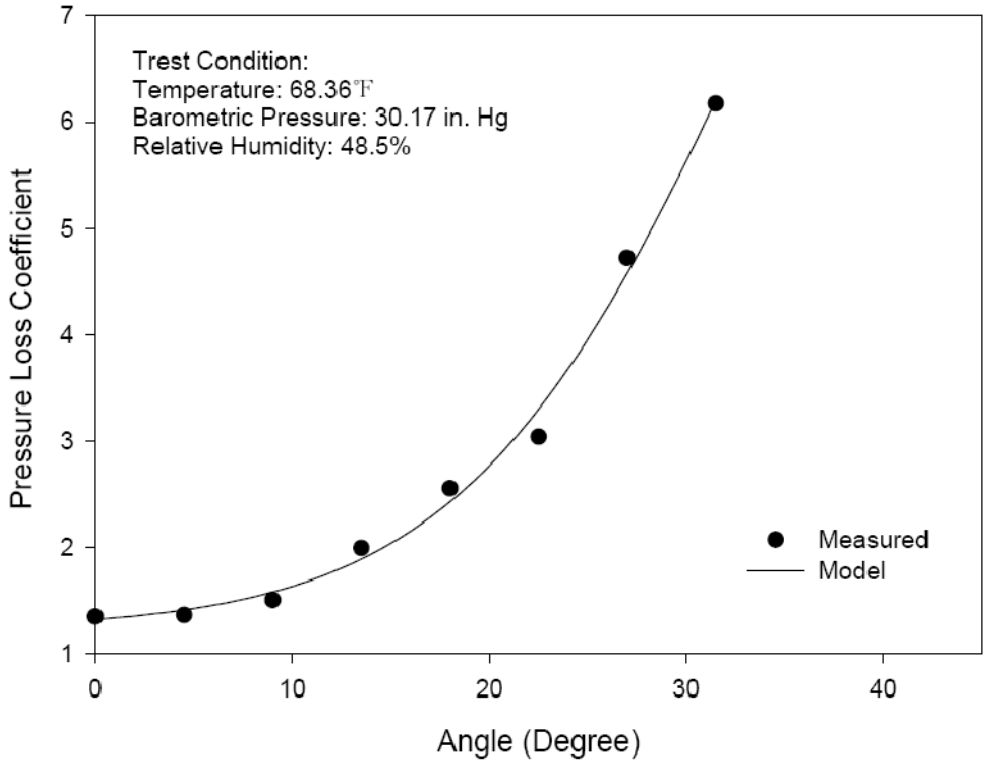

Fig. A-9 Pressure Loss Coefficient vs. Damper Position for OB8

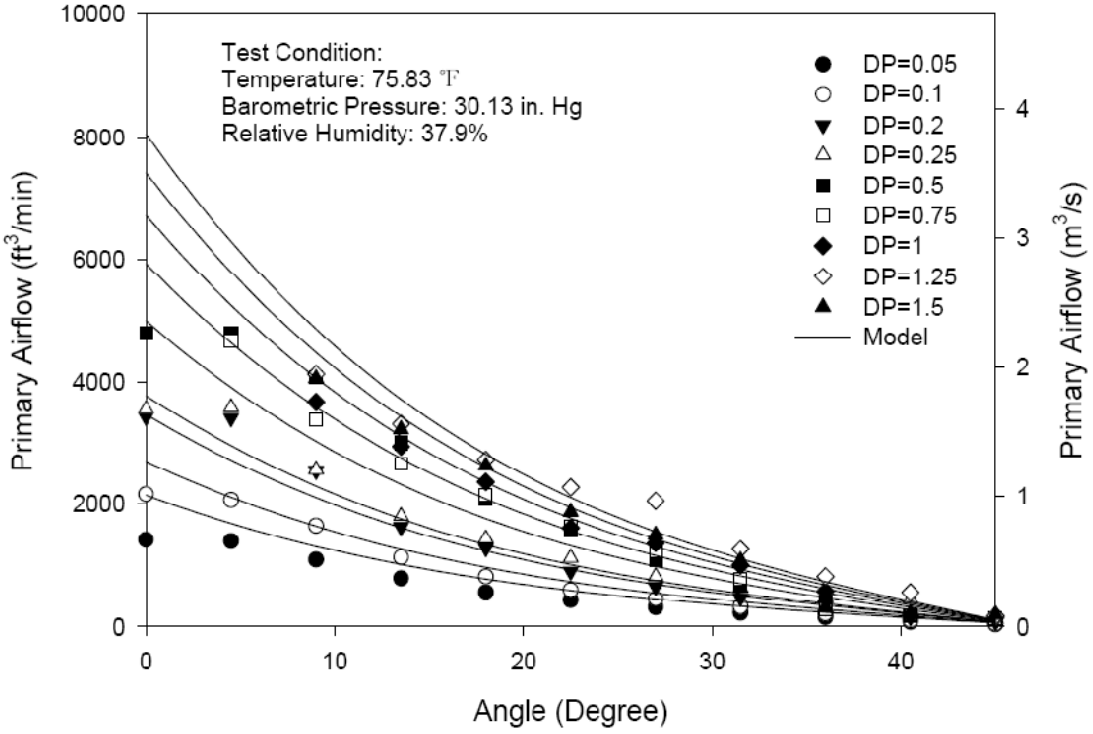

Fig. A-10 Primary Airflow vs. Damper Position for OB12

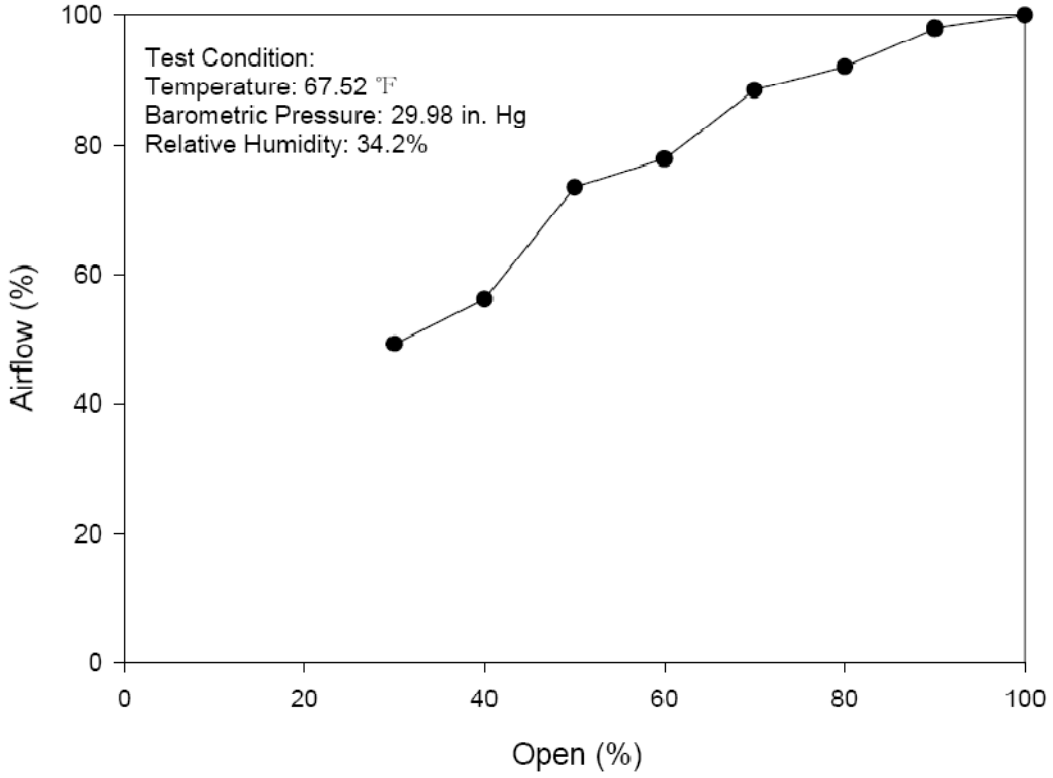

Fig. A-11 Primary Airflow Percentage vs. Damper Position for OB12

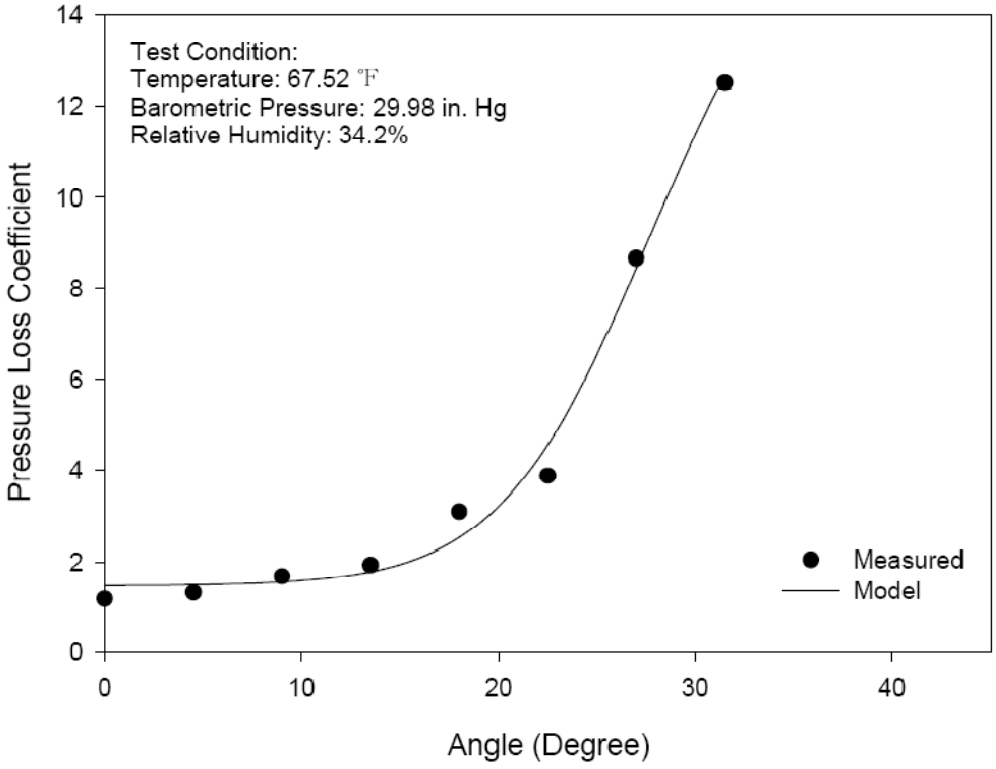

Fig. A-12 Pressure Loss Coefficient vs. Damper Position for OB12

APPENDIX B

FAN AIRFLOW

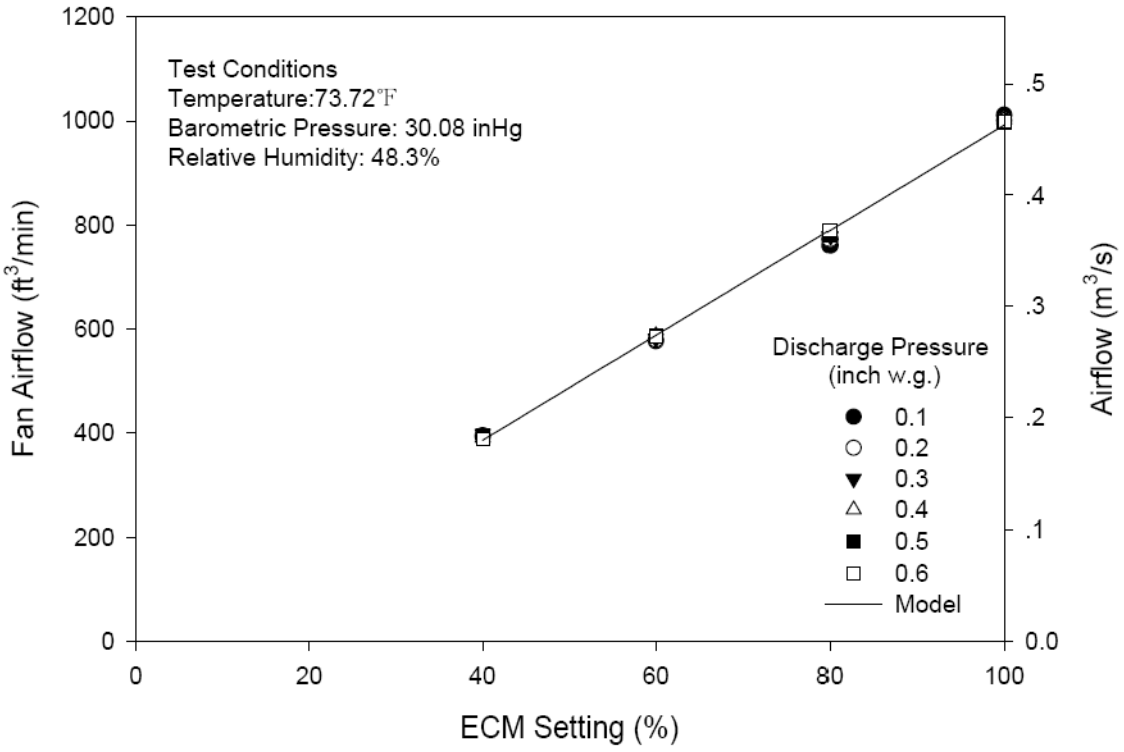

Fig. B-1 Fan Airflow vs. ECM Settings for F_S8A

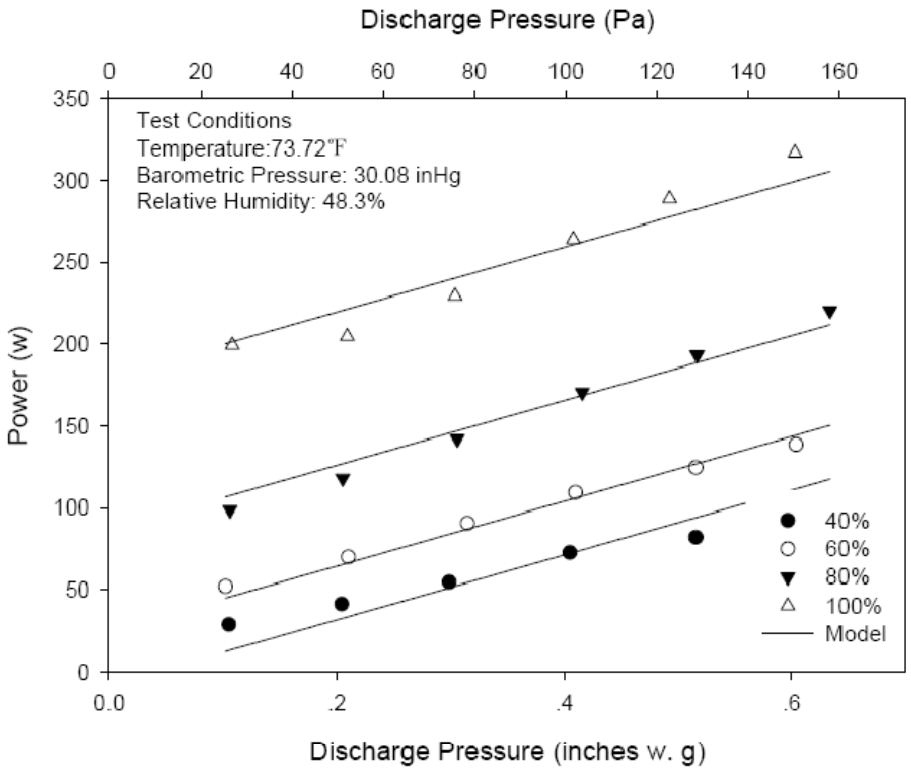

Fig. B-2 Fan Power vs. Discharge Pressure for F_S8A

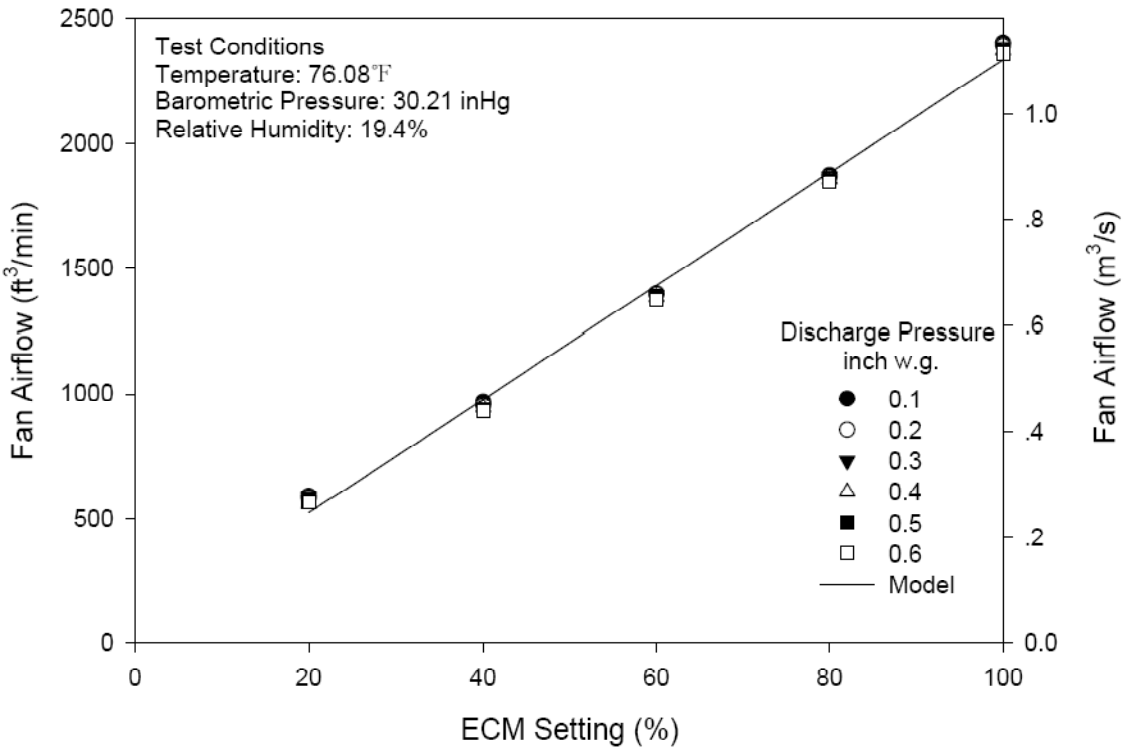

Fig. B-3 Fan Airflow vs. ECM Settings for F_S12A

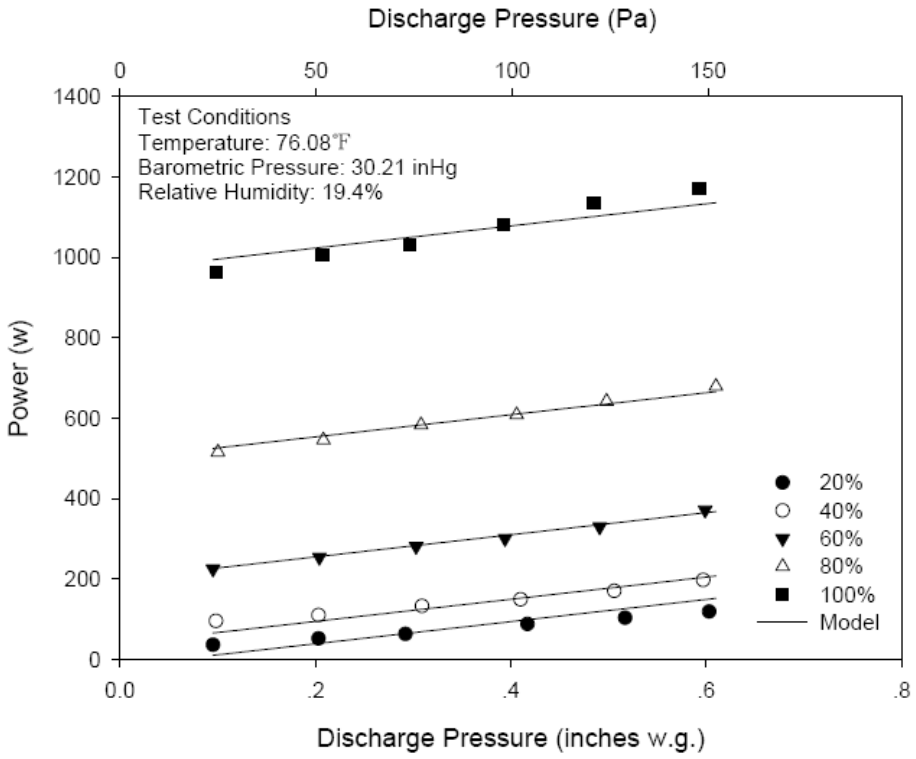

Fig. B-4 Fan Power vs. Discharge Pressure for F_S12A

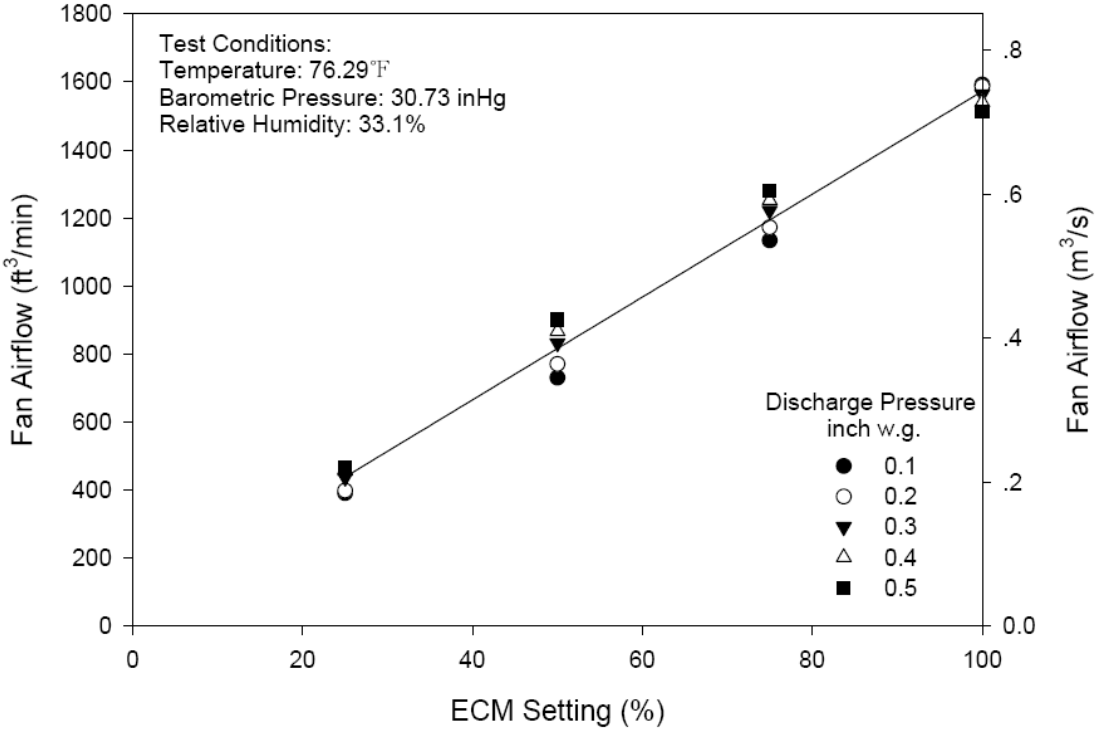

Fig. B-5 Fan Airflow vs. ECM Settings for F_S8B

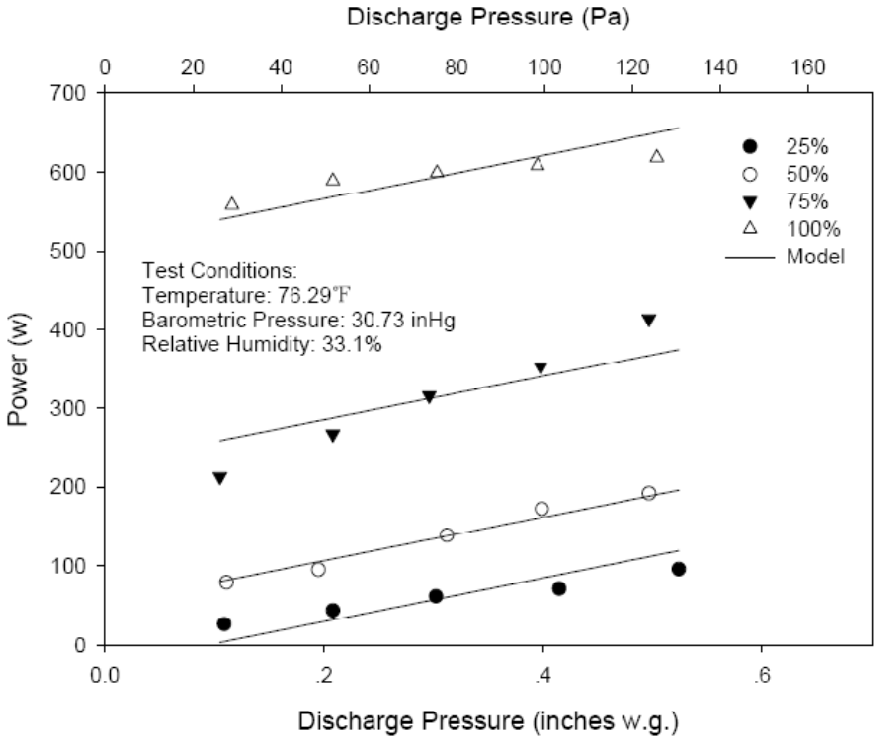

Fig. B-6 Fan Power vs. Discharge Pressure for F_S8B

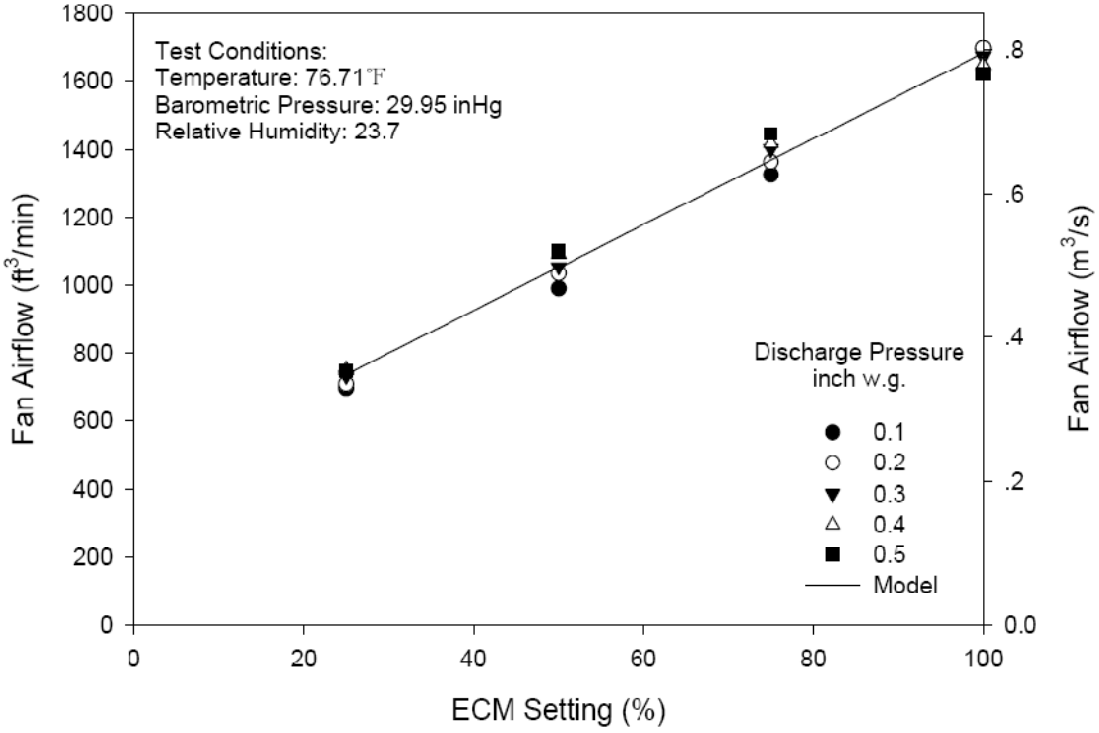

Fig. B-7 Fan Airflow vs. ECM Settings for F_S12B

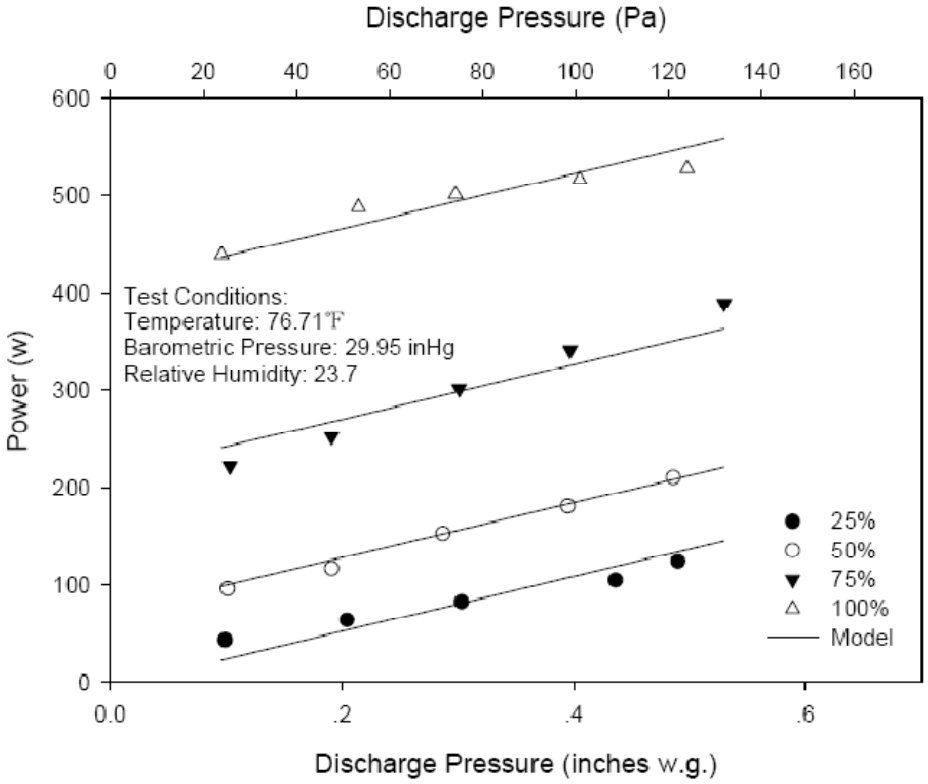

Fig. B-8 Fan Power vs. Discharge Pressure for F_S12B

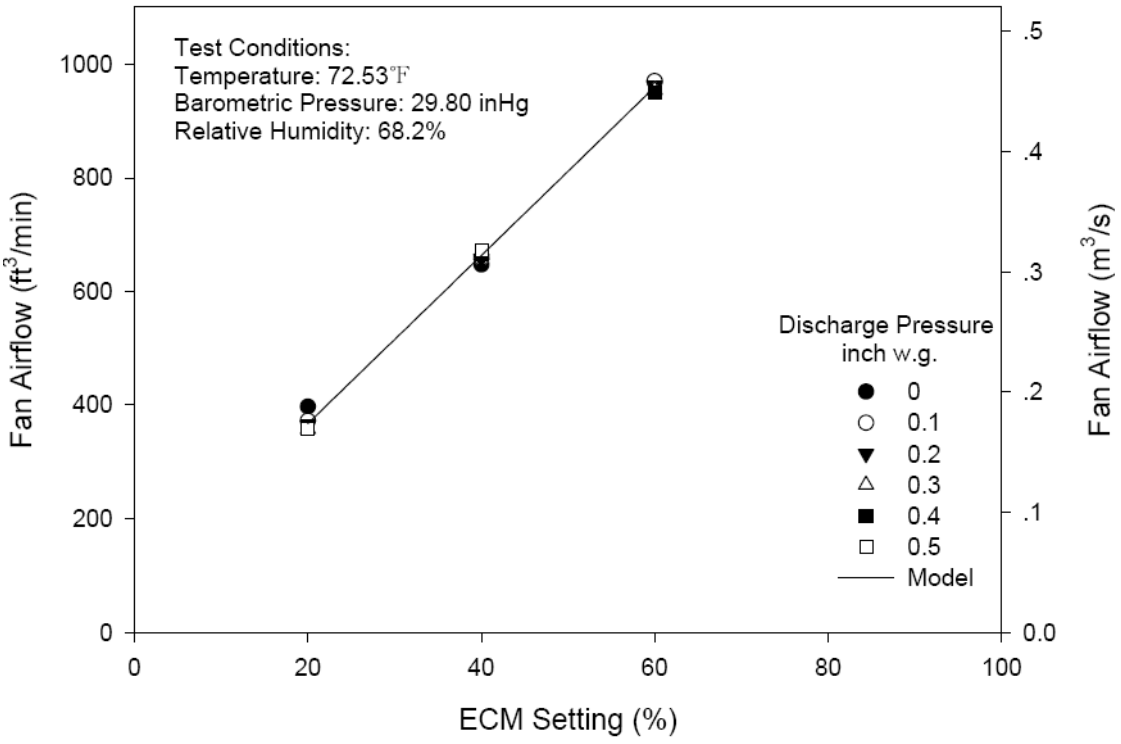

Fig. B-9 Fan Airflow vs. ECM Settings for F_S8C_M1

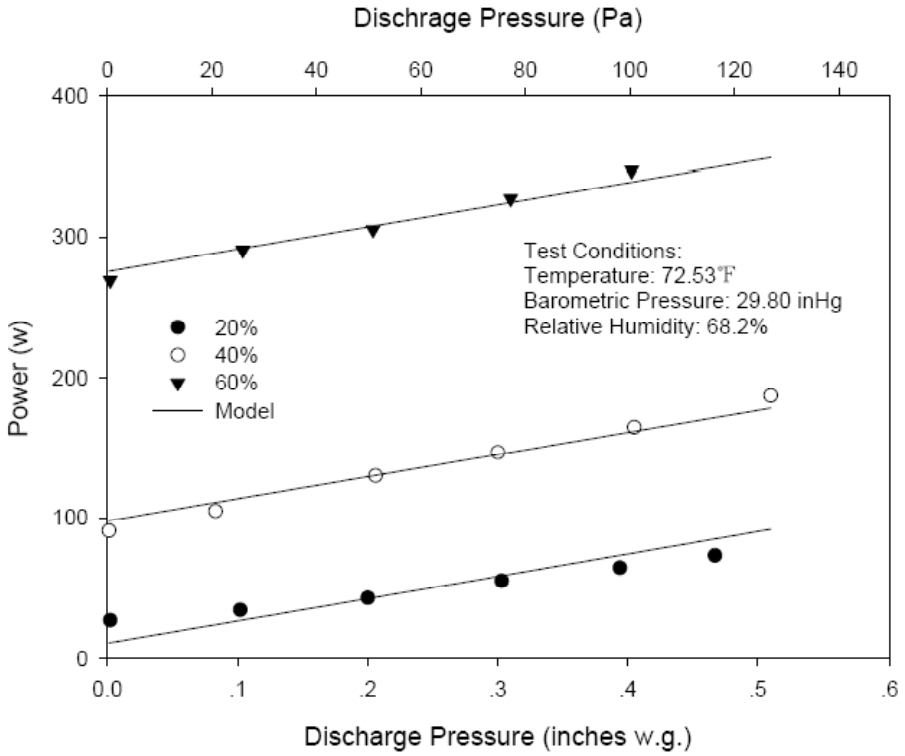

Fig. B-10 Fan Power vs. Discharge Pressure for F_S8C_M1

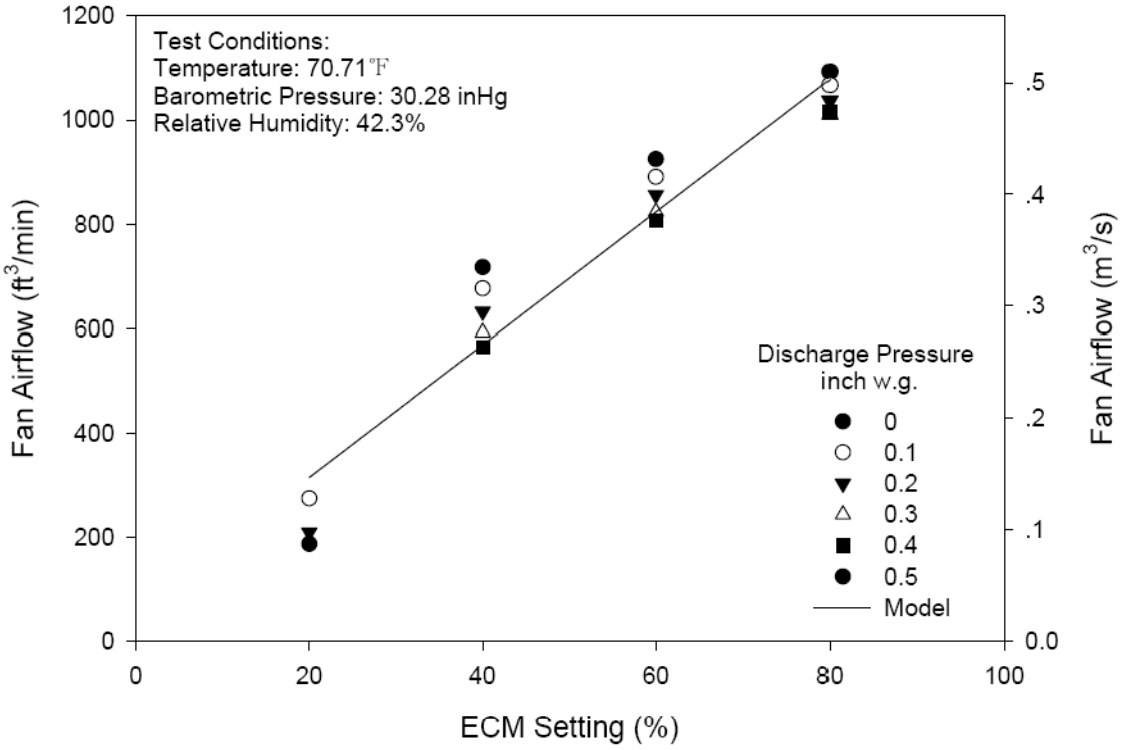

Fig. B-11 Fan Airflow vs. ECM Settings for F_S8C_M2

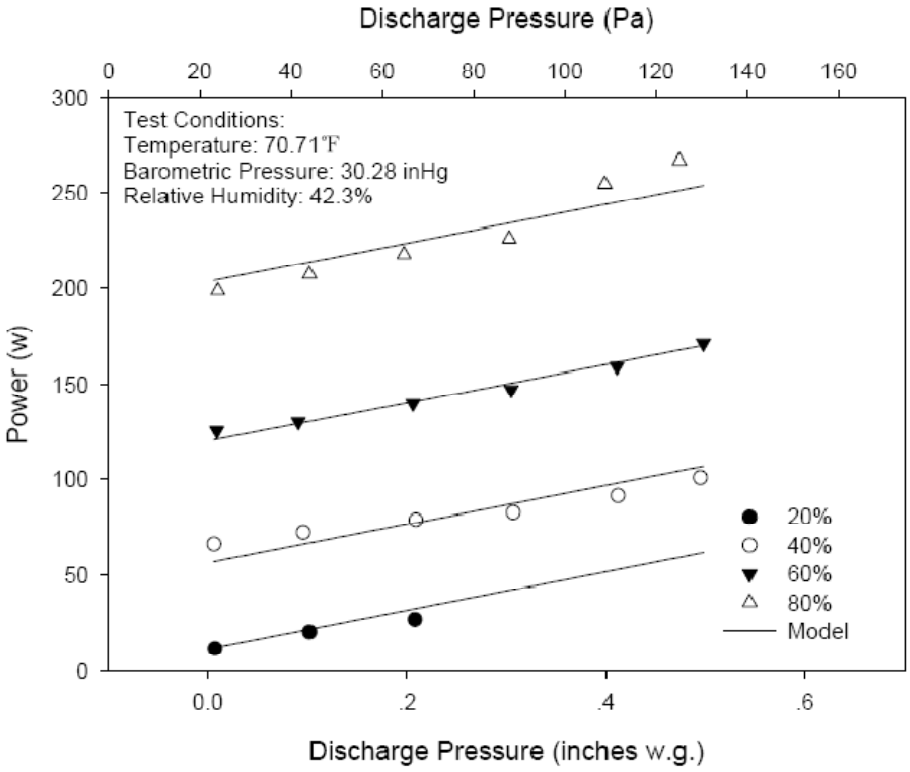

Fig. B-12 Fan Power vs. Discharge Pressure for F_S8C_M2

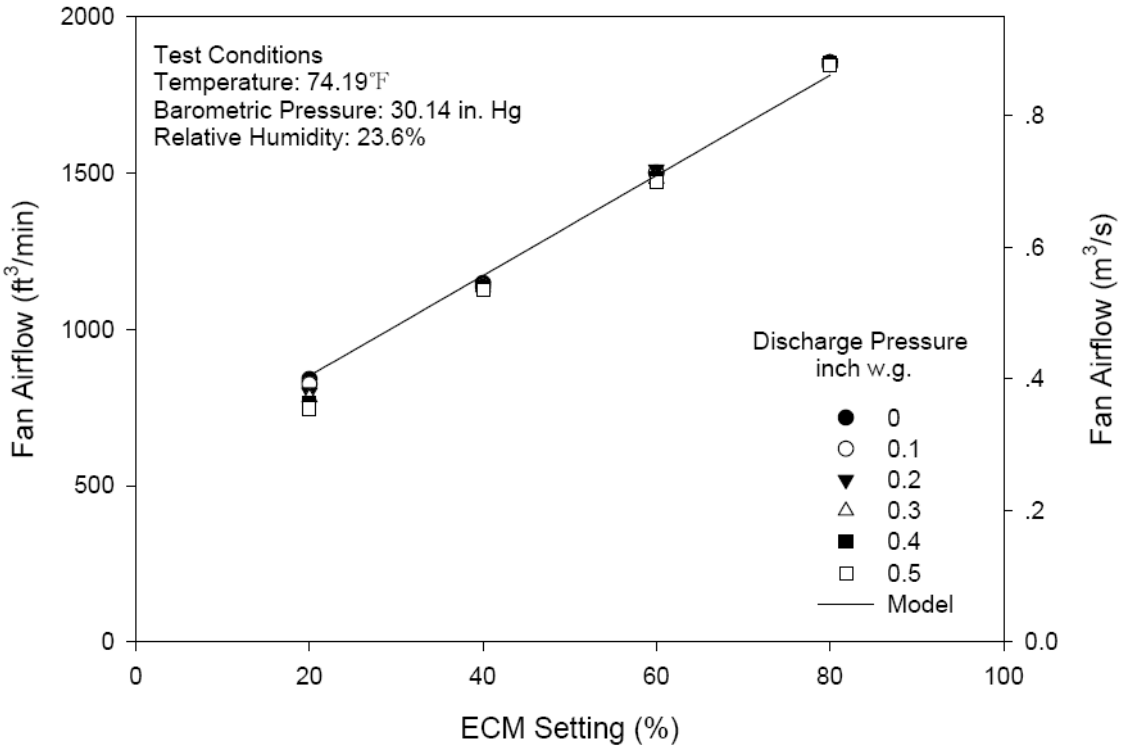

Fig. B-13 Fan Airflow vs. ECM Settings for F_S12C_M1

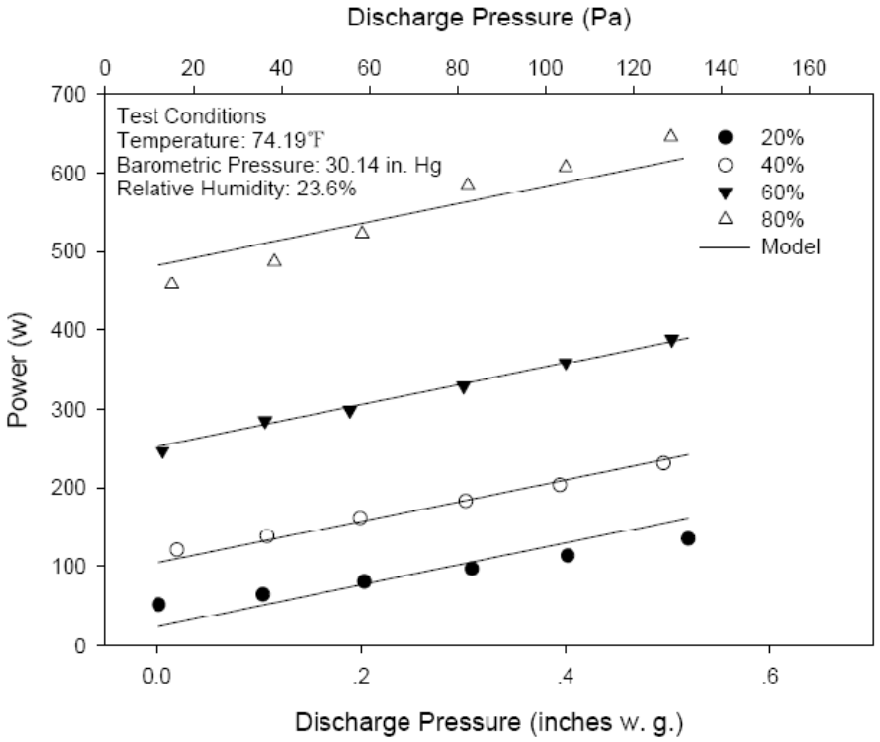

Fig. B-14 Fan Power vs. Discharge Pressure for F_S12C_M1

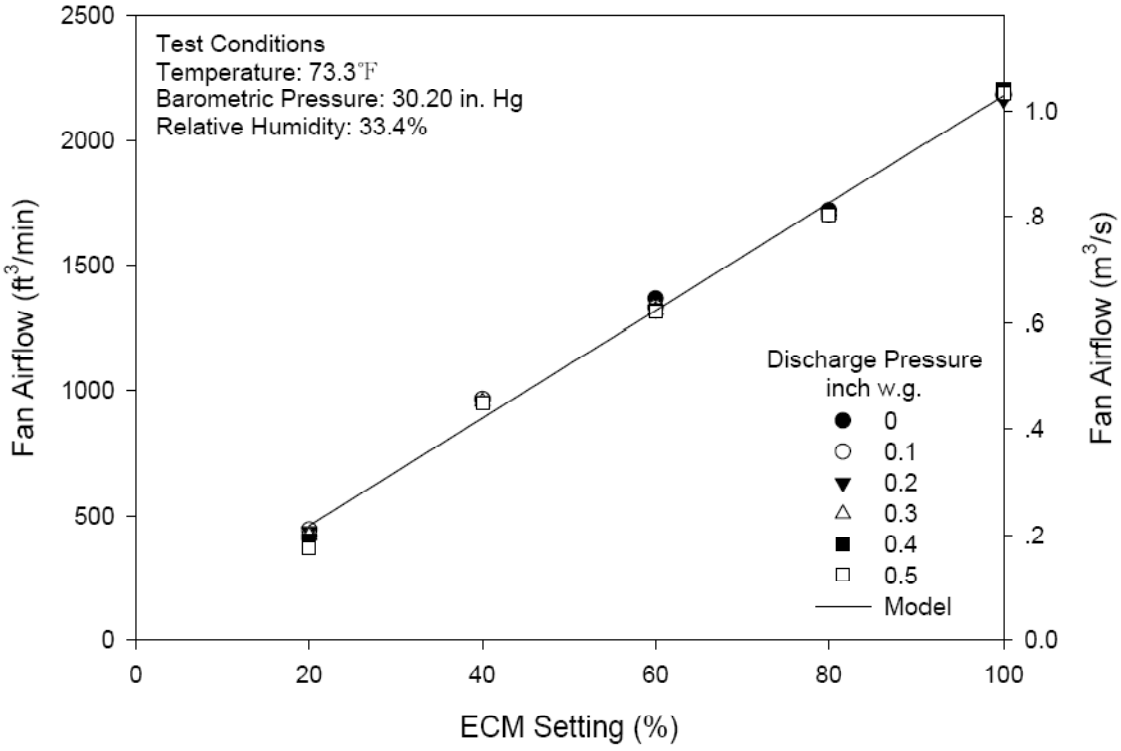

Fig. B-15 Fan Airflow vs. ECM Settings for F_S12C_M2

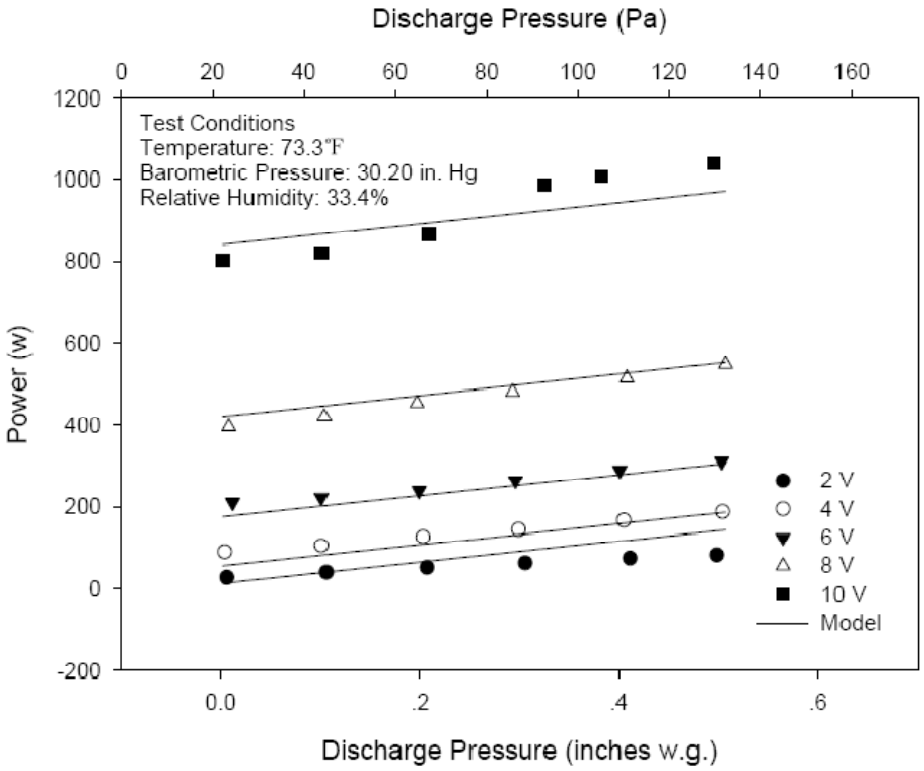

Fig. B-16 Fan Power vs. Discharge Pressure for F_S12C_M2

APPENDIX C

PLENUM AIRFLOW

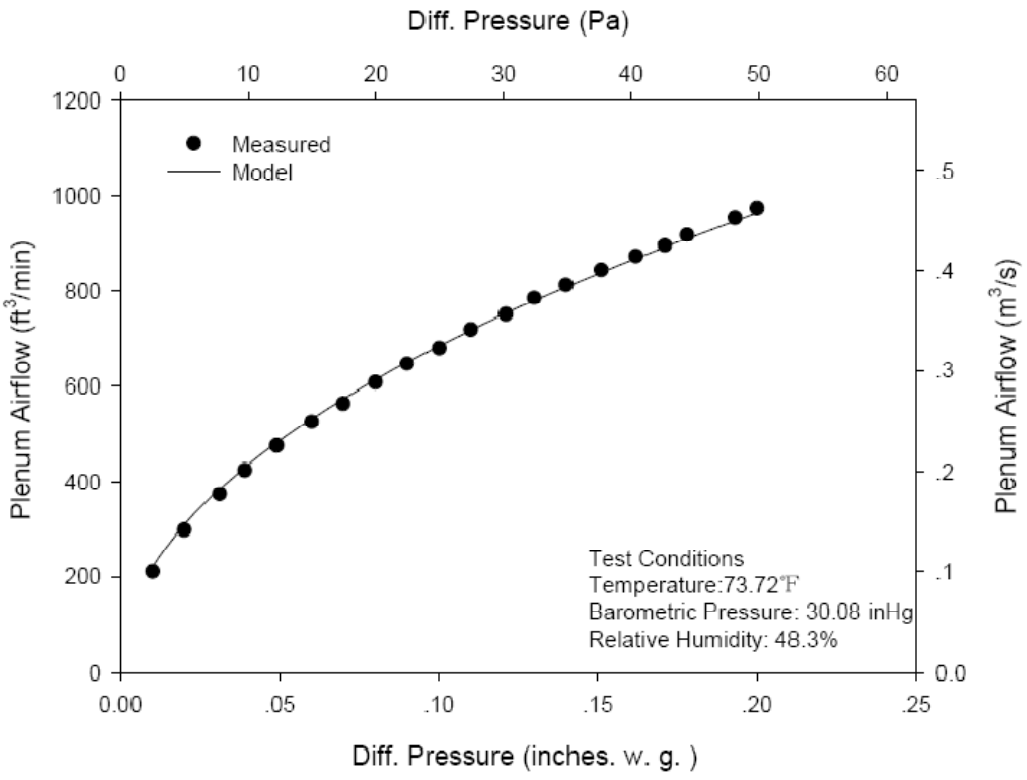

Fig. C-1 Plenum Airflow vs. Diff. Pressure for S8A

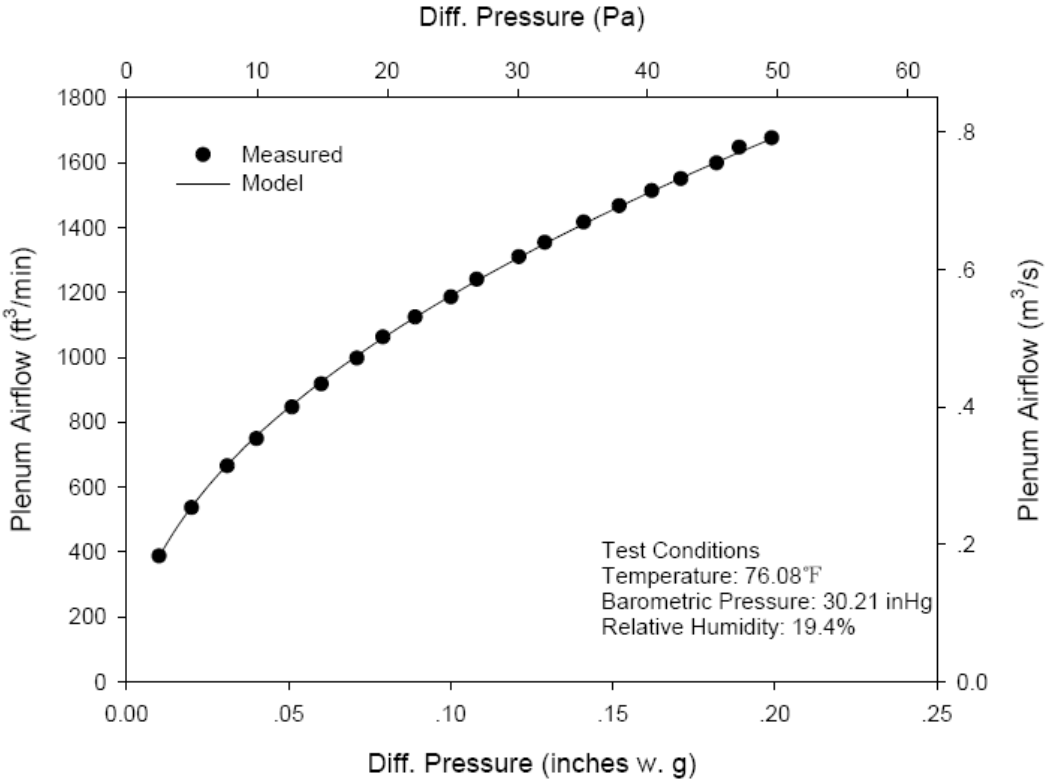

Fig. C-2 Plenum Airflow vs. Diff. Pressure for S12A

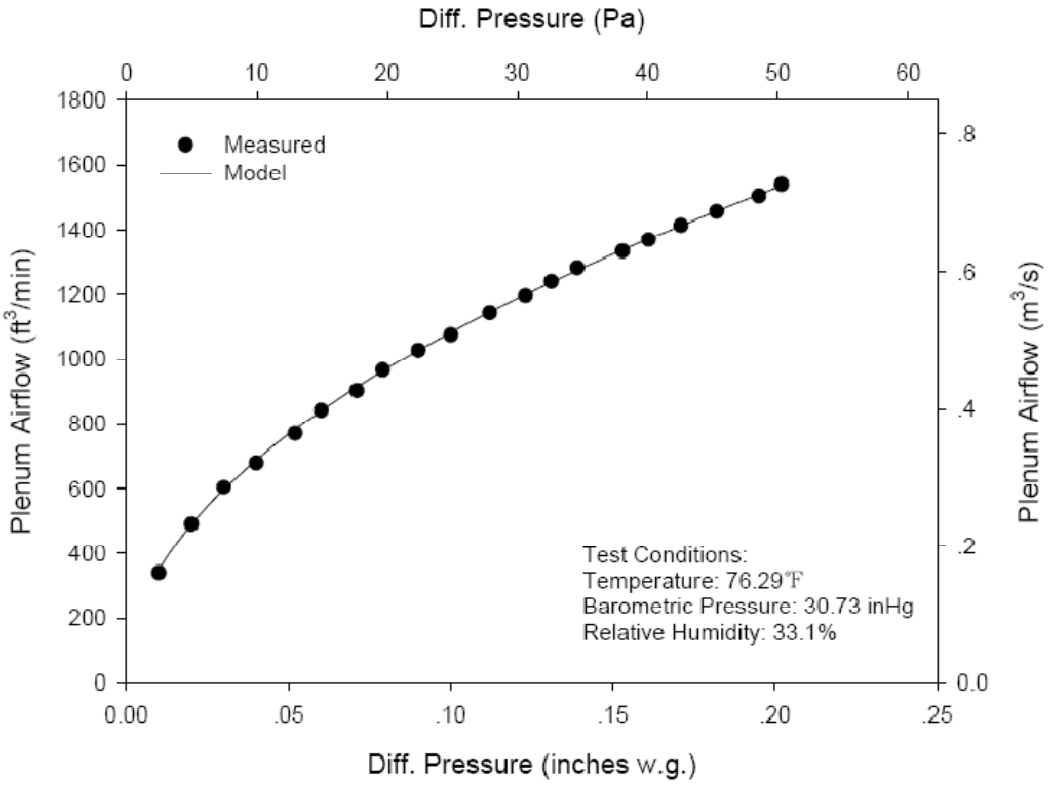

Fig. C-3 Plenum Airflow vs. Diff. Pressure for S8B

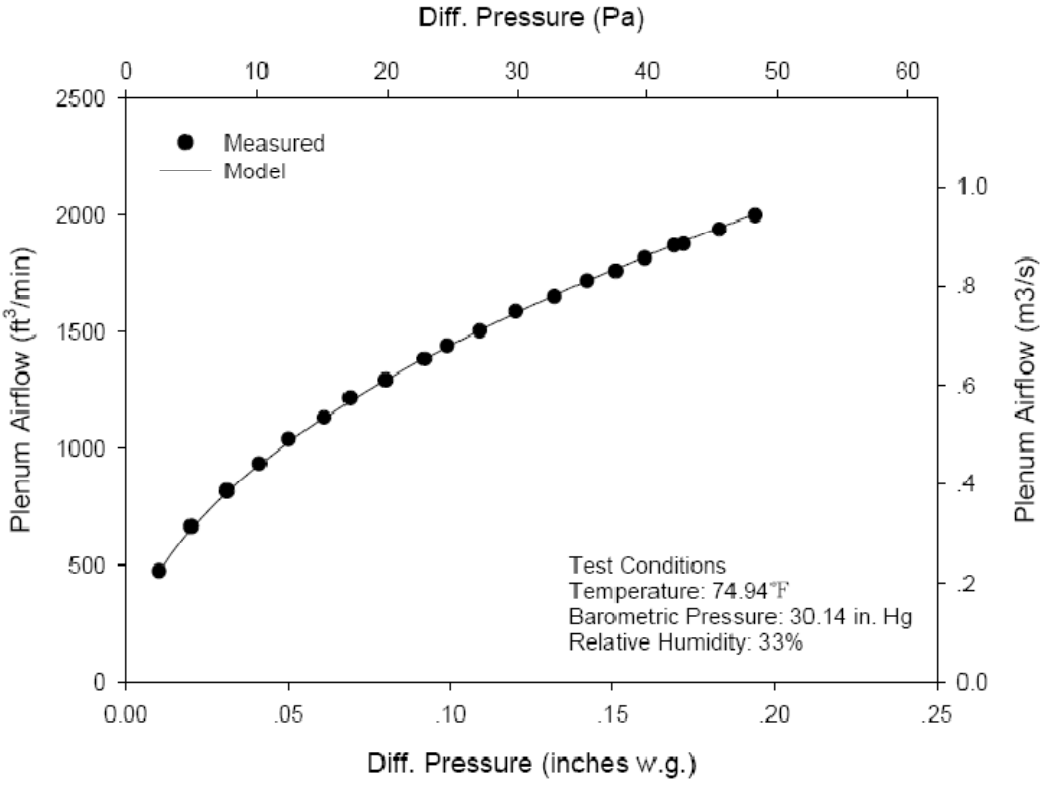

Fig. C-4 Plenum Airflow vs. Diff. Pressure for S12B

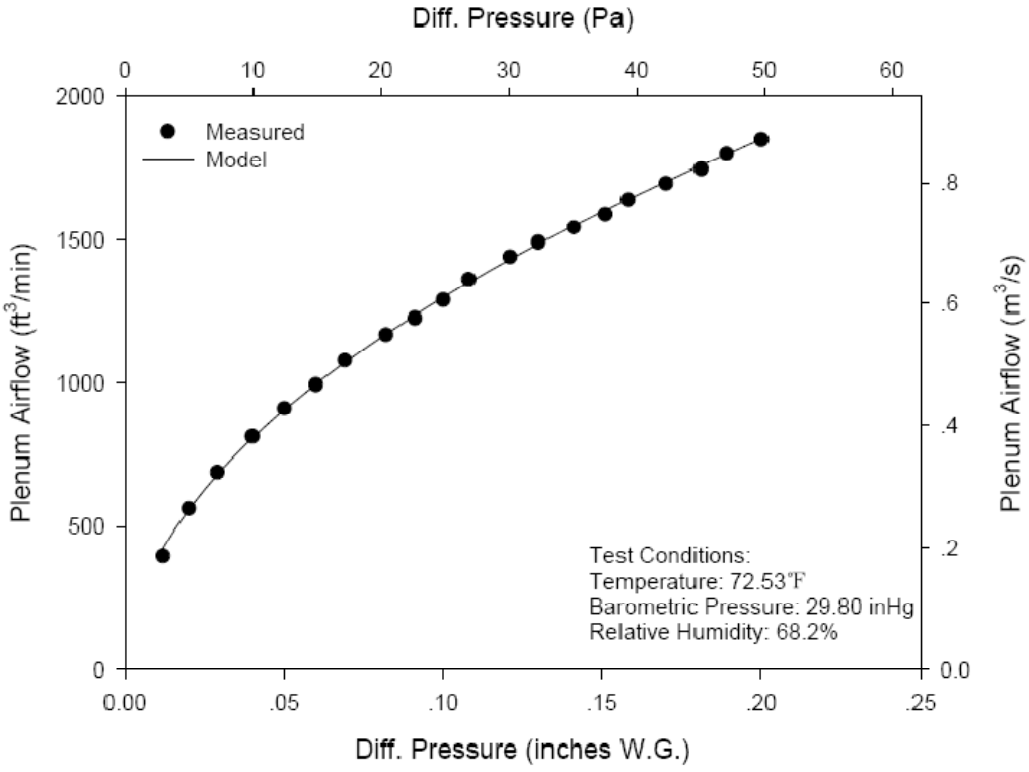

Fig. C-5 Plenum Airflow vs. Diff. Pressure for S8C_M1

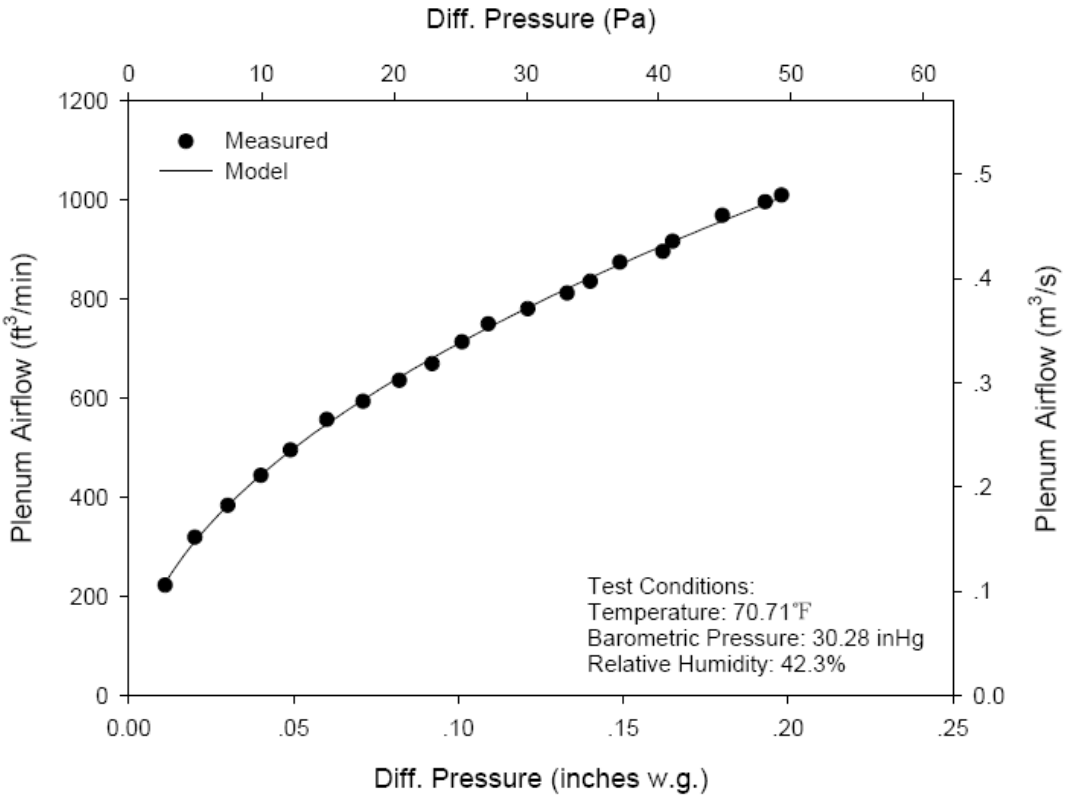

Fig. C-6 Plenum Airflow vs. Diff. Pressure for S8C_M2

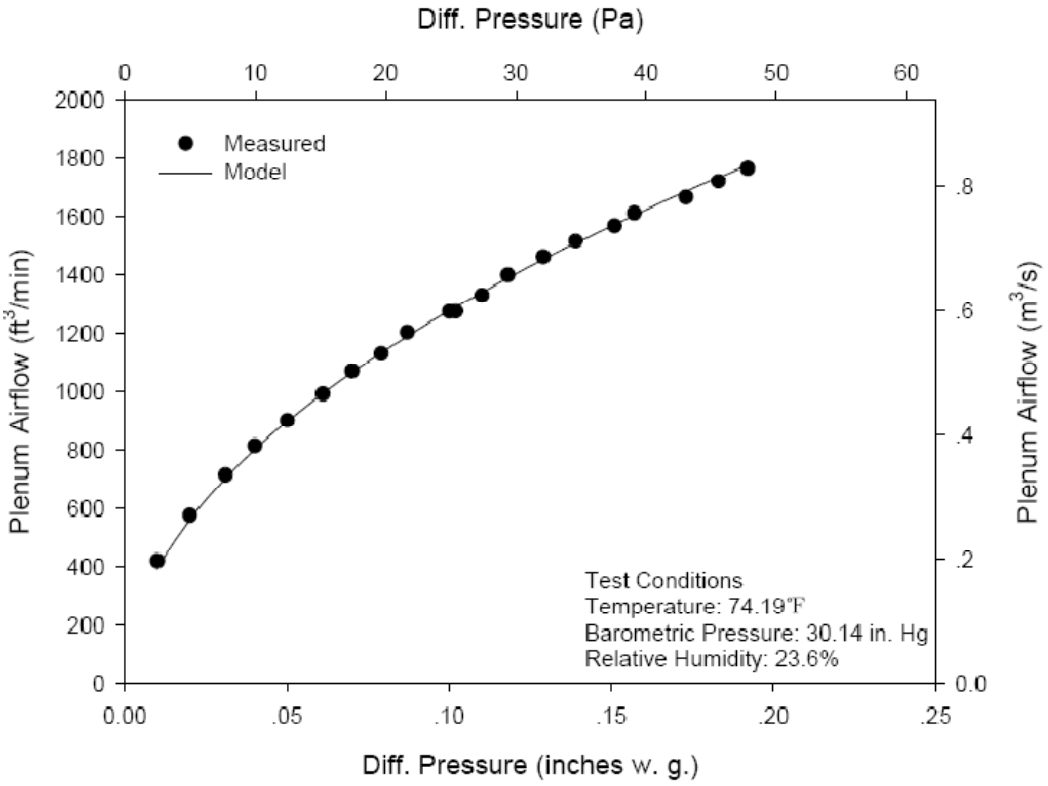

Fig. C-7 Plenum Airflow vs. Diff. Pressure for S12C_M1

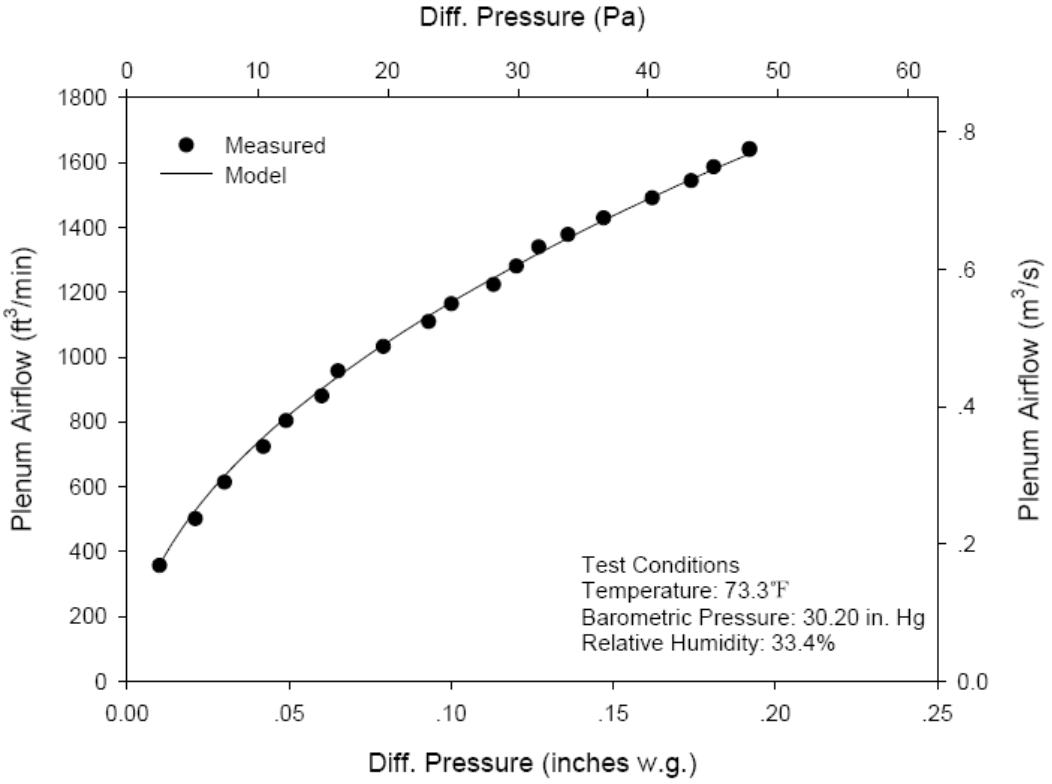

Fig. C-8 Plenum Airflow vs. Diff. Pressure for S12C_M2

APPENDIX D

VERIFICATION OF MODELS

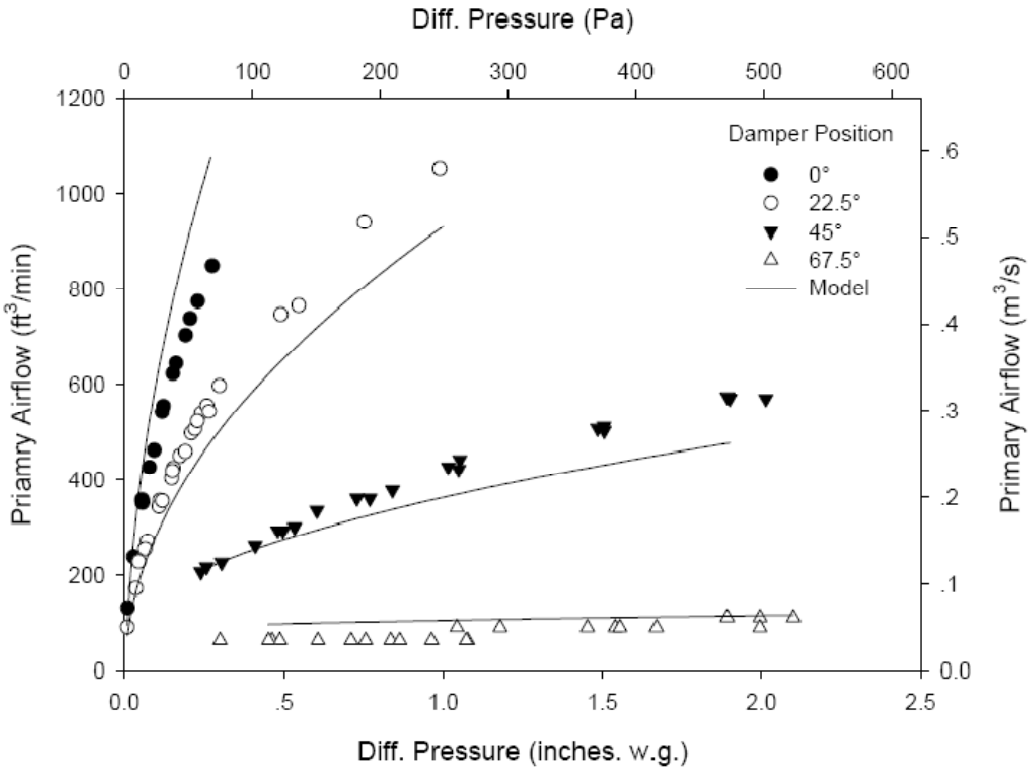

Fig. D-1 Comparison in Primary Airflow for S8A

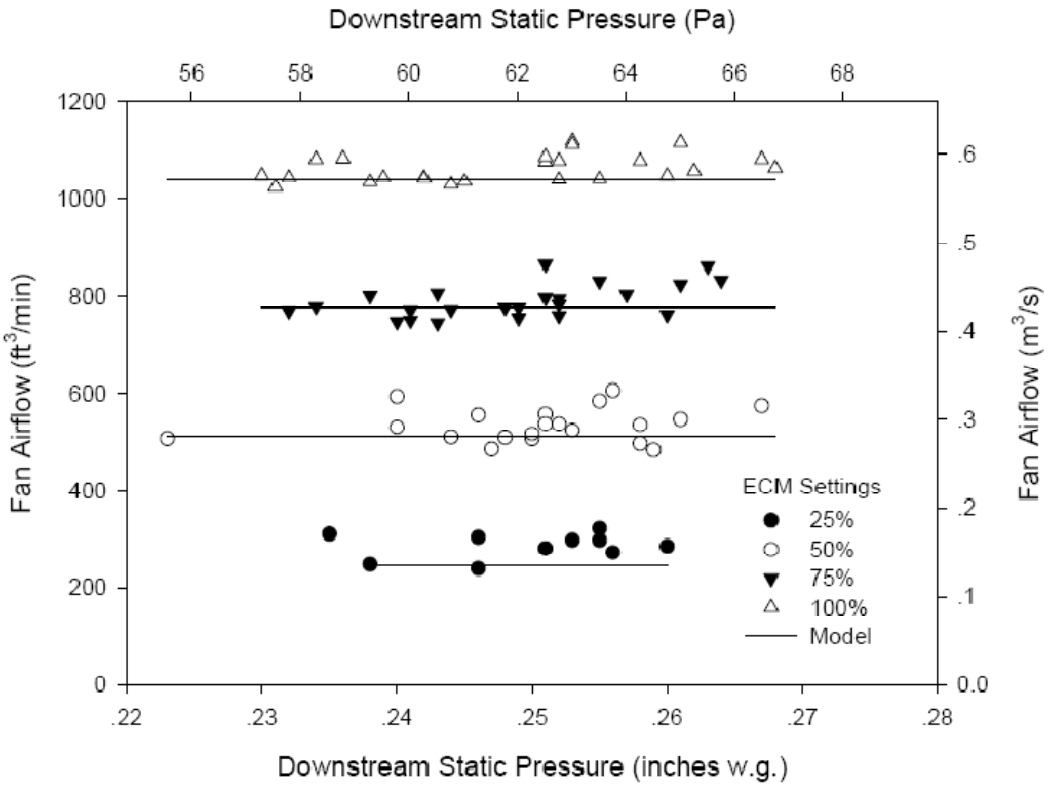

Fig. D-2 Comparison in Fan Airflow for S8A

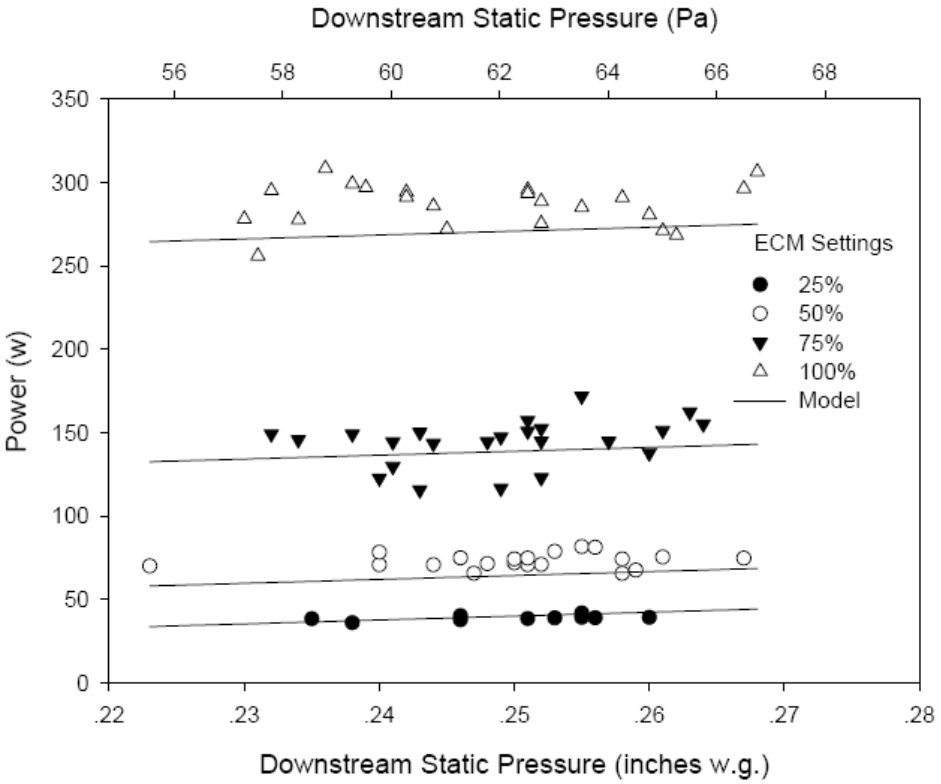

Fig. D-3 Comparison in Power Consumption for S8A

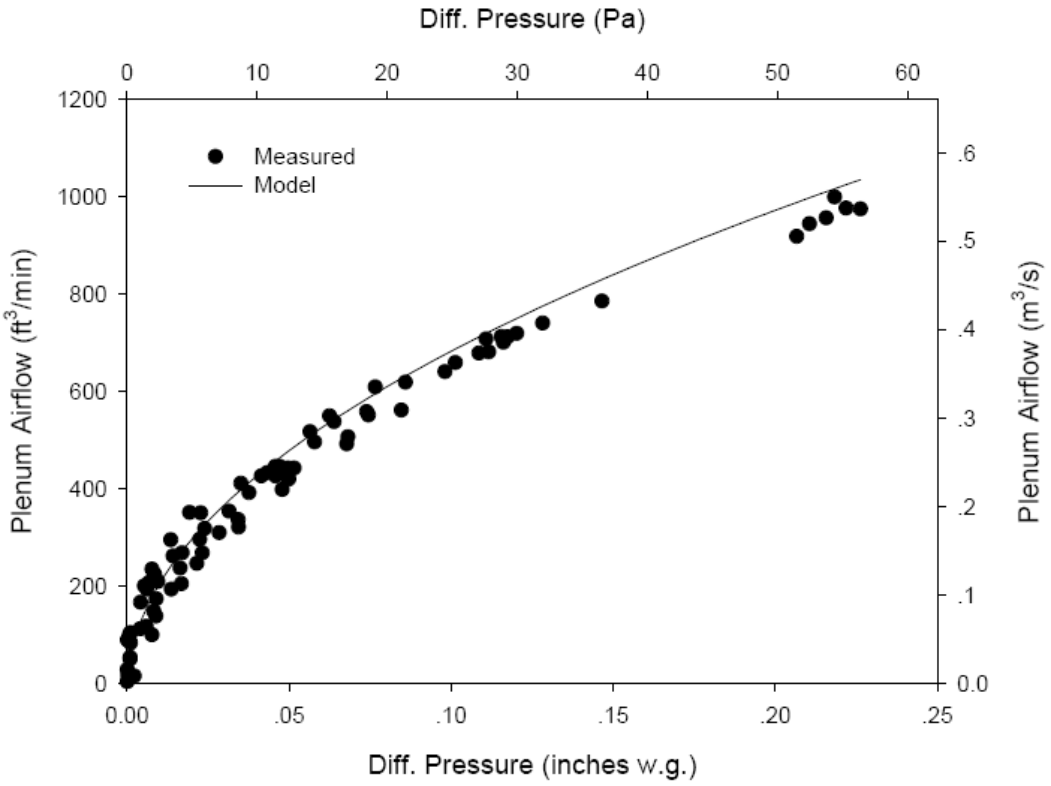

Fig. D-4 Comparison in Plenum Airflow for S8A

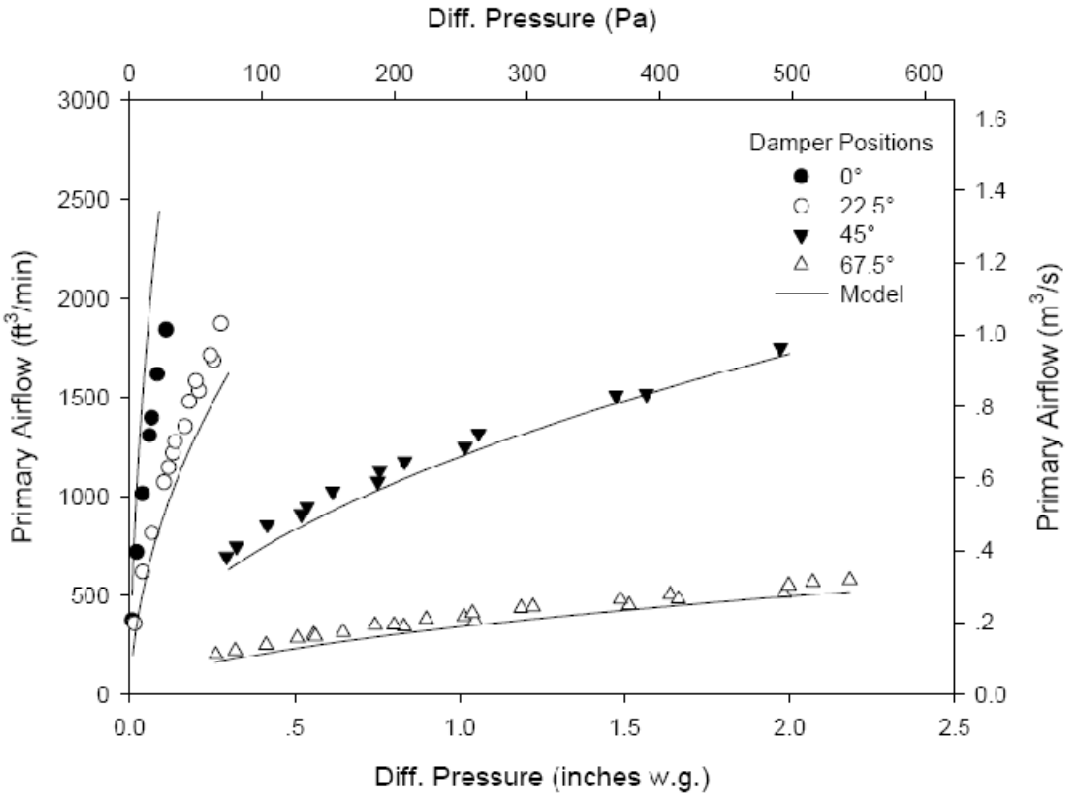

Fig. D-5 Comparison in Primary Airflow for S12A

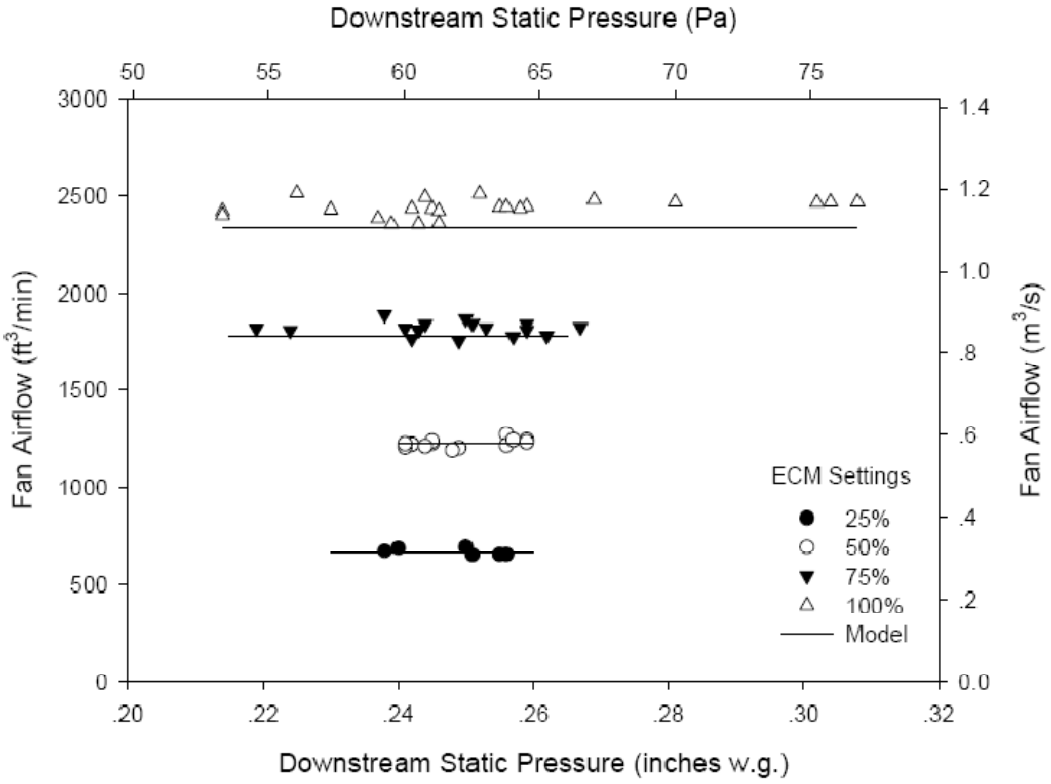

Fig. D-6 Comparison in Fan Airflow for S12A

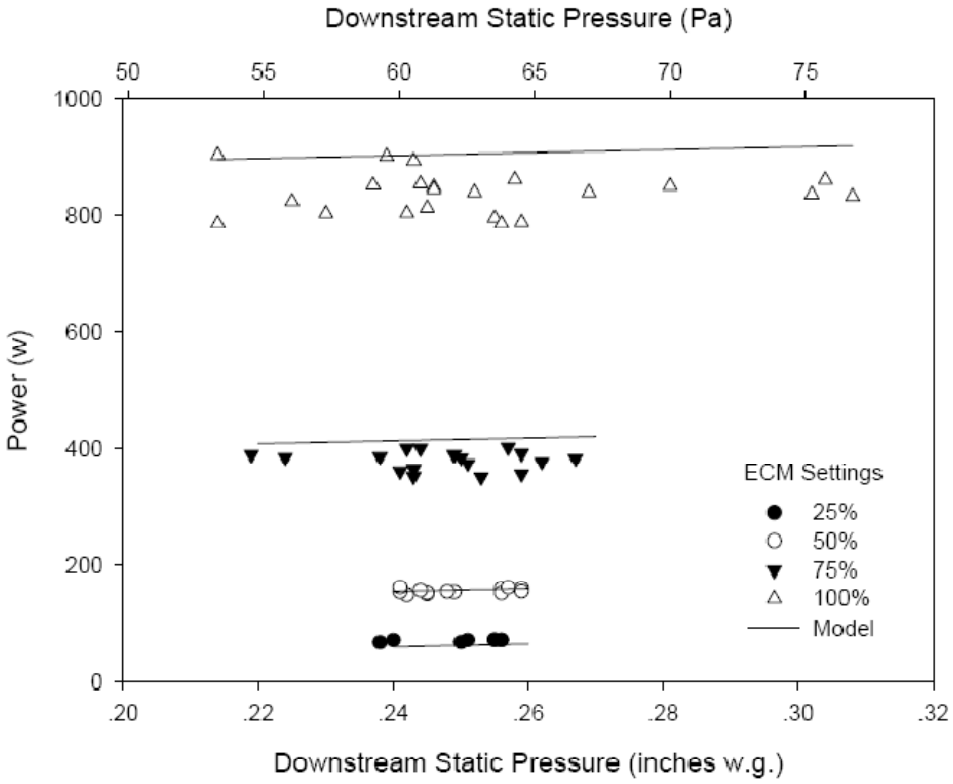

Fig. D-7 Comparison in Power Consumption for S12A

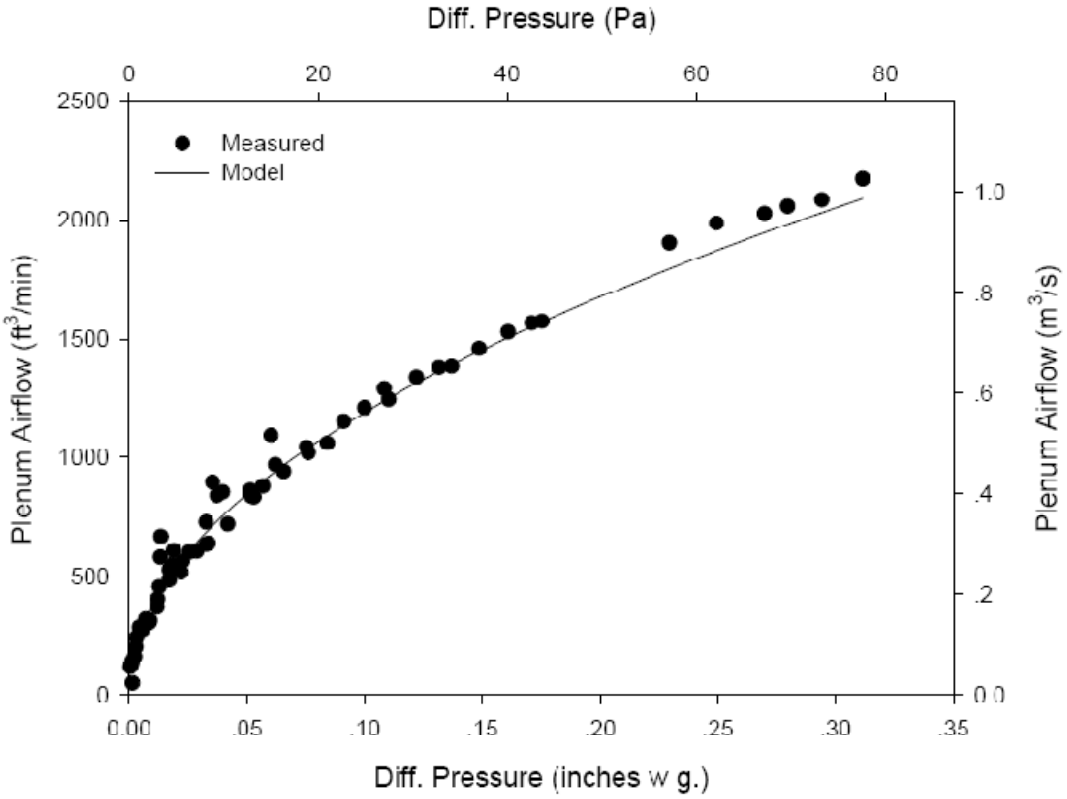

Fig. D-8 Comparison in Plenum Airflow for S12A

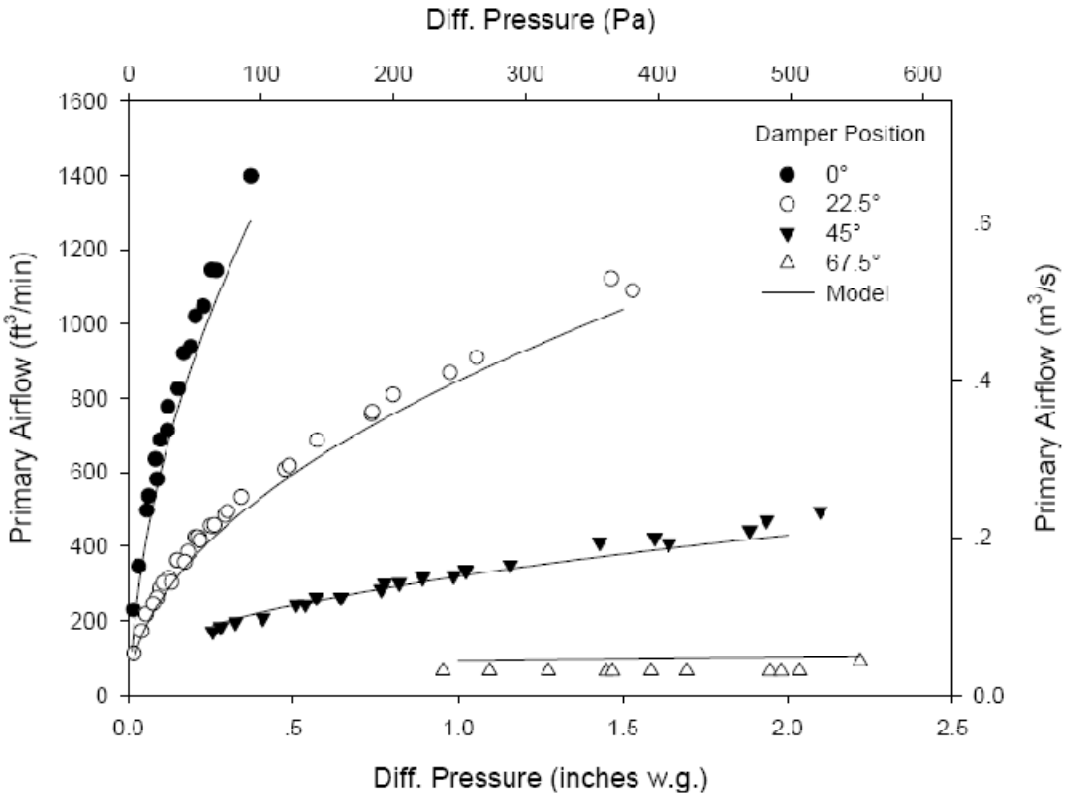

Fig. D-9 Comparison in Primary Airflow for S8B

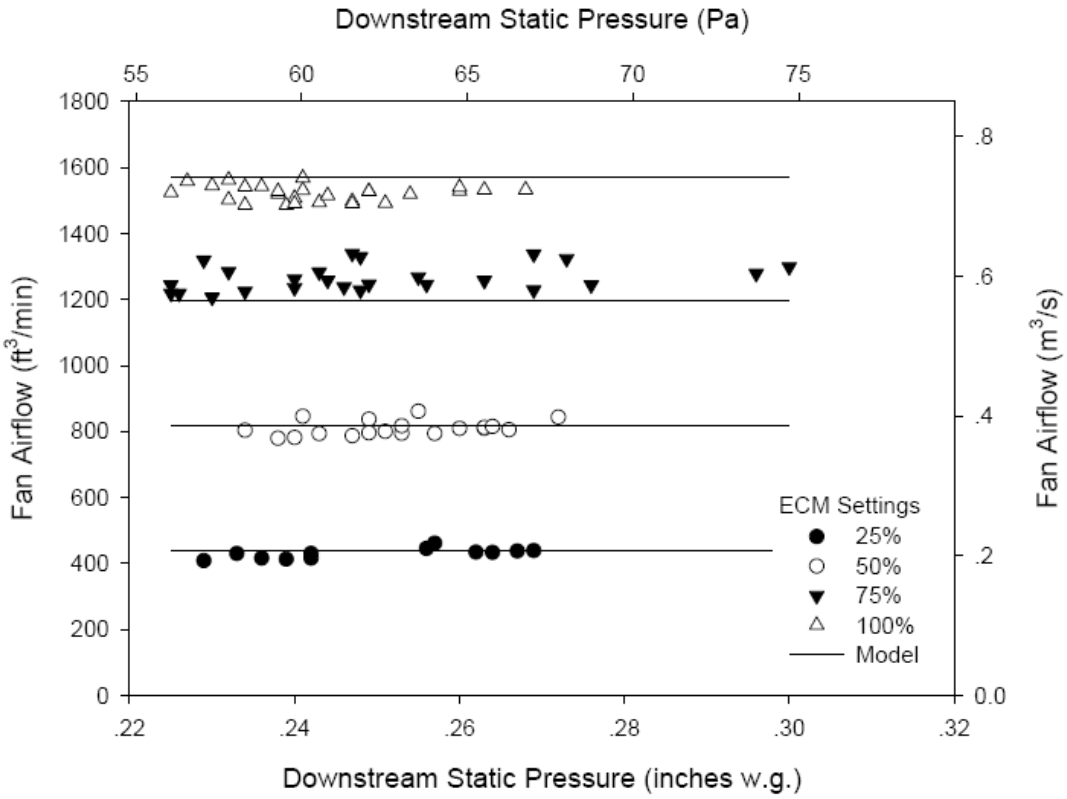

Fig. D-10 Comparison in Fan Airflow for S8B

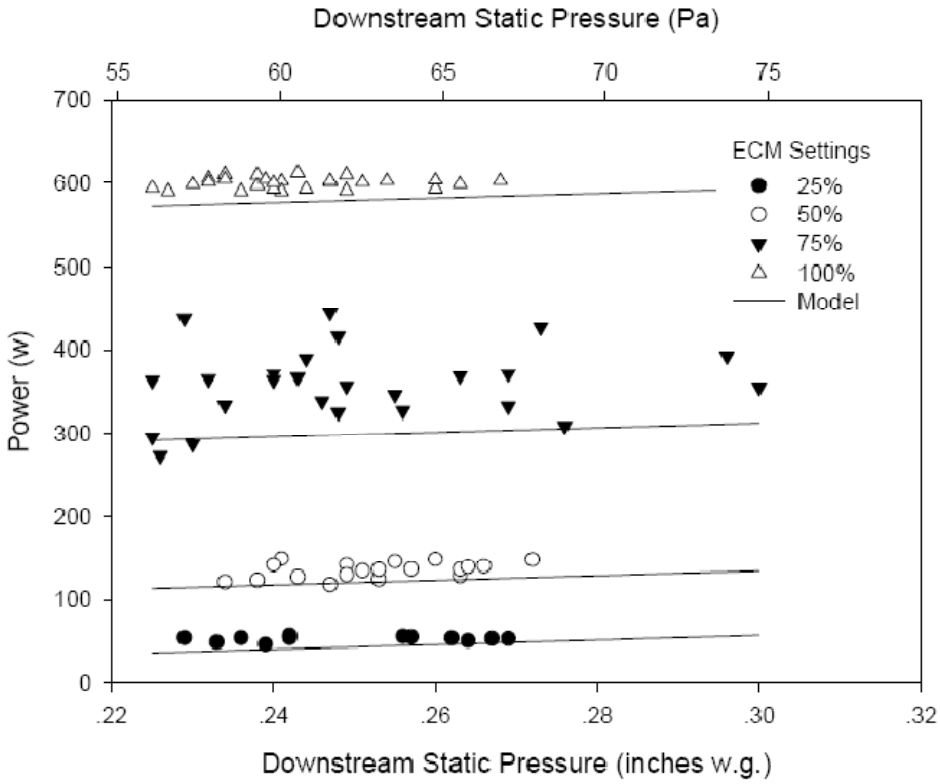

Fig. D-11 Comparison in Power Consumption for S8B

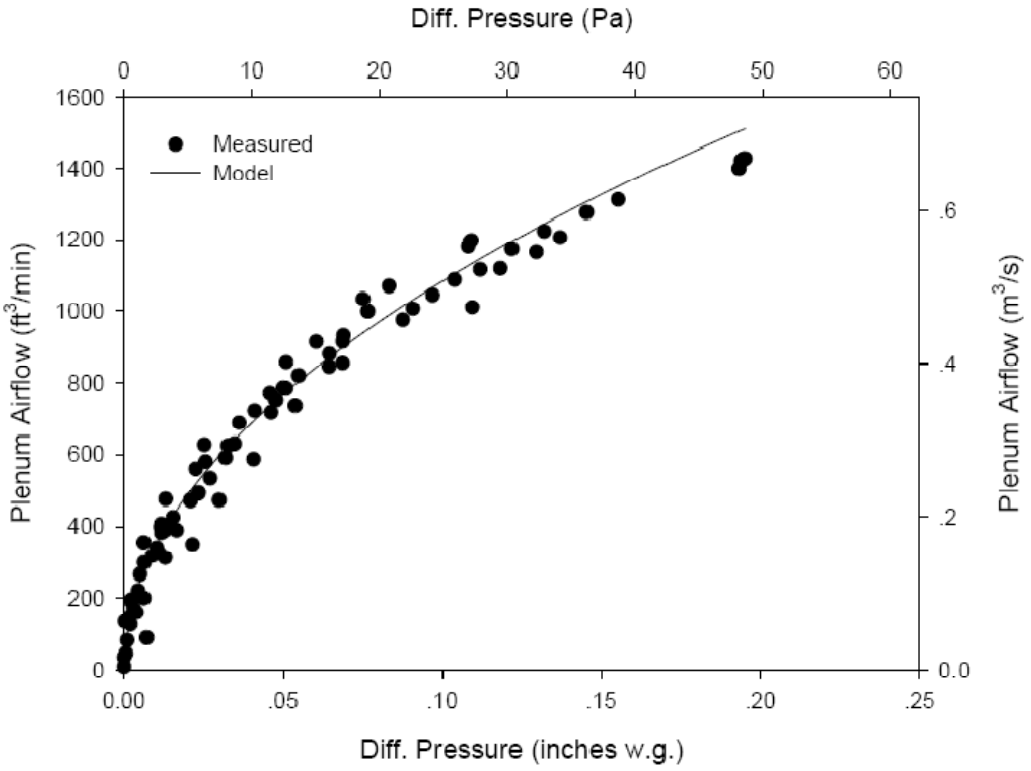

Fig. D-12 Comparison in Plenum Airflow for S8B

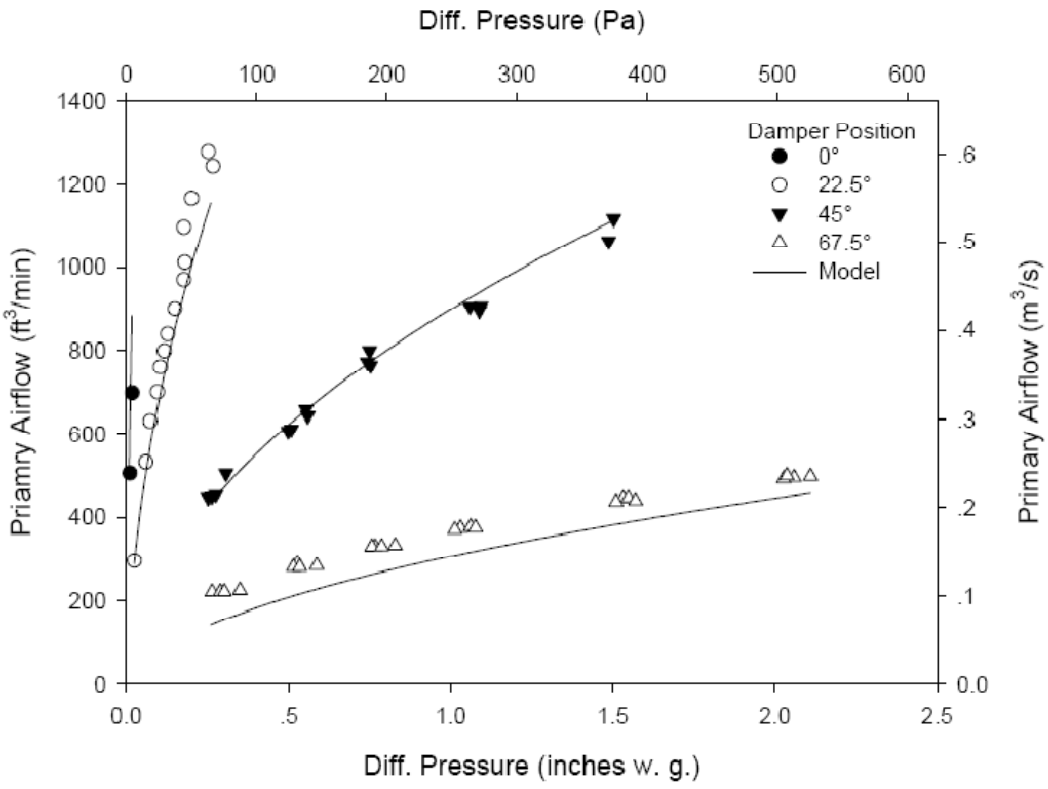

Fig. D-13 Comparison in Primary Airflow for S12B

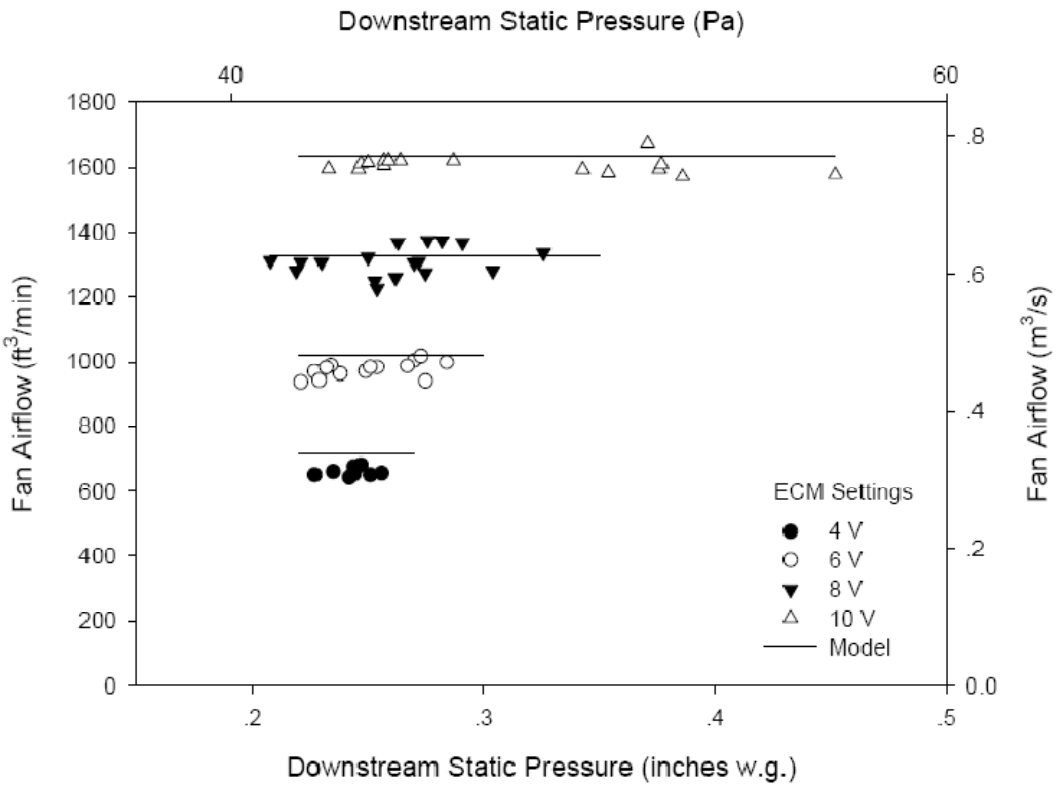

Fig. D-14 Comparison in Fan Airflow for S12B

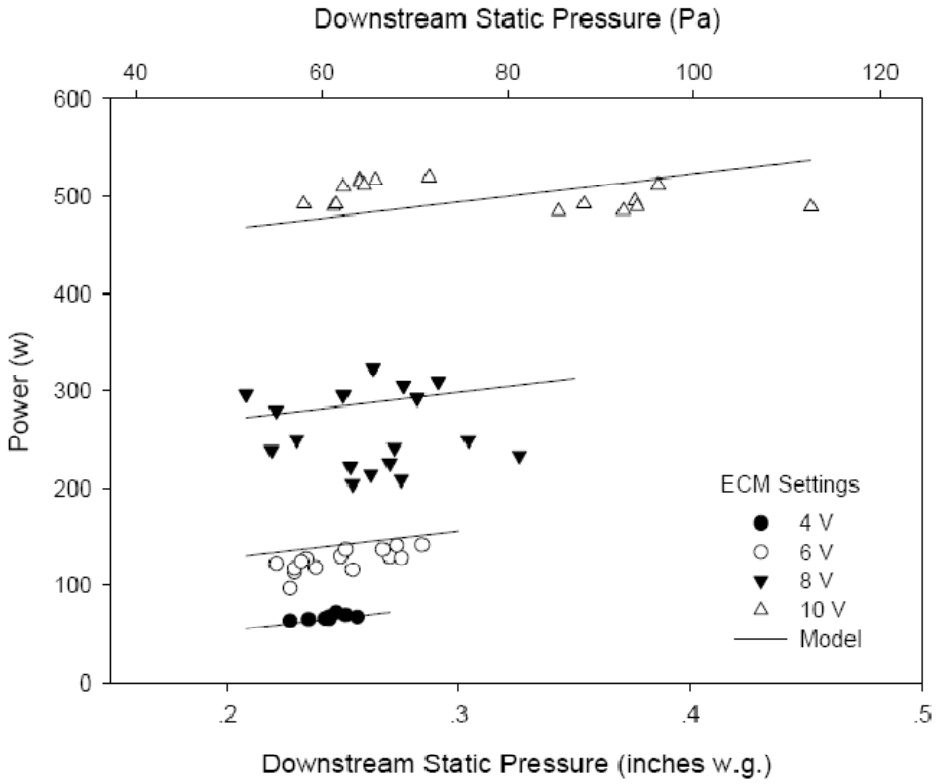

Fig. D-15 Comparison in Power Consumption for S12B

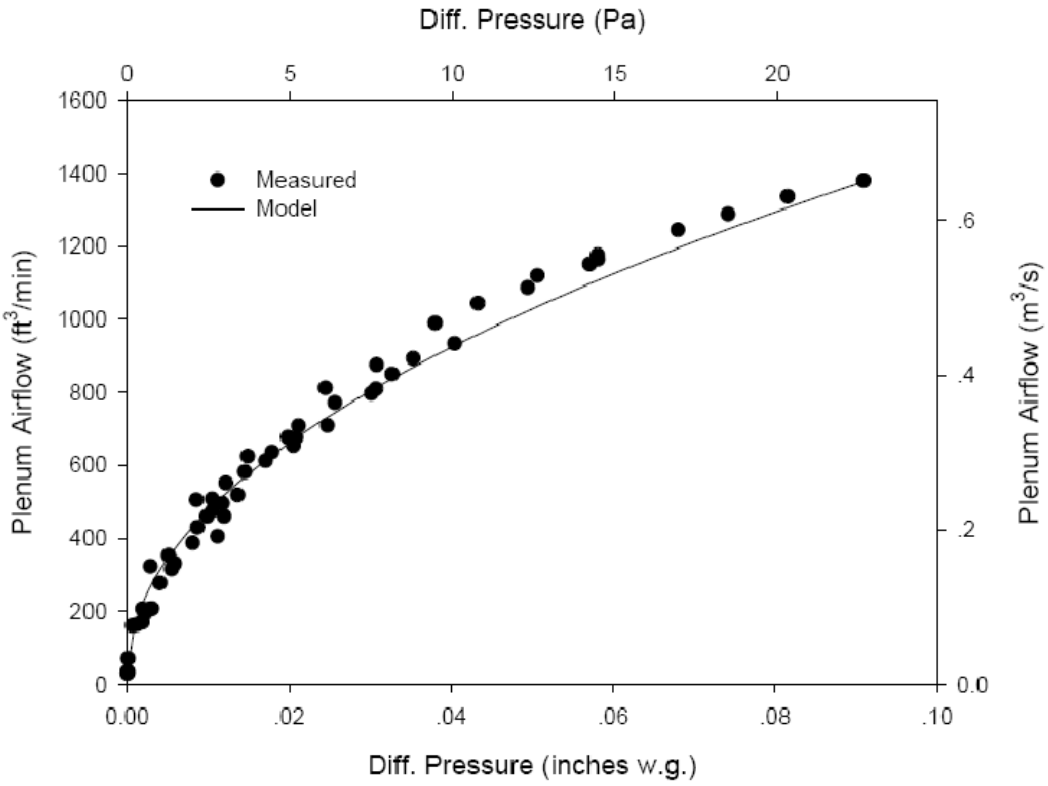

Fig. D-16 Comparison in Plenum Airflow for S12B

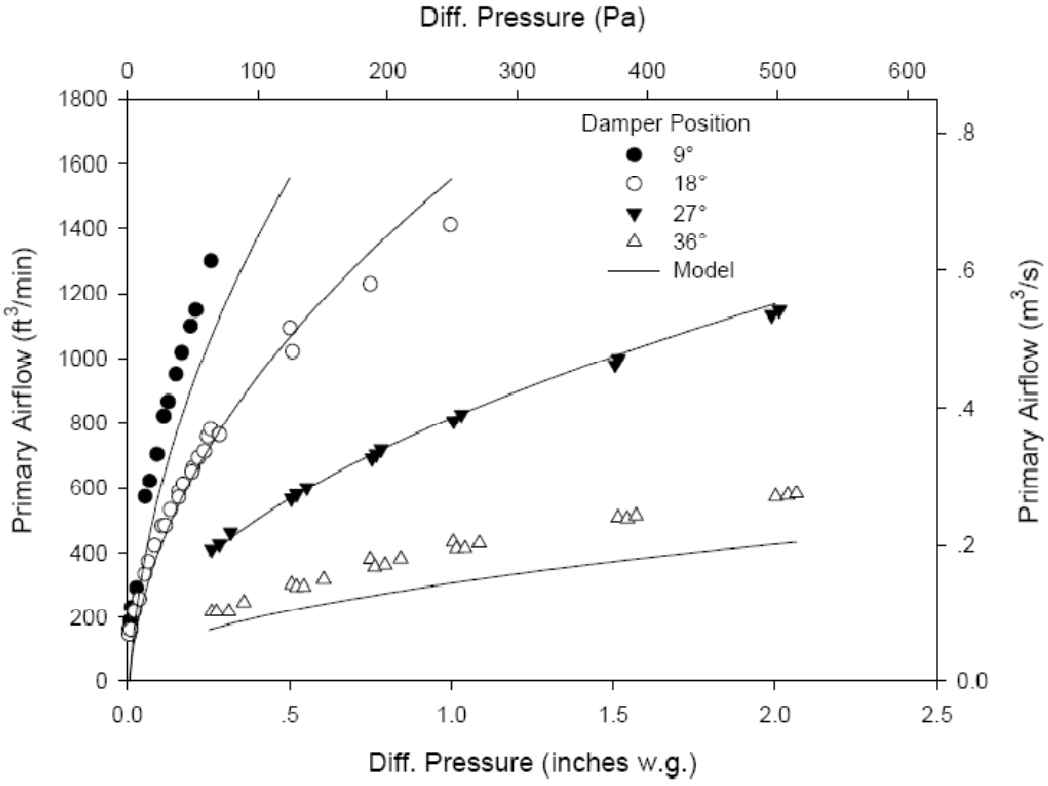

Fig. D-17Comparison in Primary Airflow for S8C_M1

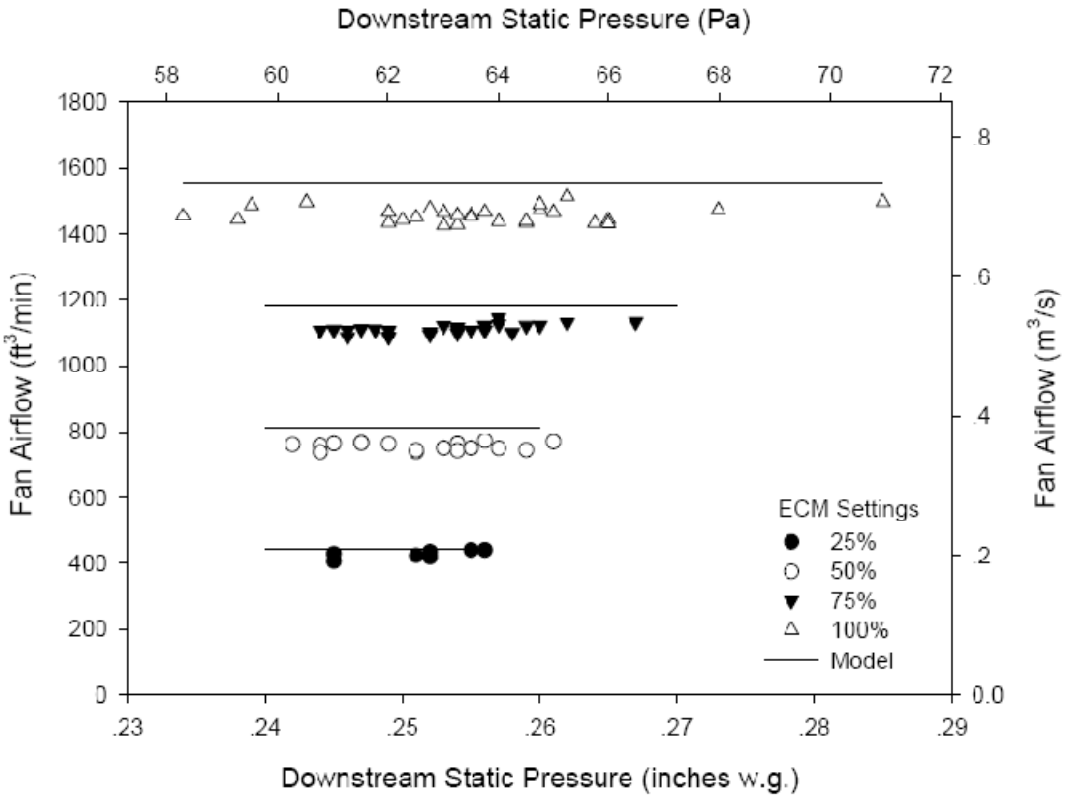

Fig. D-18 Comparison in Fan Airflow for S8C_M1

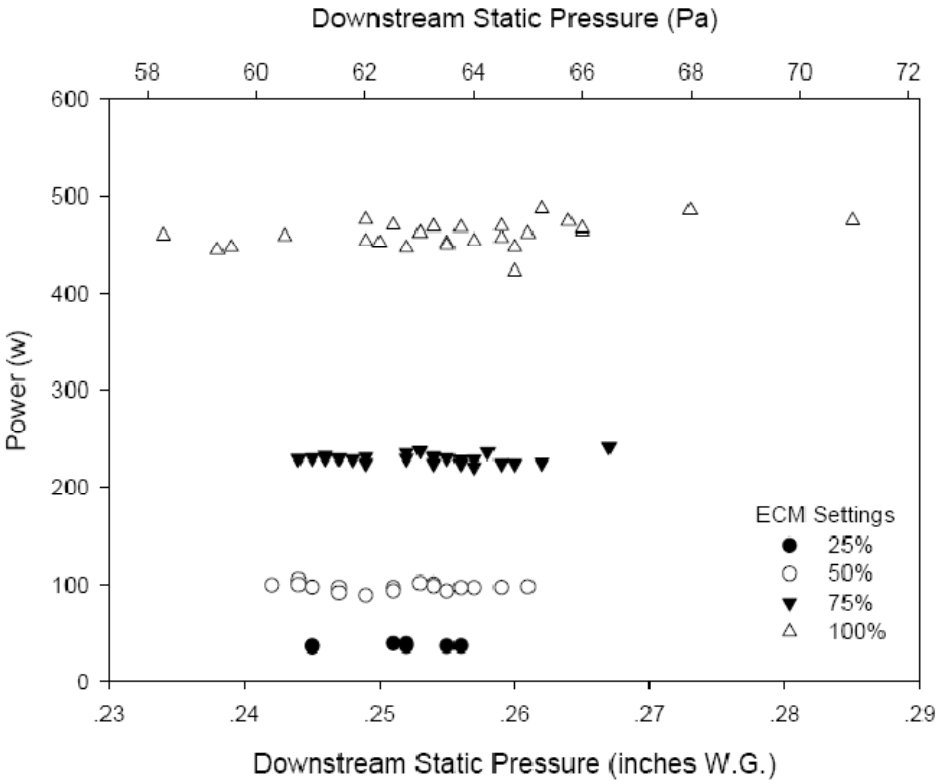

Fig. D-19 Comparison in Power Consumption for S8C_M1

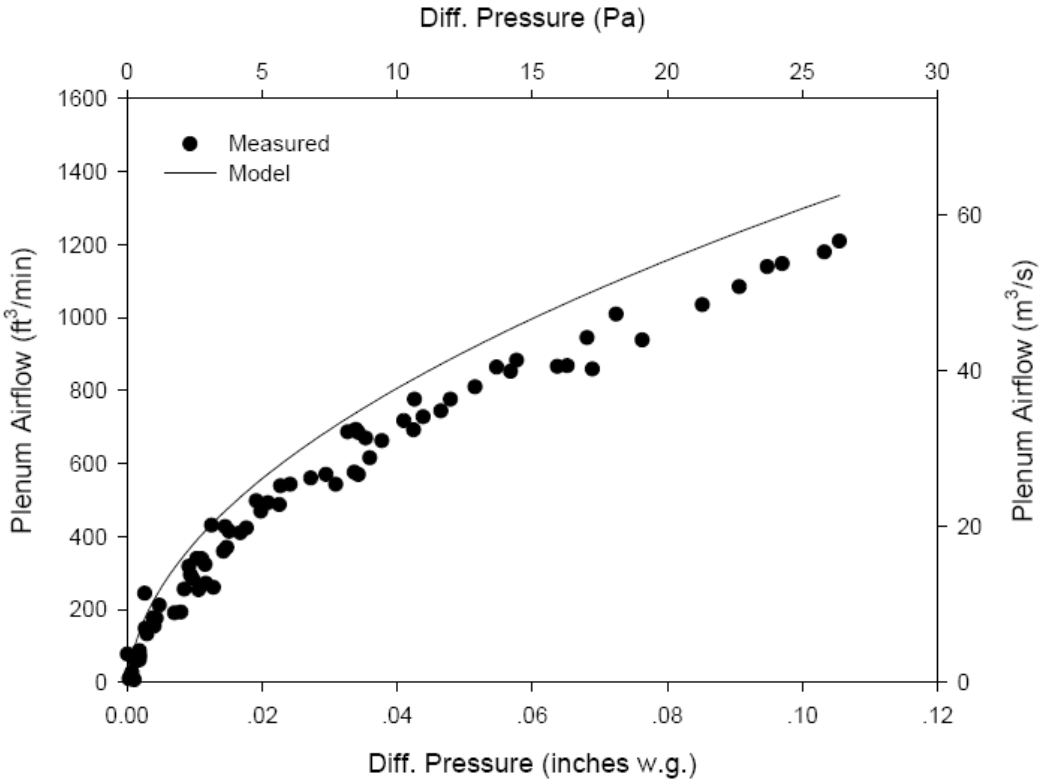

Fig. D-20 Comparison in Plenum Airflow for S8C_M1

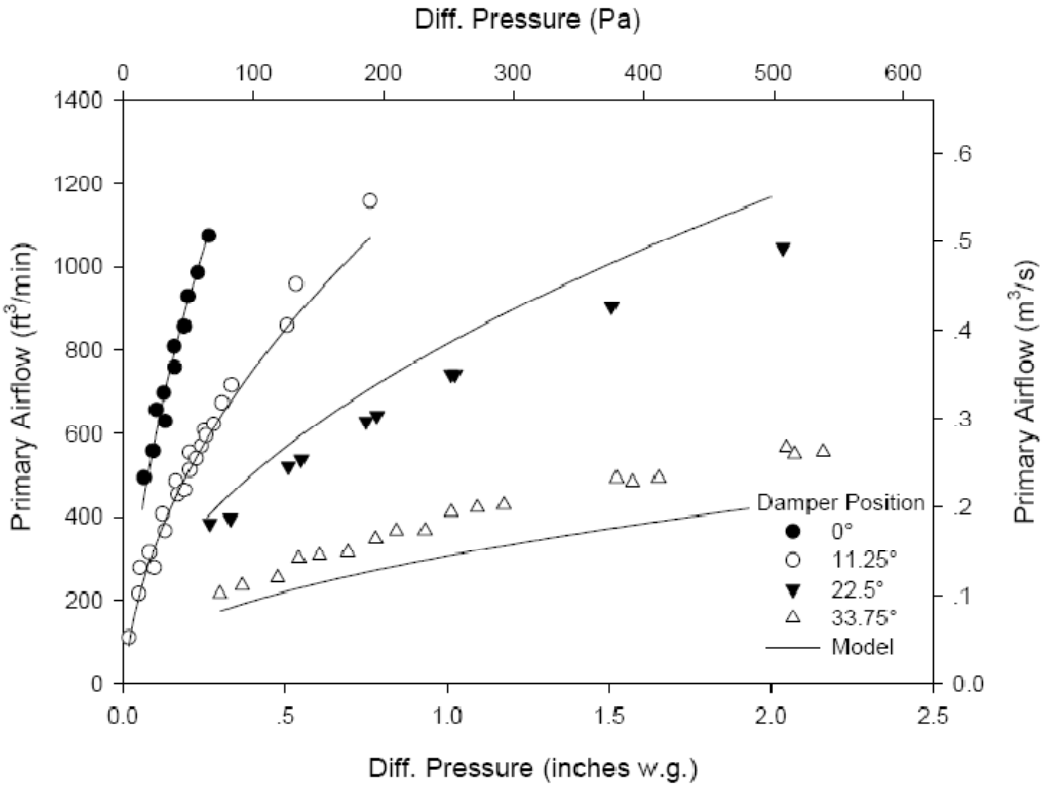

Fig. D-21 Comparison in Primary Airflow for S8C_M2

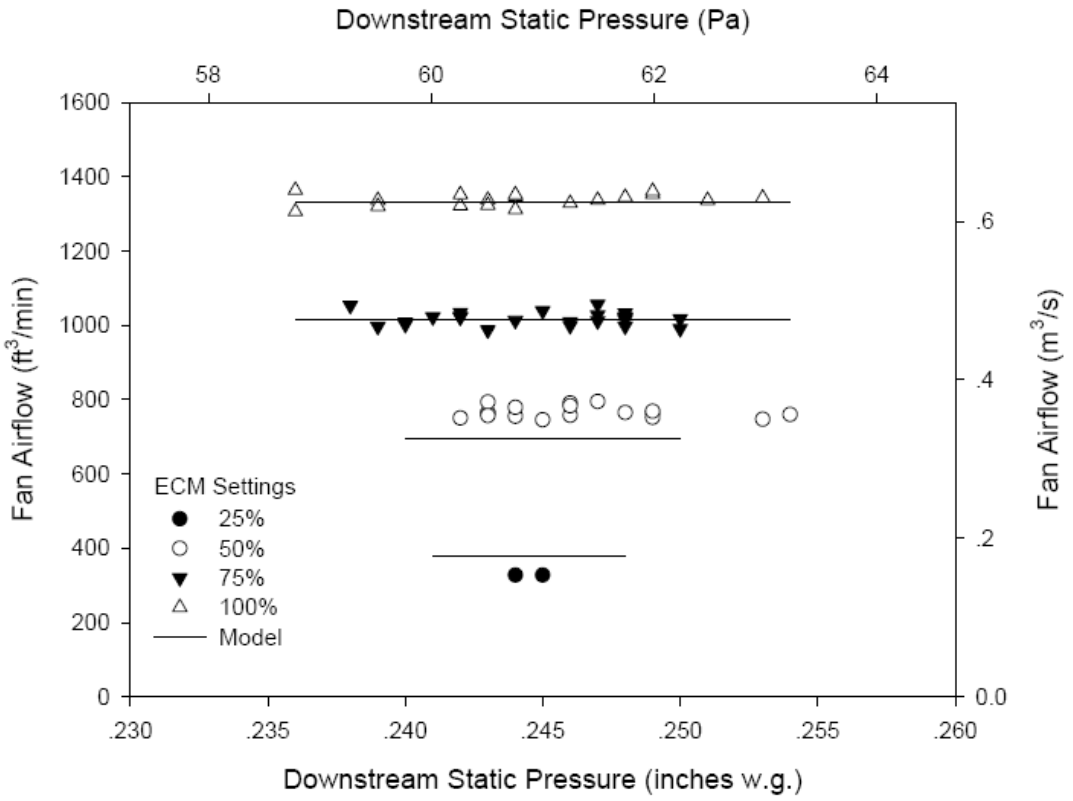

Fig. D-22 Comparison in Fan Airflow for S8C_M2

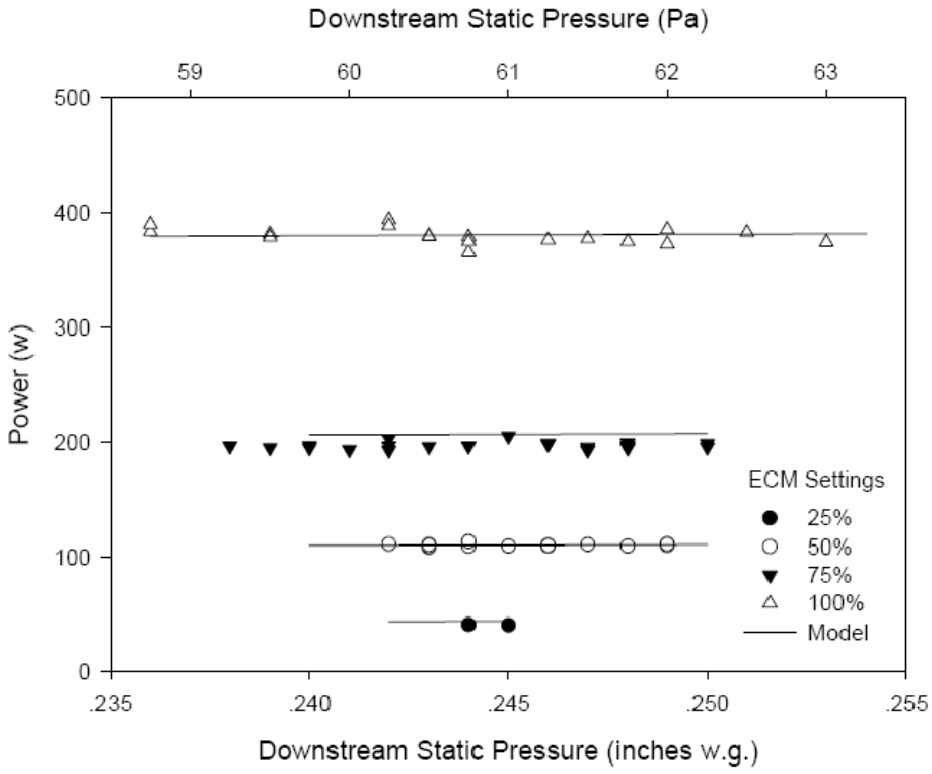

Fig. D-23 Comparison in Power Consumption for S8C_M2

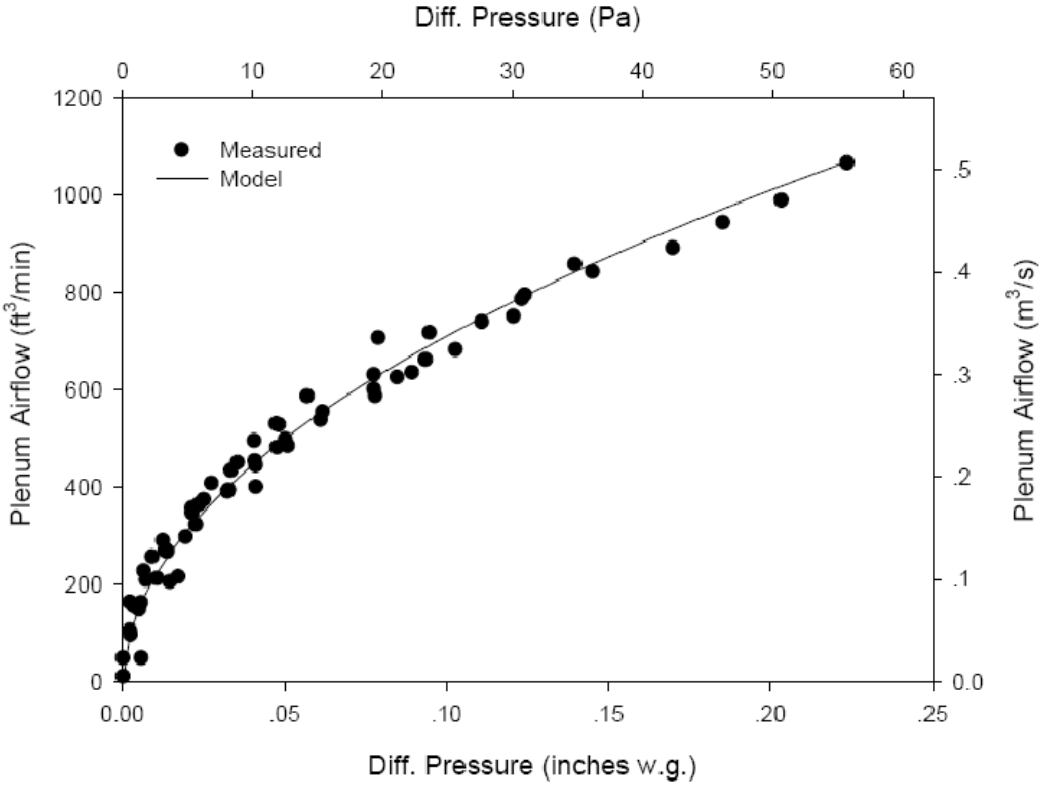

Fig. D-24 Comparison in Plenum Airflow for S8C_M2

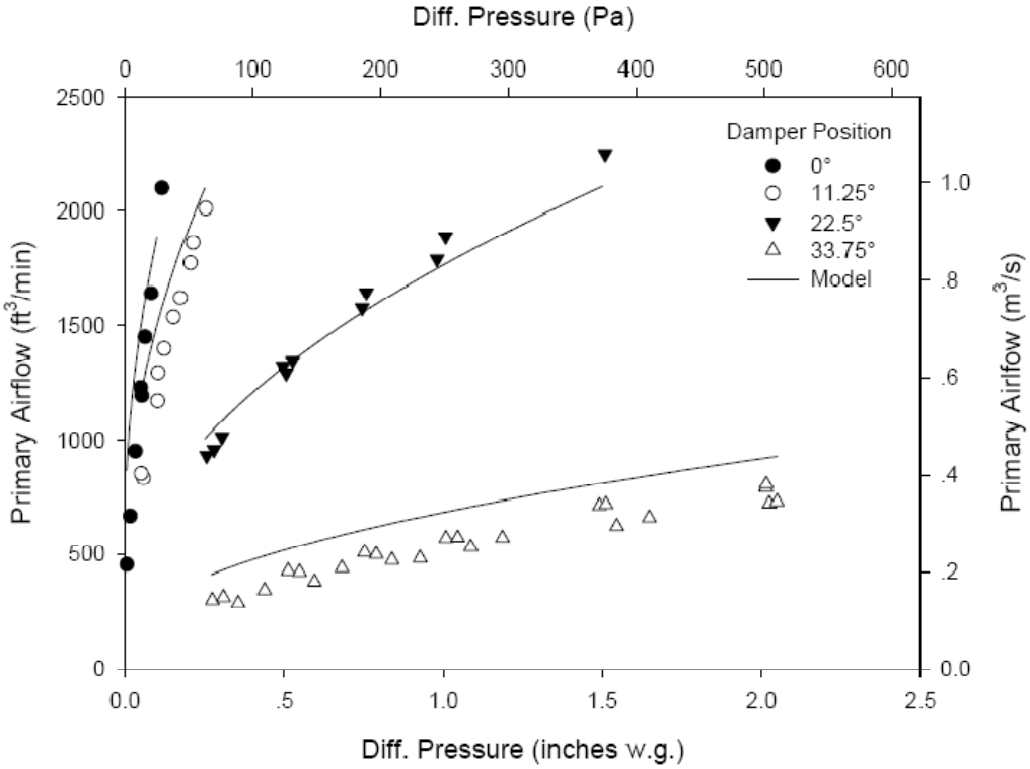

Fig. D-25 Comparison in Primary Airflow for S12C_M1

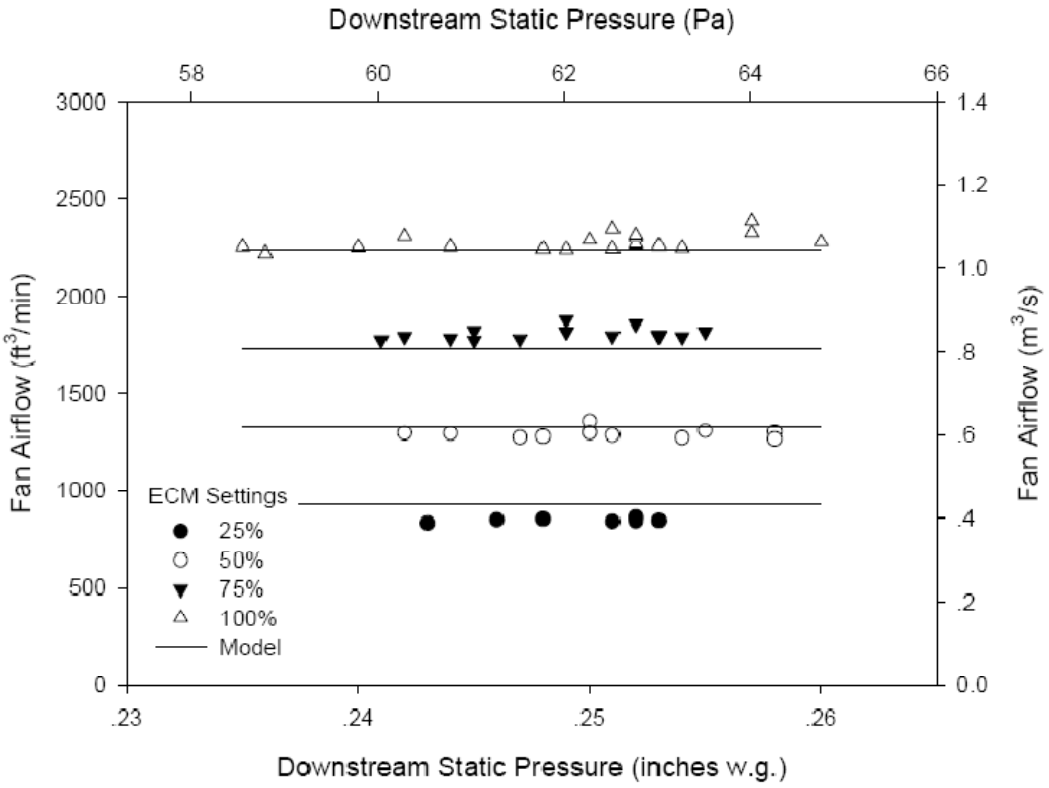

Fig. D-26 Comparison in Fan Airflow for S12C_M1

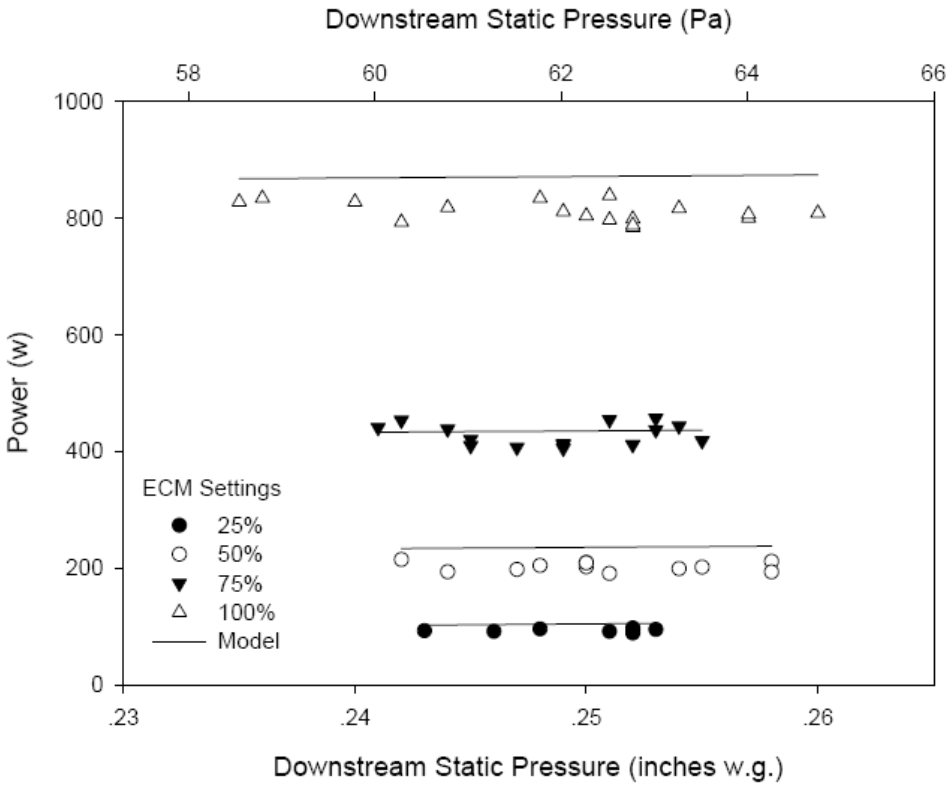

Fig. D-27 Comparison in Power Consumption for S12C_M1

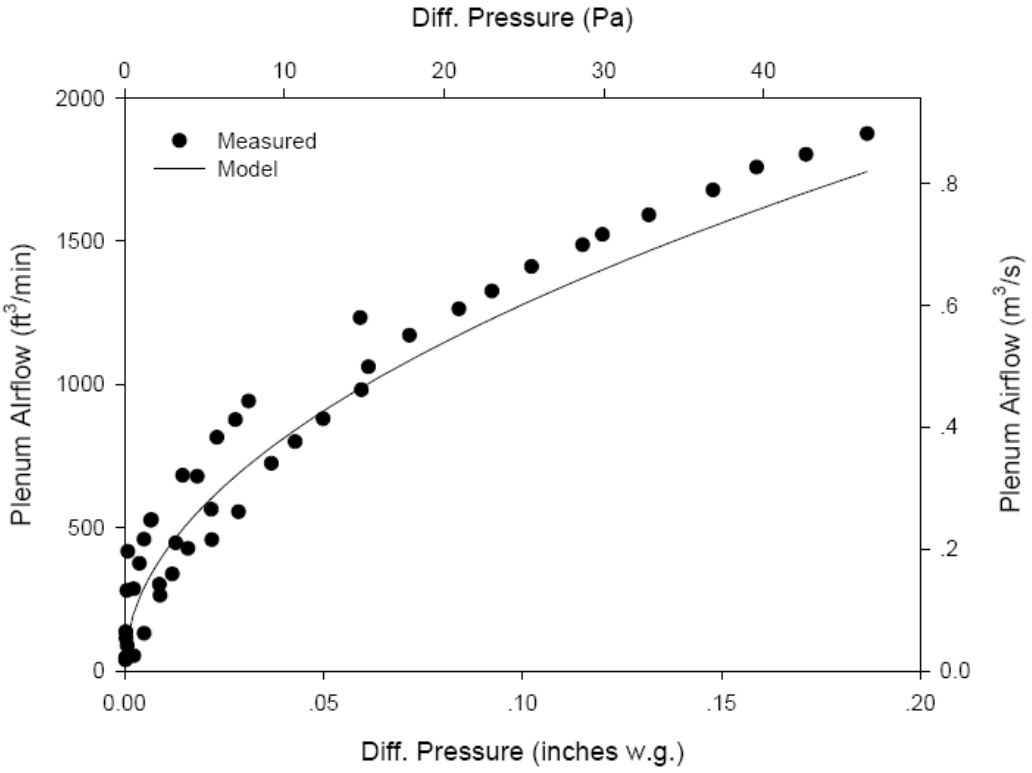

Fig. D-28 Comparison in Plenum Airflow for S12C_M1

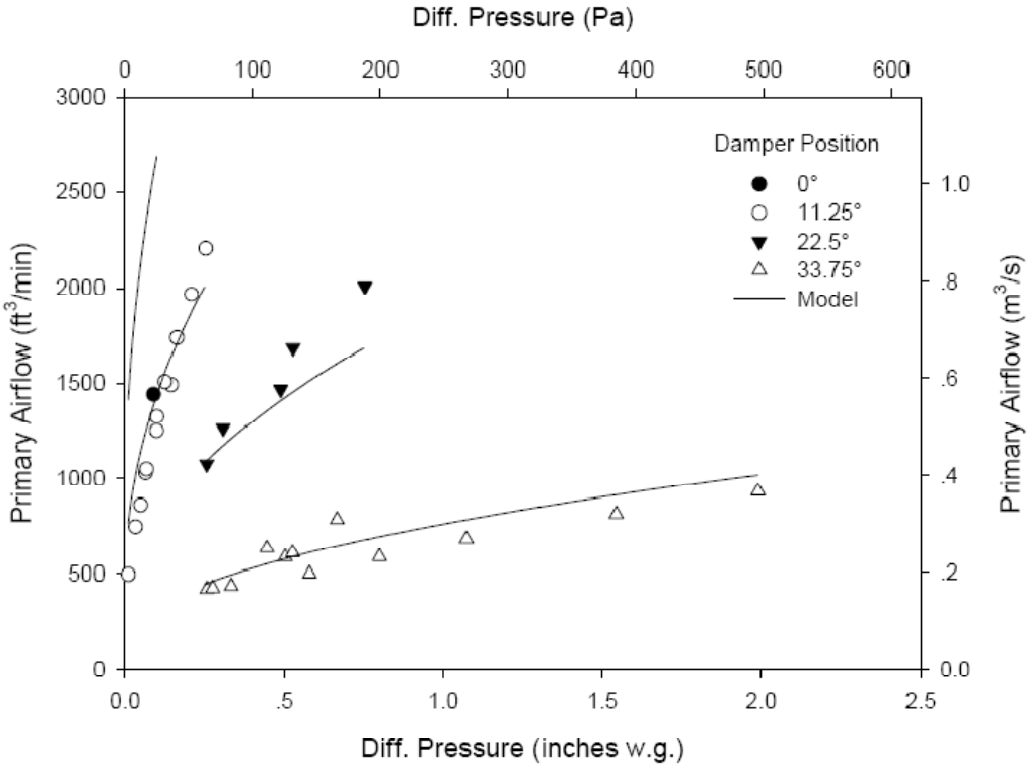

Fig. D-29 Comparison in Primary Airflow for S12C_M2

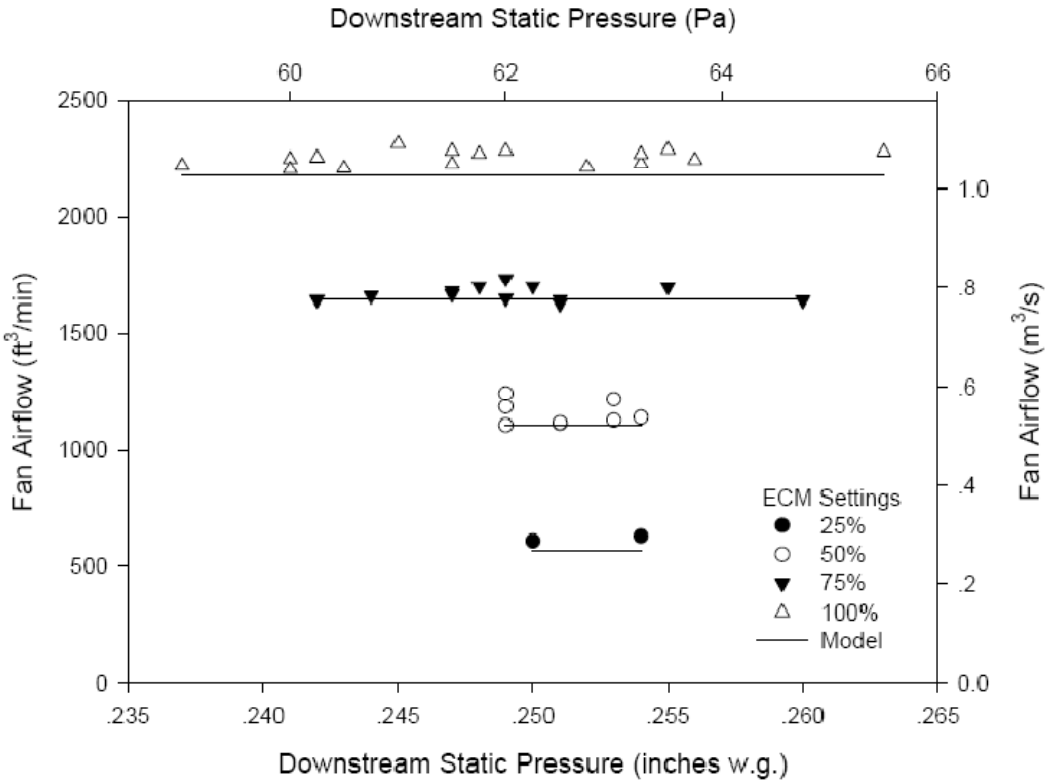

Fig. D-30 Comparison Fan Airflow for S12C_M2

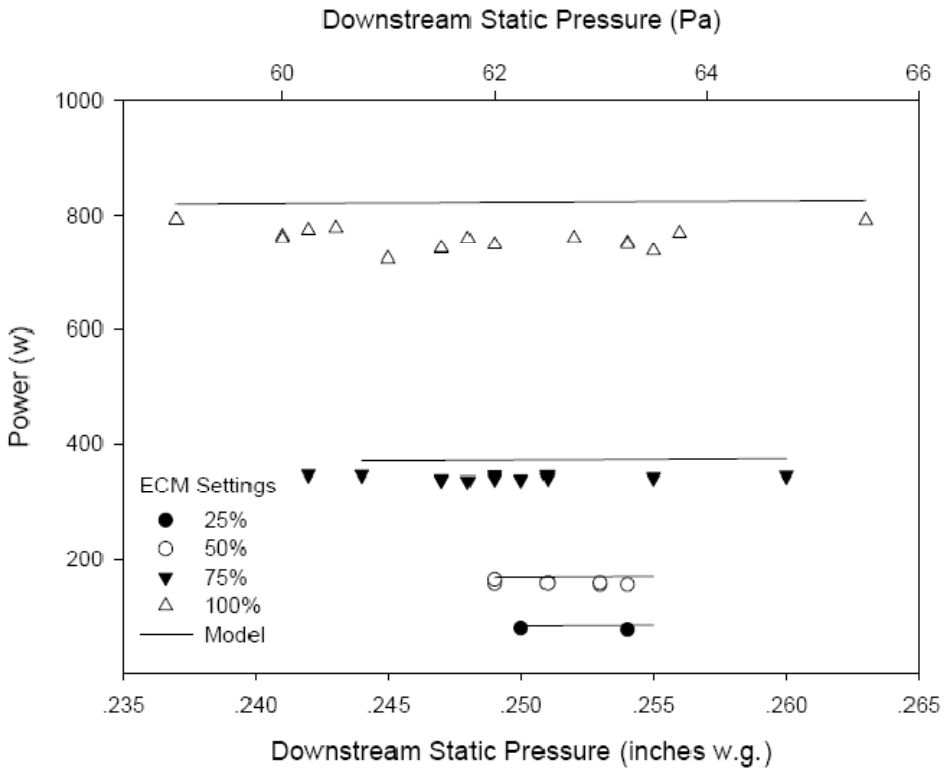

Fig. D-31 Comparison in Power Consumption for S12C_M2

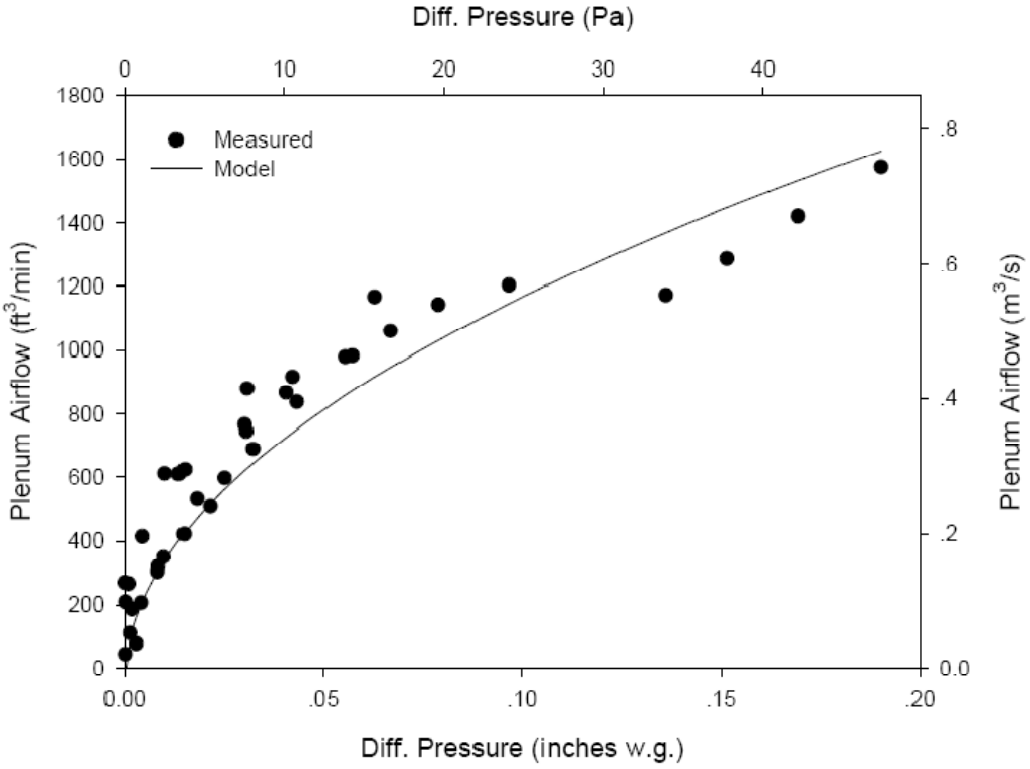

Fig. D-32 Comparison in Plenum Airflow for S12C_M2

APPENDIX E

VERIFICATION ON APPARATUS

A new inlet flow chamber was required in primary airflow test. This chamber has never been used for this project by previous students. To verify the accuracy of this chamber, it was connected directly to the outlet flow chamber without VAV terminal units. The summary of two airflow chambers is shown in Table E-1and the results of verification on apparatus are shown in Table E-2.

Table E-1 Summary of Airflow Chamber Characteristics

Type	Name	Maximum Airflow CFM (m^3/s)	Available Nozzles' Diameters Inch (m)	Fan Power (w)	Controller	Motor
Outlet	Blue	5000	3, 5, 5 & 8	10	VSD	AC Induction
Inlet	Black	8000	3, 3, 4, 4, 6, 6 & 7	30		

From the experimental data it was concluded that the new inlet flow chamber was not as accurate as the chambers used in previous studies because of its relatively large dimension compared to the other two chambers. For the same amount of airflow, a larger chamber would generate a lower differential pressure which was hard to take an accurate

measurement. However, it was found that if the differential pressure was kept within the range of 1 inch w.g. to 3 inches w.g., the accuracy would be acceptable. This requirement was achieved by choosing appropriate nozzle combinations.

Table E-2 Verification on Two Airflow Chambers

Test Point	Figure 15 (Black)		Figure 12 (Blue)		Difference	Percentage	Nozzle Combination	
	Volume Flow Rate	Differential Pressure	Volume Flow Rate	Differential Pressure			Figure 15	Figure 12
	cfm	inches w.g.	cfm	inches w.g.	cfm	%	inches	inches
1	171.1	0.819	170.0	0.799	-1.100	-0.647	3	3
2	202.4	1.144	202.0	1.128	-0.400	-0.198		
3	222.5	1.383	222.1	1.365	-0.400	-0.180		
4	244.1	1.665	244.3	1.652	0.200	0.082		
5	274.8	2.111	274.0	2.084	-0.800	-0.292		
6	285.3	2.277	285.2	2.259	-0.100	-0.035		
7	296.0	2.452	295.5	2.430	-0.500	-0.169		
8	305.8	2.619	306.1	2.607	0.300	0.098		
9	316.0	2.797	316.6	2.792	0.600	0.190		
10	326.1	2.981	327.0	2.984	0.900	0.275		
11	501.1	0.897	502.6	0.892	1.500	0.298	4+3	5
12	524.4	0.982	527.9	0.984	3.500	0.663		
13	540.8	1.044	543.8	1.044	3.000	0.552		
14	601.5	1.292	606.4	1.300	4.900	0.808		
15	648.9	1.504	655.6	1.521	6.700	1.022		
16	705.9	1.781	713.0	1.802	7.100	0.996		
17	757.0	2.050	767.3	2.091	10.300	1.342		
18	816.0	2.385	827.0	2.435	11.000	1.330		
19	868.8	2.707	883.6	2.787	14.800	1.675		
20	917.0	3.021	936.6	3.141	19.600	2.093		

Table E-2 Continued

Test Point	Figure 15 (Black)		Figure 12 (Blue)		Difference Percentage		Nozzle Combination	
	Volume Flow Rate	Differential Pressure	Volume Flow Rate	Differential Pressure			Figure 15	Figure 12
	cfm	inches w.g.	cfm	inches w.g.	cfm	%	inches	inches
21	660.3	0.941	664.9	0.842	4.600	0.692		
22	694.8	1.042	700.6	0.935	5.800	0.828		
23	765.9	1.266	775.2	1.145	9.300	1.200		
24	831.7	1.493	844.0	1.358	12.300	1.457		
25	904.9	1.769	920.5	1.618	15.600	1.695	4+4	3+5
26	975.4	2.057	992.8	1.885	17.400	1.753		
27	1044.7	2.363	1065.8	2.177	21.100	1.980		
28	1111.8	2.679	1137.5	2.485	25.700	2.259		
29	1144.2	2.840	1171.7	2.640	27.500	2.347		
30	1179.3	3.020	1210.9	2.824	31.600	2.610		
31	1247.5	1.382	1259.9	1.397	12.400	0.984		
32	1350.6	1.621	1367.8	1.649	17.200	1.257		
33	1398.0	1.737	1420.0	1.778	22.000	1.549		
34	1448.6	1.866	1471.7	1.912	23.100	1.570	3+3+4+4	5+5
35	1501.9	2.007	1529.4	2.067	27.500	1.798		
36	1597.3	2.273	1627.5	2.346	30.200	1.856		
37	1699.3	2.577	1735.3	2.674	36.000	2.075		
38	1844.9	3.046	1887.0	3.176	42.100	2.231		

Table E-2 Continued

Test Point	Figure 15 (Black)		Figure 12 (Blue)		Difference	Percentage	Nozzle Combination	
	Volume Flow Rate	Differential Pressure	Volume Flow Rate	Differential Pressure			Figure 15	Figure 12
	cfm	inches w.g.	cfm	inches w.g.	cfm	%	inches	inches
39	1222.5	0.881	1216.9	0.933	-5.600	-0.460		
40	1282.7	0.970	1275.9	1.026	-6.800	-0.533		
41	1398.2	1.153	1399.7	1.236	1.500	0.107		
42	1518.4	1.360	1522.3	1.463	3.900	0.256		
43	1632.6	1.574	1641.0	1.703	8.400	0.512	3+4+6	3+5+5
44	1752.7	1.816	1764.6	1.973	11.900	0.674		
45	1853.8	2.035	1873.4	2.229	19.600	1.046		
46	1977.3	2.319	2003.4	2.556	26.100	1.303		
47	2034.7	2.457	2064.4	2.717	29.700	1.439		
48	2094.8	2.608	2126.3	2.888	31.500	1.481		

APPENDIX F

CALCULATION OF PRESSURE LOSS COEFFICIENT THROUGH DAMPERS

Four Excel spreadsheets were used to calculate the pressure loss coefficient through the dampers with different type and size. All of the four forms are shown in this section.

BF8

Test Seting No.	Nozzle Combination (in)	Blower Setting (V)
2	3+4+6	6.00

Test Points (Damper Voltage)	Damper Angle α (Degree)	Damper Angle α (Radiant)	γ (non-dimensional)
0.00	0.00	0.00	1.00
1.00	9.00	0.16	0.84
2.00	18.00	0.31	0.69
3.00	27.00	0.47	0.55
4.00	36.00	0.63	0.41
5.00	45.00	0.79	0.29
6.00	54.00	0.94	0.19
7.00	63.00	1.10	0.11
8.00	72.00	1.26	0.05
9.00	81.00	1.41	0.01
10.00	90.00	1.57	0.00

Test Points (Damper Voltage)	Volume Flow Rate Q (CFM)	Percent of Max Flow (%)
0.00	**1358.40**	100.00
1.00	**1355.50**	99.79
2.00	**1242.80**	91.49
3.00	**1093.70**	80.51
4.00	**932.30**	68.63
5.00	**810.20**	59.64
6.00	**710.60**	52.31
7.00	**652.20**	48.01
8.00	**630.40**	46.41
9.00	**616.20**	45.36
10.00	**601.60**	44.29

Fig. F-1 Data and Results Spreadsheet for BF8

Test Points (Damper Voltage)	Density ρ (lbm/ft^3)	Area (ft^2)	Upstream Velocity V (ft/s)
0.00	0.07	**0.35**	64.86
1.00	0.07	**0.35**	64.72
2.00	0.07	**0.35**	59.34
3.00	0.07	**0.35**	52.22
4.00	0.07	**0.35**	44.51
5.00	0.07	**0.35**	38.68
6.00	0.07	**0.35**	33.93
7.00	0.07	**0.35**	31.14
8.00	0.07	**0.35**	30.10
9.00	0.07	**0.35**	29.42
10.00	0.07	**0.35**	28.72

Test Points (Damper Voltage)	Upstream Velocity Pressure P (in w.g.)	Upstream Static Pressure Ps (in w.g.)	Total Pressure Loss ΔPt (in w.g.)	Pressure Loss Coefficient k (non-dimensional)
0.00	0.94	**0.45**	1.39	1.47
1.00	0.94	**0.45**	1.39	1.48
2.00	0.79	**0.85**	1.64	2.08
3.00	0.61	**1.43**	2.04	3.33
4.00	0.44	**1.94**	2.39	5.37
5.00	0.34	**2.36**	2.69	8.02
6.00	0.26	**2.57**	2.83	10.95
7.00	0.22	**2.71**	2.93	13.45
8.00	0.20	**2.83**	3.03	14.92
9.00	0.19	**2.80**	2.99	15.42
10.00	0.19	**2.80**	2.99	16.14

Fig. F-1 Continued

BF12

Test Seting No.	Nozzle Combination (in)	Blower Setting (V)
1	4+6+6+7	6.00

Test Points (Damper Voltage)	Damper Angle α (Degree)	Damper Angle α (Radiant)	γ (non-dimensional)
0.00	0.00	0.00	1.00
1.00	9.00	0.16	0.84
2.00	18.00	0.31	0.69
3.00	27.00	0.47	0.55
4.00	36.00	0.63	0.41
5.00	45.00	0.79	0.29
6.00	54.00	0.94	0.19
7.00	63.00	1.10	0.11
8.00	72.00	1.26	0.05
9.00	81.00	1.41	0.01
10.00	90.00	1.57	0.00

Test Points (Damper Voltage)	Volume Flow Rate Q (CFM)	Percent of Max Flow (%)
0.00	**3062.30**	100.00
1.00	**2939.90**	96.00
2.00	**2208.50**	72.12
3.00	**1939.90**	63.35
4.00	**1790.90**	58.48
5.00	**1589.30**	51.90
6.00	**1397.70**	45.64
7.00	**1345.50**	43.94
8.00	**1355.40**	44.26
9.00		
10.00		

Fig. F-2 Data and Results Spreadsheet for BF12

Test Points (Damper Voltage)	Density ρ (lbm/ft^3)	Area (ft^2)	Upstream Velocity V (ft/s)
0.00	0.07	**0.79**	64.98
1.00	0.07	**0.79**	62.39
2.00	0.07	**0.79**	46.87
3.00	0.07	**0.79**	41.17
4.00	0.07	**0.79**	38.00
5.00	0.07	**0.79**	33.73
6.00	0.07	**0.79**	29.66
7.00	0.07	**0.79**	28.55
8.00	0.07	**0.79**	28.76

Test Points (Damper Voltage)	Upstream Velocity Pressure Pv (in w.g.)	Upstream Static Pressure Ps (in w.g.)	Total Pressure Loss ΔPt (in w.g.)	Pressure Loss Coefficient k (non-dimensional)
0.00	0.95	**0.14**	1.09	1.15
1.00	0.87	**0.32**	1.19	1.36
2.00	0.49	**1.42**	1.91	3.88
3.00	0.38	**1.84**	2.22	5.83
4.00	0.32	**2.07**	2.40	7.39
5.00	0.26	**2.42**	2.68	10.48
6.00	0.20	**2.86**	3.05	15.48
7.00	0.18	**2.99**	3.17	17.34
8.00	0.19	**3.07**	3.25	17.54

Fig. F-2 Continued

OB8

Test Seting No.	Nozzle Combination (in)	Blower Setting (V)
4	3+4+6	6.00

Test Points (Damper Voltage)	Damper Angle α (Degree)	Damper Angle α (Radiant)	γ (non-dimensional)
0.00	0.00	0.00	1.00
0.50	4.50	0.08	0.89
1.00	9.00	0.16	0.78
1.50	13.50	0.24	0.67
2.00	18.00	0.31	0.56
2.50	22.50	0.39	0.46
3.00	27.00	0.47	0.36
3.50	31.50	0.55	0.26
4.00			
4.50			
5.00			

Test Points (Damper Voltage)	Volume Flow Rate Q (CFM)	Percent of Max Flow (%)
0.00	**1,384.10**	100.00
0.50	**1,381.70**	99.83
1.00	**1,348.60**	97.44
1.50	**1,258.70**	90.94
2.00	**1,177.00**	85.04
2.50	**1,121.20**	81.01
3.00	**980.10**	70.81
3.50	**888.80**	64.22
4.00		
4.50		
5.00		

Fig. F-3 Data and Results Spreadsheet for OB8

Test Points (Damper Voltage)	Density ρ (lbm/ft^3)	Area (ft^2)	Upstream Velocity V (ft/s)
0.00	0.07	**0.35**	66.09
0.50	0.07	**0.35**	65.97
1.00	0.07	**0.35**	64.39
1.50	0.07	**0.35**	60.10
2.00	0.07	**0.35**	56.20
2.50	0.07	**0.35**	53.53
3.00	0.07	**0.35**	46.80
3.50	0.07	**0.35**	42.44

Test Points (Damper Voltage)	Upstream Velocity Pressure P (in w.g.)	Upstream Static Pressure Ps (in w.g.)	Total Pressure Loss ΔPt (in w.g.)	Pressure Loss Coefficient k (non-dimensional)
0.00	0.98	**0.34**	1.32	1.35
0.50	0.98	**0.36**	1.33	1.37
1.00	0.93	**0.47**	1.40	1.51
1.50	0.81	**0.81**	1.62	1.99
2.00	0.71	**1.10**	1.81	2.56
2.50	0.64	**1.31**	1.95	3.04
3.00	0.49	**1.83**	2.32	4.72
3.50	0.40	**2.09**	2.49	6.17

Fig. F-3 Continued

OB12

Test Seting No.	Nozzle Combination (in)	Blower Setting (V)
3	4+6+6+7	6.00

Test Points (Damper Voltage)	Damper Angle α (Degree)	Damper Angle α (Radiant)	γ (non-dimensional)
0.00	0.00	0.00	1.00
0.50	4.50	0.08	0.89
1.00	9.00	0.16	0.78
1.50	13.50	0.24	0.67
2.00	18.00	0.31	0.56
2.50	22.50	0.39	0.46
3.00	27.00	0.47	0.36
3.50	31.50	0.55	0.26
4.00	36.00	0.63	0.17
4.50			
5.00			

Test Points (Damper Voltage)	Volume Flow Rate Q (CFM)	Percent of Max Flow (%)
0.00	**3028.70**	100.00
0.50	**2969.70**	98.05
1.00	**2788.50**	92.07
1.50	**2678.80**	88.45
2.00	**2358.60**	77.87
2.50	**2226.50**	73.51
3.00	**1704.10**	56.27
3.50	**1496.70**	49.42
4.00	**1345.70**	44.43
4.50		
5.00		

Fig. F-4 Data and Results Spreadsheet for OB12

Test Points (Damper Voltage)	Density ρ (lbm/ft^3)	Area (ft^2)	Upstream Velocity V (ft/s)	
0.00	0.07	**0.79**	64.27	
0.50	0.07	**0.79**	63.02	
1.00	0.07	**0.79**	59.17	
1.50	0.07	**0.79**	56.85	
2.00	0.07	**0.79**	50.05	
2.50	0.07	**0.79**	47.25	
3.00	0.07	**0.79**	36.16	
3.50	0.07	**0.79**	31.76	
4.00	0.07	**0.79**	28.56	

Test Points (Damper Voltage)	Upstream Velocity Pressure Pv (in w.g.)	Upstream Static Pressure Ps (in w.g.)	Total Pressure Loss ΔPt (in w.g.)	Pressure Loss Coefficient k (non-dimensional)
0.00	0.93	**0.17**	1.10	1.18
0.50	0.89	**0.29**	1.18	1.32
1.00	0.79	**0.54**	1.32	1.69
1.50	0.72	**0.68**	1.40	1.93
2.00	0.56	**1.18**	1.74	3.10
2.50	0.50	**1.44**	1.94	3.87
3.00	0.29	**2.25**	2.54	8.66
3.50	0.23	**2.61**	2.83	12.51
4.00	0.18	**2.96**	3.14	17.17

Fig. F-4 Continued

APPENDIX G

CALCULATION PROCESS OF THE SERIES FPTU MODEL

The airflow performance of the FPTUs can be characterized by solving the group of equations consisted of Equations (G-1), (G-2), (G-3) and (G-4).

$$Q_{primary} = \left(a_1 + b_1 \times \sqrt{P_{upstream} - P_{internal}}\right) \times (1 + c_1 \times \gamma + d_1 \times \gamma^2 + e_1 \times \gamma^3) + f_1 \quad \text{(G-1)}$$

$$Q_{fan} = a_2 + b_2 \times \eta \quad \text{(G-2)}$$

$$Q_{plenum} = \left(a_4 + b_4 \times \sqrt{|P_{internal}|}\right) \times \left(1 + c_4 \times \theta + d_4 \times \theta^2\right) \quad \text{(G-3)}$$

$$Q_{fan} = Q_{plenum} + Q_{primary} \quad \text{(G-4)}$$

The intermediate variables A and B are defined in Equations (G-5) and (G-6).

$$A = 1 + c_1 \times \gamma + d_1 \times \gamma^2 + e_1 \times \gamma^3 \quad \text{(G-5)}$$

$$B = 1 + c_4 \times \theta + d_4 \times \theta^2 \quad \text{(G-6)}$$

Then the Equations (G-1) and (G-3) can be written in this form:

$$Q_{primary} = \left(a_1 + b_1 \times \sqrt{P_{upstream} - P_{internal}}\right) \times A + f_1 \quad \text{(G-7)}$$

$$Q_{plenum} = \left(a_4 + b_4 \times \sqrt{|P_{internal}|}\right) \times B \quad \text{(G-8)}$$

Put Equations (G-7) and (G-8) into Equation (G-4):

$$\left(a_1 + b_1 \times \sqrt{P_{upstream} - P_{internal}}\right) \times A + f_1 + \left(a_4 + b_4 \times \sqrt{|P_{internal}|}\right) \times B = a_2 + b_2 \times \eta \quad \text{(G-9)}$$

Then reform the Equation (G-9):

$$a_1 \times A + b_1 \times A \times \sqrt{P_{upstream} - P_{internal}} + f_1 + a_4 \times B + b_4 \times B \times \sqrt{-P_{internal}} = a_2 + b_2 \times \eta \quad \text{(G-10)}$$

The intermediate variables C, D and E are defined in the Equations (G-11) to (G-13):

$$C = a_2 + b_2 \times \eta - a_1 \times A - f_1 - a_4 \times B \quad \text{(G-11)}$$

$$D = b_1 \times A \quad \text{(G-12)}$$

$$E = b_4 \times B \quad \text{(G-13)}$$

The Equation (G-10) is simplified:

$$D \times \sqrt{P_{upstream} - P_{internal}} + E \times \sqrt{-P_{internal}} = C \quad \text{(G-14)}$$

Move the term $E \times \sqrt{-P_{internal}}$ to the left side and square both sides:

$$D^2 \times \left(P_{upstream} - P_{internal}\right) = C^2 - 2 \times C \times E \times \sqrt{-P_{internal}} - E^2 \times P_{internal} \quad \text{(G-15)}$$

Then transform Equation (G-15) into this form:

$$D^2 \times P_{upstream} - D^2 \times P_{internal} - C^2 + E^2 \times P_{internal} = -2 \times C \times E \times \sqrt{-P_{internal}} \quad \text{(G-16)}$$

Combine the terms with $P_{internal}$:

$$(E^2 - D^2) \times P_{internal} + \left(D^2 \times P_{upstream} - C^2\right) = -2 \times C \times E \times \sqrt{-P_{internal}} \quad \text{(G-17)}$$

The intermediate variable F is defined in Equation (G-18)

$$F = \left(D^2 \times P_{upstream} - C^2\right) \quad \text{(G-18)}$$

Square both sides and transform:

$$(E^2 - D^2)^2 \times {P_{internal}}^2 + [2 \times F \times (E^2 - D^2) + 4 \times C^2 \times E^2] \times P_{upstream} + F^2 = 0 \quad \text{(G-19)}$$

Equation (G-19) is a quadratic equation with internal pressure $P_{internal}$. Then the internal pressure $P_{internal}$ can be expressed in equation (G-20).

$$P_{internal} = \frac{-(2\times F\times(E^2-D^2)+4\times C^2\times E^2)+\sqrt{[2\times F\times(E^2-D^2)+4\times C^2\times E^2]^2-4\times(E^2-D^2)^2\times F^2}}{2\times(E^2-D^2)^2} \quad \text{(G-20)}$$

VITA

Peng Yin was born in Zhengzhou, China and graduated from Shanghai Ocean University with a Bachelor of Science in thermal energy and power engineering, Shanghai in June 2008. In September 2008 he enrolled in the Master of Science program in Department of Mechanical Engineering at Texas A&M University. He received his Master of Science degree in August 2010. He is going to pursue a Ph.D. in mechanical engineering after graduation.

Mr. Yin may be reached at 3126 TAMU, College Station, TX 77843-3126. His email address is solomonyp@gmail.com.